Xiaobo Ren

Effect of welding residual stress on fracture

Xiaobo Ren

Doctoral Thesis

NTNU
Norwegian University of
Science and Technology

NTNU
Norwegian University of
Science and Technology

NTNU

Xiaobo Ren

Effect of welding residual stress on fracture

Thesis for the degree of philosophiae doctor

Trondheim, June 2010

Norwegian University of
Science and Technology
Faculty of Engineering Science and Technology
Department of Structural Engineering

NTNU
Norwegian University of
Science and Technology

Effect of welding residual stress on fracture

Xiaobo Ren

Norwegian University of Science and Technology
Faculty of Engineering Science and Technology
Department of Structural Engineering
Trondheim, Norway

To my wife, parents and other family members

Preface

This doctoral thesis is submitted to the Norwegian University of Science and Technology (NTNU) for the degree of Philosophiae Doctor. This work has been carried out at Department of Structural Engineering and supported by the Research Council of Norway through the "STORFORSK" Project No.167397/V30, RESIA. Prof. Zhiliang Zhang has been my supervisor.

Different people have different perspective for a PhD. I have it as a dream deeply in my heart and regard it as a meaningful journey of my whole life. I enjoy the process much more than the ending. I could never have accomplished this task without the inspiration of so many generous people.

First, I would like to acknowledge my supervisor Prof. Zhiliang Zhang who initially offered me the opportunity to do this work and experience different culture and life. I appreciate his encouragement, great ideas, excellent advice and critical reviews for this work. Most importantly, I want to express my gratitude for him as a model of life to follow: positive, optimistic, self-confident and honest.

I would also like to express my sincere thanks to Prof. Wenxian Wang at Taiyuan University of Technology where I got my Bachelor degree and Prof. Hongyang Jing at Tianjin University where I earned my Master degree. Without their example I would not be where I am today.

I feel fortunate to have been a member of RESIA team, in which I was surrounded and inspired by professional colleagues at NTNU, SINTEF and IFE. Special thanks are directed to Mr. Bård Nyhus at SINTEF, for his valuable comments and generous help; Dr. Jun Liu at DNV, for great friendship, encouragement and help; Dr. Sigmund K. Ås at SINTEF, for his comments and help for English writing; Prof. Asbjørn Mo, Prof. Odd M. Akselsen, for their encouragement and support.

Xiaobo Ren

Abstract

Residual stresses are unavoidable in welded constructions. How to correctly predict residual stresses and assess their effect on structural integrity is a fundamental issue. One of the most difficult aspects in structural integrity assessment is to incorporate the effect of residual stresses in a safe manner, without making unduly conservative assumptions about the level of stress that may be present. Current structural assessment procedures typically assume upper bound residual stress solution, which can overestimate or underestimate the effect of residual stresses. The objective of this study is to fundamentally understand the effect of residual stresses on fracture behaviour and try to incorporate the effect into the integrity assessment procedure in a quantitative manner.

This study concerns an ideal problem. A large cylinder with a weld in the center was studied. The cylinder was simulated by a 2D plane strain modified boundary layer model with the remote boundary governed by the elastic *K-field* and *T-stress*. A sharp crack was embedded in the weld region. The eigenstrain method was employed to introduce a local tensile or compressive residual stress field into the finite element model. The concept of the study is to investigate the difference between the reference case and the case including residual stresses.

Residual stress-induced the crack-tip constraint has been investigated first. Based on the difference of the opening stress between the case with residual stresses and the reference case, a parameter R was defined to characterize the crack-tip constraint induced by residual stresses. The effects of external loading, material hardening, loading path and geometry constraint on R have also been studied. It has been found that the residual stress-induced crack-tip constraint is smaller for the case with higher geometry constraint.

Effect of residual stress on cleavage fracture toughness was investi-

gated by using the cohesive zone model with a bilinear traction-separation-law. Several cases were studied to understand the effect of residual stresses on the cleavage fracture toughness. Results suggest that the behaviour of residual stress is very similar to *T-stress*. Tensile residual stress compresses the plastic zone of the surrounding material and moves the plastic zone backward, which in turn reduces the cleavage fracture toughness. In contrast, the compressive residual stress enlarges the plastic zone and shifts the plastic zone forward, and enhances the cleavage toughness. The effect of residual stresses on cleavage fracture toughness has also been investigated for geometrically similar weld with different sizes, different damage parameters, hardening exponents and *T-stresses*.

Ductile crack growth resistance is important for assessing the structural integrity, and the effect of residual stresses on ductile crack growth resistance has also been studied. The study reveals that tensile residual stresses decrease the crack growth resistance while the compressive residual stresses have the opposite effect. With the increase of crack growth, the effect of residual stress tends to diminish. Under certain conditions, the effect of residual stresses on crack growth resistance curve is independent of the size of geometrically similar weld. Thus, a "master curve" can be obtained and applied for the integrity assessment. Effect of residual stress on the crack growth resistance also depends on the material hardening, initial void volume fraction and *T-stress*.

It has not been completed to incorporate the effect of residual stresses into the integrity assessment by a quantitative manner in this study. However, some guidelines were outlined in the thesis for future work.

List of Publications

P1 X.B. Ren, Z.L. Zhang and B. Nyhus. Effect of residual stresses on the crack-tip constraint in a modified boundary layer model, *International Journal of Solids and Structures*, 46:2629-2641, 2009.

P2 X.B. Ren, Z.L. Zhang and B. Nyhus. Effect of residual stresses on ductile crack growth resistance, *Engineering Fracture Mechanics*, 77:1325-1337, 2010.

P3 X.B. Ren, Z.L. Zhang and B. Nyhus. Effect of residual stresses on cleavage fracture toughness by using cohesive zone model, *submitted*.

P4 X.B. Ren, Z.L. Zhang and B. Nyhus. Residual stress induced crack-tip constraint: a parametric study, In *Proceeding of 17th European Conference on Fracture (ECF-17)*, Brno, Czech Republic, 2008.

P5 X.B. Ren, Z.L. Zhang and B. Nyhus. Effect of residual stresses on brittle fracture by cohesive zone modeling, In *Proceeding of 12th International Conference on Fracture (ICF-12)*, Ottawa, Canada, 2009.

P6 X.B. Ren, Z.L. Zhang and B. Nyhus. Effect of residual stresses on brittle fracture by cohesive zone modeling, In *Proceeding of 21st Nordic Seminar on Computational Mechanics (NSCM-21)*, Trondheim, Norway, 2008.

P7 X.B. Ren, Z.L. Zhang and B. Nyhus. Numerical investigation on the effect of residual stresses on the ductile crack growth resistance, In *Proceeding of 29th International Conference on Ocean, Offshore and Arctic Engineering (OMAE-2010)*, Shanghai, China, 2010.

Contents

List of Figures

Chapter 1

Introduction

1.1 Background

Welding technique has been widely used in industry to fabricate and repair the structures. The safety and integrity of welded structures is an important issue that should be take into account for both human and environment impacts. It is widely accepted that the presence of the welding residual stress can have a significant effect on the subsequent failure characteristics of engineering components and structures [1]. However, compared with the role of primary load and defects, the role of residual stress on failure and integrity assessment has received relatively little attention, which due largely to historical difficulties associated with the measurement and prediction of residual stress [2]. It has been demonstrated that the current procedures can significantly overestimate the residual stress effects in most cases and underestimate their effects in others [3]. Large savings can probably be done if the origins of residual stress are recognized, means for predicting their evolution in-service developed, and their influence on failure processes understood. In this way residual stresses can be incorporated into structural integrity assessment in a safe manner, without making unduly conservative assumptions about the levels of residual stress that may be present [4].

Project RESIA (Residual Stress Simulation for Integrity Assessment) was established with the purpose of developing the scientific platform for next generation quantitative modeling of residual stresses and associated integrity assessment for welded steel components and structures.

WP1: Integrity assessment

WP4: Model validation and demonstration

WP2: Finite element backbone

WP3: Constitutive models
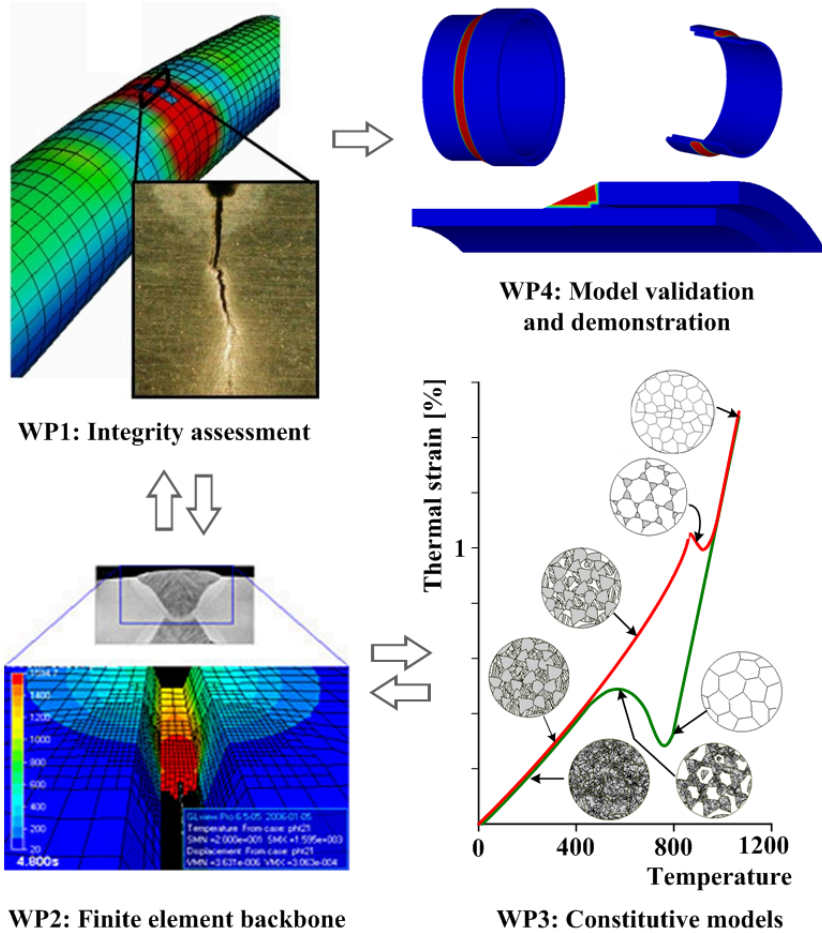
Figure 1.1: Main tasks of the RESIA project [5].

The project involves three research units, SINTEF[*], NTNU[†] and IFE[‡]. The main tasks of the project are illustrated in Figure 1.1.

The main objectives of the RESIA project are as follows [4]:

- Develop the scientific platform for next generation quantitative modeling of residual stress prediction and integrity assessment for welded steel components and structures.

- Unified constitutive equations that couple the temperature, strain rate effect, microstructure and phase transformation plasticity will be modified and extended to high strength steels.

- Develop a reliable thermal mechanical testing method for inversely retrieving the microstructure and temperature dependent material parameters used in the constitutive equations.

- Establish welding residual stress distribution for typical applications and develop an improved failure assessment procedure for effectively incorporating the quantitative effect of residual stresses.

The work presented in this thesis belongs to work-package 1 (WP1) of the RESIA project, which focuses on the effect of residual stresses on the integrity assessment from the viewpoint of fracture mechanics, such as the effect of residual stresses on crack driving force, residual stress-induced crack-tip constraint, the influence of residual stress on failure mechanisms and how to incorporate the effect of residual stress into the current integrity assessment procedure.

1.2 Fracture mechanics

The effect of residual stress on fracture is the main concern in this thesis. A description of the theory of fracture mechanics used in this study will be presented in this section, and the effect of residual stresses on fracture behaviour will also be briefly introduced.

1.2.1 Crack driving force

Crack driving force is defined as the rate of change in potential energy with the crack area, which refers to the derivative with respect to the crack area [6]. In linear elastic fracture mechanics (LEFM), the *stress intensity factor* defines the amplitude of the crack-tip singularity and is used as crack driving force parameter. For mode I loading conditions, K has the following form:

$$K_I = \sigma\sqrt{\pi a} \tag{1.1}$$

where σ is the stress and a is the crack length. When residual stress is present, the contribution to the crack driving force must be included in the

analysis, and the total stress intensity is simply the sum of the contribution from applied load and residual stresses:

$$K^{Total} = K^{Appl} + K^{Rs} \tag{1.2}$$

where the superscripts *Appl* and *Rs* denote applied load and residual stress respectively. For an elastic-plastic body a more complex analysis is required which cannot be evaluated by a simple linear addition of the various *K* terms resulting from the residual and applied stress component [2].

In elastic-plastic fracture mechanics (EPFM), two parameters are proposed and widely used as the measure of fracture toughness, and to characterize the near tip stress and strain fields: one is crack tip opening displacement (δ, CTOD) proposed by Wells [7] and *J*-integral proposed by Rice [8] for deformation plasticity (nonlinear elastic) materials. CTOD is usually defined as the displacement at the original crack tip or the displacement at the intersection of a 90° vertex with the crack flanks. Shih [9] has shown that there is a unique link between the *J* and CTOD for a given elastic-plastic material.

J-integral is a measure of the nonlinear elastic energy release rate and the intensity of the crack tip fields under *J*-dominant conditions. For a two-dimensional body with a crack directed along the x_1 axis under quasi-static conditions, a general definition of the *J*-integral is [10]:

$$J = \lim_{\Gamma \to 0} \int_{\Gamma} \left(W\delta_{1i} - \sigma_{ij}\frac{\partial u_j}{\partial x_1} \right) n_i ds \tag{1.3}$$

where *W* is the strain energy density, σ_{ij} and u_i are components of stress and displacement in Cartesian coordinates respectively, Γ is an arbitrary counterclockwise path around the crack tip, and *ds* is the path length along Γ. *J*-integral is path independent given the assumption that the strain energy density is a single-valued function of the strain (or stress), e.g. linear/nonlinear elastic materials. However, *J*-integral is not path independent in case of non-proportional loading or when residual stress is present [11, 12]. When residual stresses are regarded as secondary stresses and assumed only to contribute to the elastic part of the *J*-integral, the effect of residual stresses can be incorporated into *J*-integral as follows [13]:

$$J^{Total} = \left\{ \sqrt{J_{EL}^{Appl}} + \sqrt{J^{RS}} \right\}^2 + J_{PL}^{Appl} \tag{1.4}$$
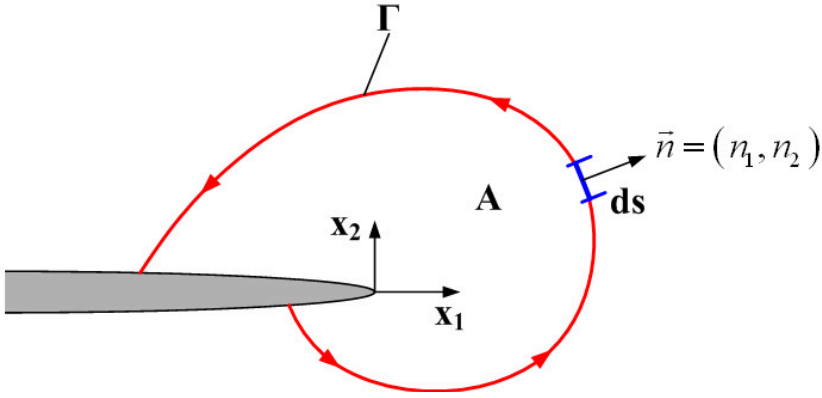
Figure 1.2: Illustration of the contour integration.

where J_{EL} and J_{PL} represent the linear elastic (small-scale yielding) and fully plastic J. The length scale of the residual stress should be considered in this case. If it is smaller than the plastic zone r_p, then it is likely that the residual stress will have little effect on the fracture behaviour because crack-tip plasticity will obliterate the underlying eigenstrains [2]. Recently, Lei [12] proposed a path-independent integral that applies to general crack problems under combined primary and secondary loads. This includes thermal stresses and residual stress and their combination with primary load, and has the following form [12, 14]:

$$J = \int_{\Gamma} \left(W \delta_{1i} - \sigma_{ij} \frac{\partial u_j}{\partial x_1} \right) n_i ds + \int_A \left(\sigma_{ij} \frac{\partial \varepsilon_{ij}}{\partial x_1} - \frac{W}{\partial x_1} \right) dA \qquad (1.5)$$

where σ_{ij}, ε_{ij} and u_i are components of stress, strain and displacement, respectively. x_1 is the direction ahead of the crack, ds is the path length on the contour Γ, A is the area surrounded by Γ and n_i is the unit vector normal to Γ (see Figure 1.2). The strain energy W is [14]

$$W = \int \sigma_{ij} (d\varepsilon_{ij}^e + d\varepsilon_{ij}^p) \qquad (1.6)$$

and the total strain is

$$\varepsilon_{ij} = \varepsilon_{ij}^e + \varepsilon_{ij}^p + \varepsilon_{ij}^0 \qquad (1.7)$$

where superscripts e, p and 0 refer to elastic, plastic and initial strains, respectively.

Hou and Pan [15] also proposed a finite element procedure to determine a potential fracture parameter J_{1d} for welded structures with residual stresses, which is based on the concept of the energy difference under the load-displacement curves of the two cracked solids with slightly different crack sizes.

1.2.2   Crack-tip constraint

Although fracture mechanics has been developed for over 50 years, the subject of "constraint effect in fracture" is relatively recent, which only started in early 1990's [16]. Constraint in fracture mechanics is a term that is widely used but vaguely defined or understood. In the present context we prefer to understand the level of constraint as an indicator of the near-tip stress state, and the constraint is regarded as the factors or conditions which influence the transferability and invalidate the one-to-one relation between the crack driving force and near-tip stress field [17]. In a weldment there are basically four factors which influence the level of a crack-tip constraint. The geometry constraint is caused by the crack size, specimen dimensions and loading mode; inhomogeneous material properties can induce the mismatch constraint at the crack tip [18–20]; Both the prestrain history [21] and the welding residual stresses influence the crack-tip constraint as well.

Conventional single parameter fracture mechanics approaches rely on the similarity of the crack tip stress and deformation fields [22]. Under well-contained near tip plasticity, a single parameter, such as the linear elastic stress intensity factor K, and the J-integral or equivalently crack tip opening displacement (CTOD), can uniquely scales the elastic-plastic near tip field. However, the single parameter characterization is not satisfied in most practical situations because certain high constraint condition can not be satisfied [23]. The arguments that a single parameter might not be sufficient to characterize the near-tip behaviour or cracked geometries under large-scale yielding condition motivated the development of two-parameter fracture theories.

According to Williams's solution, the first two terms of small-strain linear elastic expansion of the crack-tip stress field possess the following form [24]:

$$\sigma_{ij} = \frac{K_I}{\sqrt{2\pi r}} f_{ij}(\theta) + T\delta_{1i}\delta_{1j} \tag{1.8}$$

where K_I is the Mode I elastic stress intensity factor and T is a stress parallel to the crack. Larsson and Carlsson [25] demonstrated that the second term in the series was important to modify the boundary solution to fit the real crack problem, and the *T-stress* has a significant effect on the plastic zone size and shape. Du and Hancock [26] studied the effect of *T-stress* on the small scale yielding field of a crack in plain strain conditions and found that a positive *T-stress* causes plasticity to envelop the crack tip and exhibits a Prandtl field. This corresponds to the limit solution of the HRR field [27, 28] for a non-hardening material, while a compressive *T-stress* reduces the stress triaxiality state at the crack tip. Betegón and Hancock [29] suggested a two-parameter framework *J-T* to characterize the effect of the constraint induced by the geometry. But, *T-stress* is only valid in an elastic regime.

O'Dowd and Shih [30, 31] developed the *J-Q* two-parameter theory and gave a precise meaning to the term constraint caused by the geometry and loading mode. They showed that the full range of high- and low-triaxiality fields within the *J-Q* annulus are members of a family of solutions parameterized by *Q* when distances are normalized by J/σ_0, where σ_0 is the yield stress. The near-tip stress field can be expressed by two-term expansion:

$$\sigma_{ij} = \sigma_{ij}^{HRR} + Q\sigma_0 \left(\frac{r}{J/\sigma_0}\right)^q \hat{\sigma}_{ij}(\theta, n) \tag{1.9}$$

where

$$\sigma_{ij}^{HRR} = \left(\frac{J}{\alpha\varepsilon_0\sigma_0 I_n r}\right)^{\frac{1}{n+1}} \sigma_0 \tilde{\sigma}_{ij}(\theta, n) \tag{1.10}$$

is the *J*-controlled HRR stress field, r and θ are polar coordinates centered at the crack tip; n is the power hardening exponent; ε_0 is the yield strain ($\varepsilon_0 = \sigma_0/E$), and α is a material constant.

Their study showed that $|q| \ll 1$; and when $|\theta| < \pi/2$, $1 < r/(J/\sigma_0) < 5$, the stress components $\hat{\sigma}_{rr} \approx \hat{\sigma}_{\theta\theta} \approx constant$ and $|\hat{\sigma}_{r\theta}| \ll |\hat{\sigma}_{\theta\theta}|$. Thus, *Q* is a hydrostatic stress parameter. In this two-parameter formulation, *J* sets the size scale over which large stress and strains develop, and *Q* characterizes the crack-tip stress distribution and the stress triaxiality achieved ahead of the crack. *Q* is therefore a quantitative measure of the crack-tip constraint caused by geometry. It should be noted that the *J-Q* theory fails to characterize the crack-tip fields and quantify the constraint level in a bending-dominated large deformation regime. Zhu and Leis [32] proposed a bending modified *J-Q* theory, by which the crack-tip stress fields

for bending specimens at all deformation levels can be characterized. For geometry constraint characterization, Chao et al. [33], Chao and Zhu [34] also proposed J-A_2 theory, and an engineering crack-tip constraint parameter Γ was suggested by Schindler [35] as well. The above constraint measures are developed for in-plane constraint. For the effect of out-of-plane constraint, Guo extended the HRR analysis in a series of papers [36–38] to the 3D case. In Guo's solution the thickness effect entered the final result through functions $T_z(n, r, x_3)$, $I_n(n, T_z)$ and $\tilde{\sigma}_{ij}(\theta, n, T_z)$ of Eq. 1.10, and the parameter T_z is defined as:

$$T_z = \frac{\sigma_{33}}{\sigma_{11} + \sigma_{22}} \tag{1.11}$$

Within the plastic domain in front of the crack T_z changes from 0 for plane stress to 0.5 for plane strain. Guo also proposed an analytical approximate formula to compute T_z.

In welded components, the crack located at the interface between the weld metal and the heat affected zone is generally the most critical one. Because of the nature of welding, there is often a mismatch between the weld metal and the base metal. By considering the interface crack as a bi-material system, Zhang et al. [18] carried out a numerical investigation on the near-tip stress field and found that the near-tip field in the forward sector can be separated into two parts. The first is characterized by the J-integral for a reference material; the second part which influences the absolute levels of stresses at the crack tip and measures the deviation of the field from the first part can be described by a mismatch constraint parameter, M [39]:

$$\sigma_{ij} \approx \sigma_{ij}^{Ref}(J) + M\sigma_{0_{Ref}}\bar{f}_{ij}^{M}(\theta + 12\beta) \tag{1.12}$$

where $\beta = 0$ for overmatch and $\beta = 1$ for undermatch, $\sigma_{0_{Ref}}$ is the yield stress of reference material and $\bar{f}_{ij}^{M}$ represents the angular function of the difference fields caused by mismatch, which only depends on the reference material. The study also showed that radial dependence of M-field is weak. Similar studies have been carried out for the crack in the middle of weld [19, 20].

Zhang et al. [40] further studied the effect of T-stress on the crack-tip stress field of an elastic-plastic interface crack. They found that the T-stress

can shift the near-tip stress level up and down without significantly affecting the mismatch constraint parameter M, which indicates that the constraints caused by geometry and mismatch are independent of each other. A so-called J-Q-M formulation to describe the near-tip stress field in the presence of both geometry and material mismatch constraints was then proposed:

$$\sigma_{ij} \approx \sigma_{ij}^{M=0;T=0} + Q\sigma_{0_{Ref}}\hat{f}_{ij}^{Q}(\theta) + M\sigma_{0_{Ref}}\hat{f}_{ij}^{M}(\theta + 12\beta) \qquad (1.13)$$

Here, the Q parameter describes the geometry constraint. Similarly, the M value is used to rank the material mismatch effect on the crack-tip constraint.

Plastic prestrain history common in reeled pipes has also been found to influence on the crack driving force and crack-tip stress field. By considering single prestrain cycles, Eikrem et al. [21] developed a new parameter to quantify the prestrain induced crack-tip constraint:

$$P = (\frac{\triangle\sigma_{\theta\theta}}{\sigma_0})_{x/\delta=4} = \{(\frac{\sigma_{\theta\theta}}{\sigma_0})_{\varepsilon} - (\frac{\sigma_{\theta\theta}}{\sigma_0})_{\varepsilon=0}\}_{x/\delta=4}, \quad \theta = 0 \qquad (1.14)$$

where $(\frac{\sigma_{\theta\theta}}{\theta_0})_{\varepsilon}$ implies the case with prestrain history and $(\frac{\sigma_{\theta\theta}}{\theta_0})_{\varepsilon=0}$ denotes the monotonic loading case. Thus, P value represents the amplitude of the difference stress field caused by the prestrain history and can be used to rank its constraint. A three parameter formulation $CTOD$-Q-P is suggested to describe the near-tip stress field of a cracked specimen with prestrain history. Here, CTOD has been used as the crack driving force. The formulation is as following:

$$\sigma_{\theta\theta}^{\varepsilon}(x) = \sigma_{\theta\theta}^{\varepsilon=0}(x,\delta,\sigma_0,n) + Q + P \qquad at \quad \theta = 0 \qquad (1.15)$$

The study of the effect of residual stresses on the crack-tip constraint has also received attention recently. The studies carried out by Panontin and Hill [41], Hill and Panontin [42] confirm that the residual stresses contribute to both the crack driving force and the crack-tip constraint. Xu and Burdekin [43] investigated the effect of residual stresses on the crack-tip constraint and found that the tensile residual stresses parallel to the crack flank increase the constraint at the crack tip while compressive residual stresses in this direction have the opposite effect, but a biaxial residual
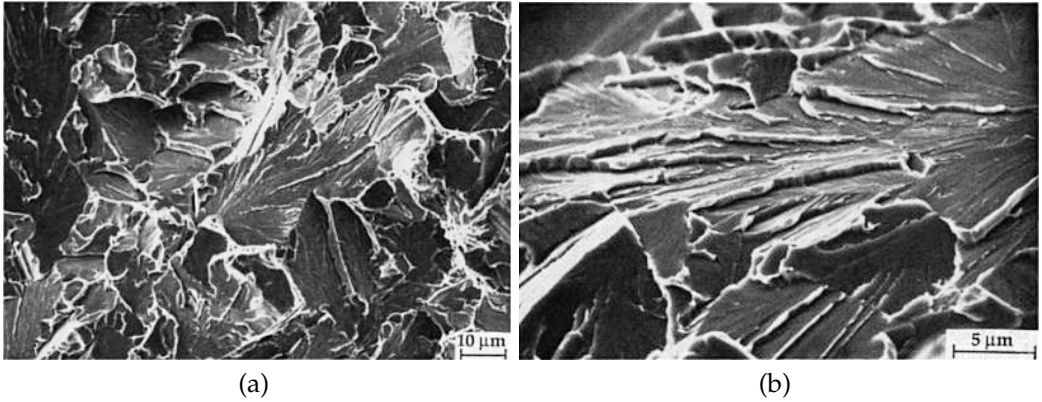
Figure 1.3: SEM fractographs of cleavage in an A 508 Class 3 alloy, (a) multifaceted surface, and (b) river patterns [6].

stress state may also increase the crack-tip constraint despite the residual stress component parallel to the crack flank being compressive. Liu et al. [44] studied a one-dimensional residual stress field perpendicular to the crack plane in single edge notched tension and bending specimens. They showed that residual stress can enhance the crack-tip constraint and defined a parameter R to characterize the effect. Following the same approach for investigating crack-tip constraint [18, 21, 30, 31] the structure and behaviour of the near-tip stress field under the combined load of a two-dimensional residual stress field and external load in a well defined modified boundary layer (MBL) model will be studied in this thesis, and the parameter R used to quantify the constraint induced by residual stresses will be further investigated.

1.2.3   Cleavage fracture

Cleavage fracture can be defined as the rapid propagation of a crack along a particular crystallographic plane [6], and there is little or no evidence of local micro-scale plasticity accompanying the unstable crack growth. Typically, cleavage fracture has multifaceted fracture surface in a polycrystalline material or so-called "river pattern", as shown in Figure 1.3. The mechanism of cleavage fracture has been well discussed in Ref. [45].

Micromechanical models using continuum representation of stress and
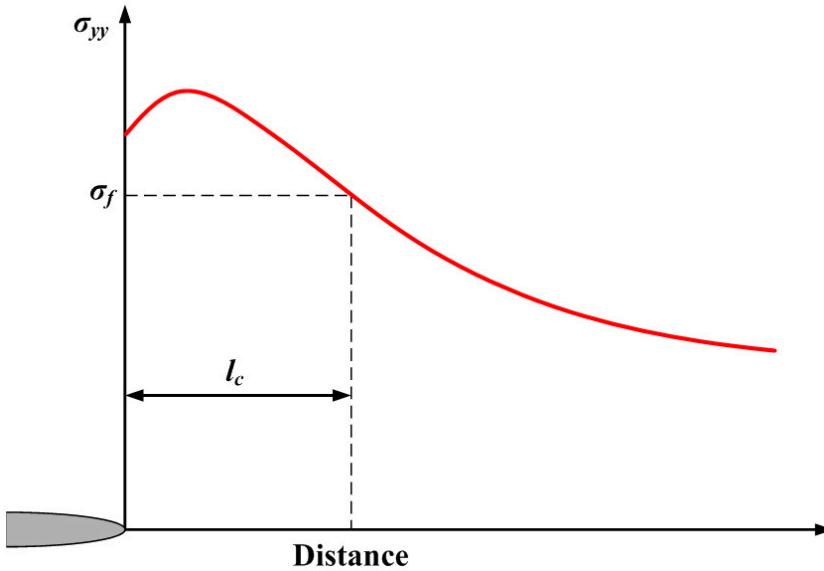
Figure 1.4: Illustration of Ritchie-Knott-Rice model.

strain are generally used to predict local conditions for cleavage fracture. For cleavage fracture to happen, the opening stress should reach the critical value σ_c at a certain distance from the crack tip l_c or within a certain volume in front of the crack tip [46]. This physical scale must be considered in studying the micromechanisms of fracture in order to consider microstructural features necessary for the physical failure mechanism. Ritchie, Knott and Rice (RKR) [47] introduced a simple model to relate fracture stress to fracture toughness, and they postulated that cleavage failure occurs when the stress ahead of the crack tip exceeds σ_f over a characteristic distance, as illustrated in Figure 1.4.

Previous studies concerning cleavage fracture indicate that the critical fracture stress ranges from 3 to 4 times the yield strength of the material, and that is relatively independent of temperature and strain rate. Estimates of the characteristic length or distance in mild steels range from 2 to 5 grain diameters [41]. However, in real elastic-plastic materials, the large plastic deformations are often necessary to initiate the cleavage fracture. Therefore, Neimitz et al. [46] proposed an alternative formulation of the RKR criterion. The cleavage fracture was demonstrated as a synergistic action of the stress and deformation at the critical moment. It has been
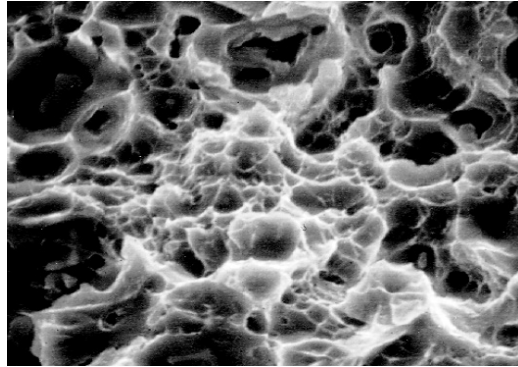
Figure 1.5: Dimple type fracture surface of A6082 aluminum alloy [49].

demonstrated that for fracture to occur it is not sufficient that the opening stress reaches the critical value alone, but it is also necessary that the location of this maximum from the crack tip must be over the distance $l \geqslant l_c$, where l_c is considered as a material parameter.

Experimental work undertaken by Mirzaee-Sisan et al. [48] indicated an apparent reduction in mean cleavage fracture toughness of an A553-B ferritic steel of 50% from conventional fracture toughness data. Panontin and Hill [41] utilized the RKR (Ritchie-Knott-Rice) [47] model to predict the effect of residual stresses on brittle fracture initiation and found that the constraint generated by the residual stress decreases the initiation toughness of brittle fracture. The fundamental understanding of the effect of residual stress on cleavage fracture toughness will be carried out in this work.

1.2.4 Ductile fracture

Ductile fracture is a common failure mechanism, which is characterized by slow crack propagation and large amount of plastic deformation. The ductile fracture usually shows dimpled fracture surface, or cup-cone fracture surface that is commonly observed in uniaxial tensile test [6]. Figure 1.5 shows the dimples observed in the fracture surface of A6028 aluminum alloy.

For polycrystalline metals, it has been observed that ductile fracture is controlled by nucleation, growth and coalescence of microvoids [49]. The common observed stages in ductile fracture are as follows [6]:
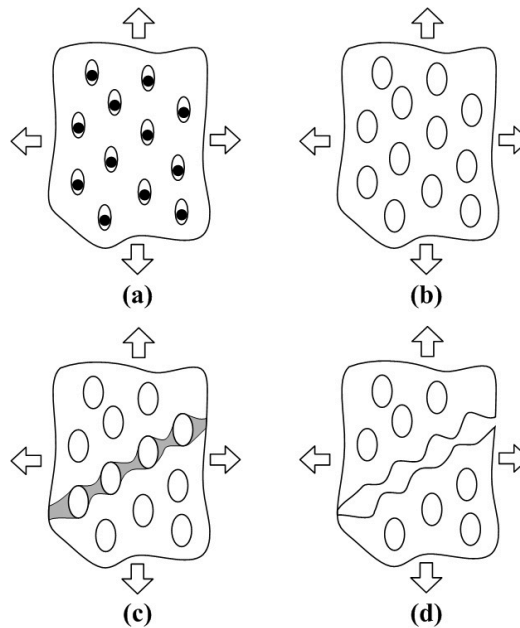
Figure 1.6: Illustration of ductile fracture mechanisms: (a) void nucleation, (b) void growth, (c) beginning of void coalescence and (d) end of void coalescence.

- Void nucleation from large inclusions and second phase particles by particle fracture or interracial decohesion [50].

- Growth of the void around the particles, by means of plastic strain and hydrostatic stress.

- Coalescence of the growing void with adjacent voids.

The mechanism of ductile fracture is illustrated in Figure 1.6. It should be noted that process before void coalescence, the plastic deformation of a void containing material is dilatational and macroscopically homogeneous. i.e. process (a) and (b). Once the coalescence process begins, the homogeneous deformation terminates and shifts to a localized plastic deformation [49].

It has been found that residual stress can influence the ductile fracture behaviour. Panontin and Hill [41] predicted the brittle and ductile initiation by micromechanical models and showed that the effect of residual

stress on the ductile fracture initiation toughness is negligible. Sherry et al. [51] demonstrated that a high strength low toughness aluminum alloy AL2024-T351 showed a marked reduction in initiation and tearing toughness for specimens containing a mechanically induced residual stress field. Experimental work undertaken by Sharples et al. [52] on wide plate specimens has also demonstrated that residual stress can significantly influence the ductile tearing behaviour of engineering materials. However, the experiments performed by Mirzaee-Sisan et al. [53] on the AISI Type 361H stainless steel indicates a negligible impact on ductile tearing toughness at load ratio L_r close to 1, i.e. close to the plastic collapse of the specimen. The observation is in contrast to their previous experiments performed on the A533B unstable cleavage fracture in ferritic steels at $-150°C$ [48]. A reduction of approximately 46% was observed in apparent fracture toughness for specimens containing a residual stress field compared with specimens in the as-received condition. Mahmoudi et al. [54] employed a local out-of-plane compression method to introduce residual stresses into C(T) specimens for aluminum alloys A12024, and the ductile tearing resistance of A12024 also decreased when tensile residual stresses are present. To date, the fundamental understanding of the effect of the residual stresses on ductile fracture resistance remains an open challenge. Thus, the effect of residual stress on ductile fracture behaviour will be investigated in this thesis.

1.3   Integrity assessment

1.3.1   Description

Structural integrity assessment is the techniques used to assess the fitness-for-purpose of critical components and welded structures, which is fundamental to the safe and economic operation of structural components. Such approaches can be used at the design stage to provide assurance for new structures, at the fabrication phase to ensure the integrity in the construction and at the operation phase to provide assurance throughout the life of the structure [55]. Used correctly, they can prevent over-design and unnecessary inspection and provide the tools to enable a balance between safety and economy to be achieved.

The procedure of structural integrity assessment consists following four

tasks [55]:

- Determination of the time profile of all the significant external loads and operating temperature, and performing a complete stress analysis including evaluation of the residual stresses in and around the weld seams in all critical locations.

- Mechanical fracture characterization of the base and weld materials, e.g. tensile properties, fracture toughness etc. The investigation of a possible variation of the fracture toughness in heat affected zone (HAZ) is also important.

- Obtaining a reliable map of significant existing flaws through a variety of non-destructive flaw detection techniques. The distribution, size, and the nature of flaws should be obtained.

- Carrying out the appropriate fracture and safety assessment.

Several codes and procedures have been defined for integrity assessment, e.g. BS 7910 [56], the low-temperature fracture assessment procedure R6 [57], the high-temperature procedure R5 [58] and structural integrity assessment procedure for European industry, SINTAP [59]. Existing defect assessment approaches present the results of an assessment in terms of either a failure assessment diagram (FAD) or a crack driving force (CFD) [60], as illustrated in Figure 1.7. In the FAD approach, the combination of loading and the materials resistance to the fracture is represented by a point on an FAD; failure is conceded when the point lies outside a bounding failure assessment curve. In the CFD method, the crack driving force, such as J-integral or CTOD is represented by a curve which describes the increase in CFD with increasing load; failure is conceded when the parameter reaches a limiting value derived from fracture toughness tests [60].

1.3.2 FAD method

The FAD method is probably the most widely used methodology for structural integrity assessment, which is easy to implement and also very versatile [6]. The concept of a two-criterion FAD to describe the interaction between brittle fracture and fully ductile rupture was introduce by Dowling and Townley [61] and Harrison et al. [62]. The first FAD was derived
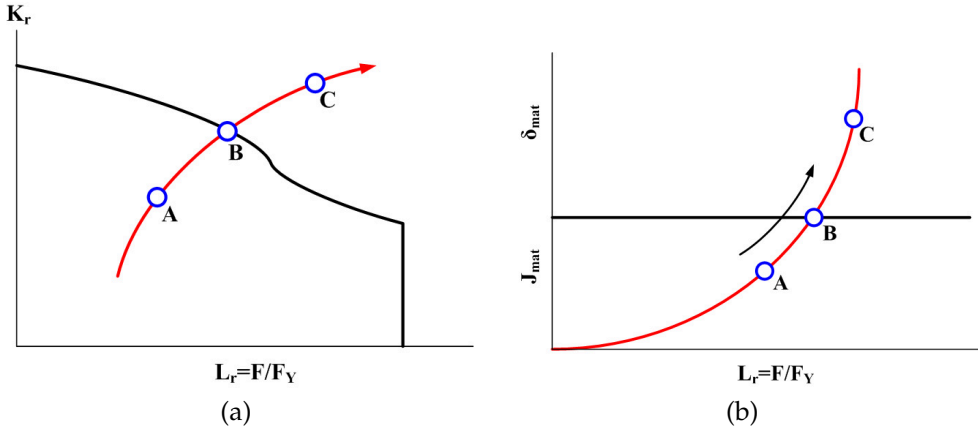
Figure 1.7: Illustration of integrity assessment approaches, (a)Failure Assessment Diagram (FAD), and (b) Crack Driving Force (CDF) curve. A: safe, B: critical and C: unsafe [55].

from a modified version of the strip-yield model. Considering primary loading on its own, the basis of the FAD is the use of two dimensionless parameters [63], the load ratio L_r and the toughness ratio K_r. K_r was defined as follows:

$$K_r = \frac{K_I}{K_{mat}} \tag{1.16}$$

where K_I is applied tensile (Mode I) stress intensity factor, K_{mat} is the material toughness measured by the stress intensity factor. It should be noted that toughness can be measured in terms of the J-integral or CTOD and converted to the equivalent K_{mat}. The load ratio L_r is defined as follows:

$$L_r = \frac{\sigma_{ref}}{\sigma_Y} \tag{1.17}$$

where σ_Y is the yield stress, and σ_{ref} is the reference stress and defined as:

$$\sigma_{ref} = (P/P_0)\sigma_0 \tag{1.18}$$

where P is the remote load and P_0 is the reference load.

BS 7910:1999 [56] procedure includes three assessment levels, which are in order of increasing complexity and decreasing conservatism [64],

- Level 1: a preliminary screening procedure.

- Level 2: the usual assessment method for structural applications and that generally used for offshore structures. The level 2 method yields realistic predictions for situations, where ductile tearing is limited.

- Level 3: this procedure is appropriate to ductile materials which exhibit stable tearing.

A particular conservatism in integrity assessment procedure may arise from the application of high constraint toughness values to assess low constraint structure components [55]. Thus, constraint-based failure assessment diagrams [65, 66] have been developed and included in R6 procedure [67] and SINTAP procedure [68]. To assess constraint effect, both the structural constraint and the dependence of material toughness on constraint should be considered. The latter dependence can be assessed by comparing a constraint dependent toughness K_{mat}^c with K_{mat} measured under high constraint conditions. For negative constraint, the relation between K_{mat}^c and K_{mat} can be approximated expressed as [65]

$$K_{mat}^c = K_{mat}[1 + \alpha(-\beta L_r)^p] \tag{1.19}$$

where α, p are constants and β represents the structural constraint, being defined (under primary load only) either in terms of the elastic *T-stress* ($\beta_T L_r = T/\sigma_y$) or the elastic-plastic *Q-stress* ($\beta_Q L_r = Q$) [55]. For positive constraint, $K_{mat}^c \approx K_{mat}$. Eq. 1.19 can be written in a equivalent form as [65], and a modified FAD including the effect of constraint can be obtained as:

$$K_r = f(L_r)[1 + \alpha(-\beta L_r)^p] \tag{1.20}$$

1.3.3 Treatment of residual stresses

Residual stresses can have a detrimental effect on structural integrity and are an important consideration in the defect assessment of welded structures [64]. Under linear elastic conditions, residual stresses can be treated by the superposition principle, as shown in Eq. 1.2. However, local or global plastic deformation may relax or redistribute residual stresses. Figure 1.8 schematically shows how residual stress contribute to the crack driving force, and the modification of FAD.
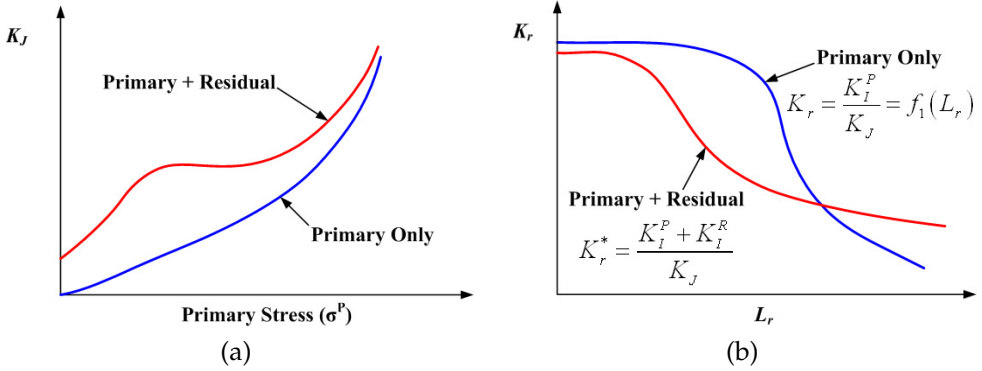
Figure 1.8: Schematic plot of the contribution of residual stress on (a) driving force, and (b) failure assessment diagram [6].

Residual stresses are usually treated as the secondary stresses and included in current integrity assessment procedures. BS 7910 and R6 procedure includes the residual stress through the modification of K_r as [14]

$$K_r = (K_I^P + K_I^S)/K_{mat} + \rho \tag{1.21}$$

where K_I^P and K_I^S are the stress intensity factors for the primary and secondary stresses, respectively, and ρ is a factor covering interactions. In Ref. [57], ρ is defined as

$$\rho = \psi - \phi(K_I^S/K_p^S - 1) \tag{1.22}$$

where K_p^S is the effective elastic-plastic stress intensity factor for the secondary loading and is related to the J-integral associated with the secondary stress, i.e. $K_p^S = \sqrt{E'J^S}$. ψ and ϕ are functions of L_r and the ratio $[K_p^S/(K_I^P/L_r)]$.

R6 and SINTAP also give an alternative but equivalent definition of K_r as

$$K_r = (K_I^P + VK_I^S)/K_{mat} \tag{1.23}$$

where the factor V now covers interaction [14], and is defined as [64]

$$V = K_p^S/K_I^S(1 + \psi/\phi) \tag{1.24}$$

When residual stresses are accounted for in integrity assessment procedures, the detailed information on the residual stress distribution in

the component is very important and should be known [69]. However, such information is often not directly available, and upper-bound residual stress profiles are generally recommended for use. Thus, it is fatal to predict or measure realistic residual stress distribution, and well-characterized residual stress profiles can be obtained [70]. An accurate measurement of the crack driving force that includes the residual stress can be another approach to incorporate the effect of residual stress into the structural integrity assessment. To this end, the modified *J*-integral proposed by Lei [12] can be a good candidate.

1.4 Objectives

The objective of this thesis is to investigate and quantify the effect of the residual stress on fracture behaviour, and further incorporate the effect into the structural integrity assessment procedure. The main objectives of this thesis are as follows:

- Employ an efficient method to introduce residual stresses into the finite element model. Tensile residual stress is generally detrimental for structures, thus, introducing a proper tensile stress field near the crack tip is the starting point of the study.

- Crack tip constraint is a very important factor to take into account when performing the structural integrity assessment. However, the effect of residual stresses on the crack-tip constraint has not been systematically studied. Thus, the residual stress-induced crack-tip constraint will be investigated in this thesis, and a new constraint parameter R will be defined and further investigated.

- Understand the effect of residual stresses on cleavage fracture and ductile crack growth resistance. It is also aimed to link the effect of residual stresses on failure mechanisms to parameter R.

- With the above framework, the effect of residual stresses will be incorporated into available integrity assessment procedure by a quantitative manner, and an improved failure assessment diagram will be proposed.

1.5   Organization of this thesis

This thesis consists of eight chapters. The first chapter introduces the background of the thesis, the ground theory of this study and the objectives. Chapter 2 gives a brief review of the residual stress and its effect on fracture. The methodology employed in this thesis is described in Chapter 3. Study of the effect of residual stress on the crack-tip constraint is presented in Chapter 4. Chapter 5 summarizes the investigation of the effect of residual stress on cleavage fracture, and the effect of residual stress on ductile crack growth resistance is reported in Chapter 6. The thesis is concluded in Chapter 7, and the future work is also suggested in Chapter 8.

Chapter 2

Residual stress

2.1 Origin of residual stress

Residual stresses are those stresses which retained within a body when no external forces are acting [2], which are stationary and at equilibrium with their surroundings [71].

Residual stresses can be very detrimental to the performance of a material or the life of a component. Alternatively, beneficial residual stresses can be introduced deliberately. Residual stresses are developed during most manufacturing processes involving material deformation, heat treatment, machining or processing operations that transform the shape or change of the properties of a material, and can be regarded as a consequences of interaction among time, temperature, deformation, and microstructure, as illustrated in Figure 2.1. There are several material or material related factors that can influence the development of residual stresses, e.g. thermal conductivity, heat capacity, thermal expansion coefficient, plasticity, mechanisms of transformations, and transformation plasticity etc. [72].

The source of residual stresses can be regarded as the misfits between different regions of the materials, component or assembly, as shown in Figure 2.2. The misfit strain field could be produced by plastic deformation, thermal strain, phase-transformation or other means [73], which are referred as "eigenstrain" by Mura [74]. Residual stresses are often described by the distribution of eigenstrain ε_{kl}^* through the following form [2]:
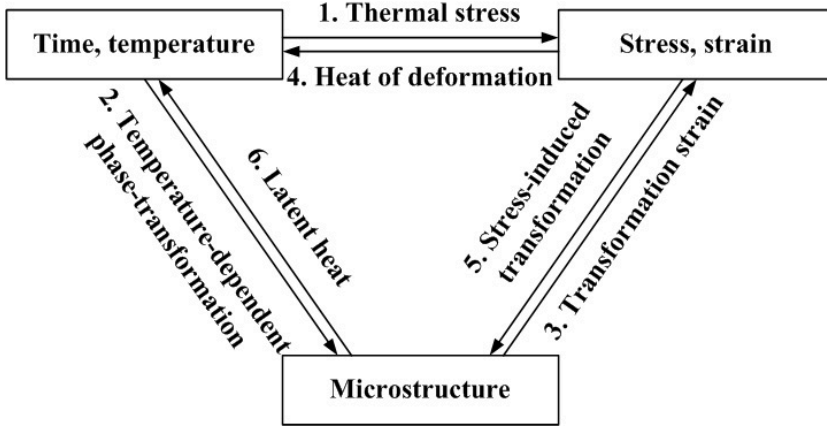
Figure 2.1: The coupling of temperature, stress and microstructure [72].

$$\sigma_{ij}(x) = -C_{ijkl}\left\{\int_{-\infty}^{\infty} C_{pqmn}\varepsilon^*_{mn}(x')G_{kp,ql}(x-x')dx' + \varepsilon^*_{kl}(x)\right\} \qquad (2.1)$$

where C_{ijkl} are elastic stiffness coefficients; the Green's function $G_{kp}(x - x')$ represents the displacement component in the k direction at x when a body force is applied at x' in the p direction in an infinitely extended material. For any field location x the integration in terms of x' needs to be carried out only over the misfitting region (i.e. where the eigenstrain is non-zero) [2]. Using Equation 2.1 it is relatively straightforward to calculate the residual stress field that arises from a given eigenstrain. However, in practice, it is only possible to measure the elastic strain at a finite number of points and thus difficult to determine the complete distribution of eigenstrain field and further calculate the residual stress field.

2.2   Classification

Residual stresses may be categorized by the cause (e.g. thermal or elastic mismatch), by the scale over which they self-equilibrate, or according to the method by which they are measured [71]. From a length scale perspective, the residual stress on continuum level that neglect the underlying microstructure are defined as type I stresses which equilibrate over a
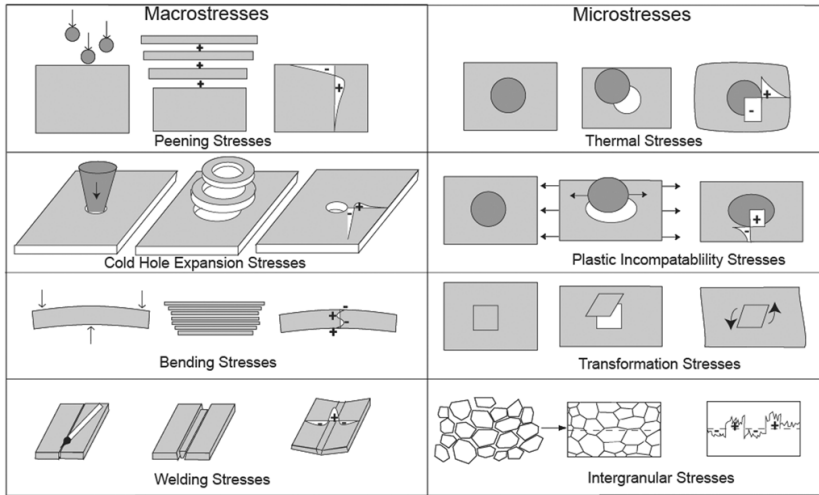
Figure 2.2: Residual stress arises from misfit either between different regions or different phases within the material. Examples of different types of macro- and micro-residual stress are illustrated schematically. In each case the process is indicated on the left, the misfit in the center and the resulting stress pattern on the right-hand side [2].

length scale comparable to the extend of the component or structure. Type II residual stresses are microstructurally related and equilibrate on a scale of a few grain diameters. Type III microstresses are arising from heterogeneous behaviour at the atomic scale, these might arise from line defects (dislocations), point defects such as might arise from radiation damage or doping with atoms of a different size [2].

In practice, it is conceptually satisfying to consider the whole three dimensional stress field within a component. However, it is usually costly and impractical to depict the whole stress field. Thus, in structural integrity assessment, residual stresses are often decomposed across a region of concern into the membrane stress σ_m, through-section bending stress σ_b and locally self-equilibrated σ_{se}. It is useful to decompose residual stresses into different components, and a length-scale concept can be applied [75]. By using the length-scale concept, a consistent characterization of stresses from various sources can be obtained based on their length scales. Also, the contributions of different stress components to fracture driving force can be quantified in terms of their characteristic length scales. Figure 2.3
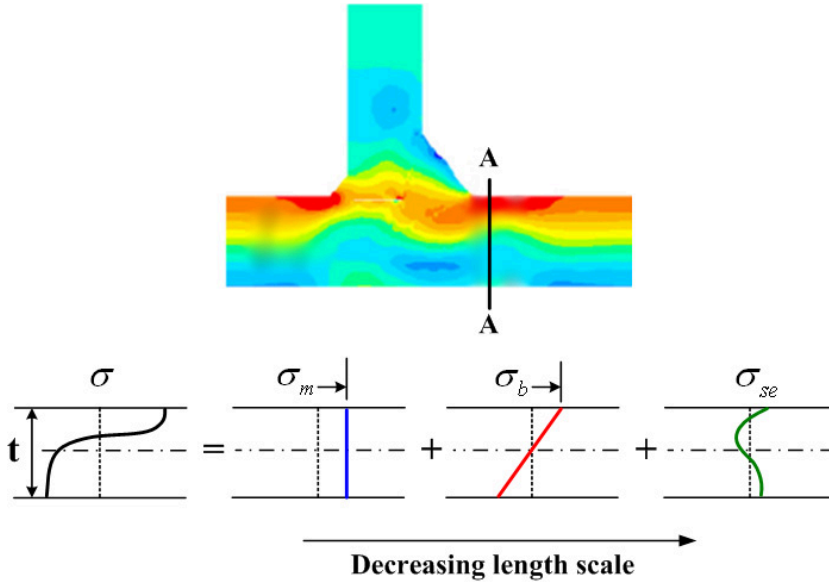
Figure 2.3: Illustration of residual stress decomposition in terms of through-thickness membrane, bending and self-equilibrating components for a T fillet weld [75].

shows a example of the decomposition of residual stress into different components with respect to the thickness of a T fillet weld [75].

2.3   Measurement techniques

Just as residual stress can present over a range of scales, from atomic scale to structural scale, failure can also occur at the material level or at macro structure level. Residual stresses tend to affect the micromechanisms of failure at smaller scale and have influence on structural integrity at the continuum level. Thus, it is very important to obtain realistic distribution of residual stresses. There are basically two types of methods to obtain the residual stress field, the numerical simulation and experimental measurement. For experimental measurement, destructive methods (e.g. sectioning, hole drilling, contour method) and non-destructive tests (NDT), such as ultrasonic, X-ray diffraction method, neutron diffraction method, are often employed. A review of residual stress measurement methods can

be found in Ref. [76]. In the following, the common used residual stress measurement techniques will be briefly introduced.

Destructive methods of residual stress measurement rely on the fact that when a cut is introduced the object deforms as the necessary components of traction due to the residual stress field reduce to zero at the newly formed surface [2]. Common to all these methods is the reconstruction of the original stress field or eigenstrain distribution, from the observed distortion. Central to this is the assumption that the redistribution that takes place as a consequence of cutting does so entirely elastically, introducing no further misfit. The most common used destructive methods are as following:

- Hole drilling method
  Hole drilling method [77] is one of the most widely used techniques for measuring residual stress near the surface of component [78]. It is simple, quick and versatile. Equipment can be laboratory-based or portable, and the technique can be applied to a wide range of materials and components. The hole-drilling method involves drilling a shallow hole around which the local surface deformations are measured by a specially designed strain-gauge rosette, as illustrated in Figure 2.4. Provided the stress is essentially constant over the drill depth the residual stress that originally existed at the hole location can then be calculated form the measured strain relaxations ε_1, ε_2 and ε_3 around it using

$$\sigma_{max}, \sigma_{min} = -\frac{E}{2}\left(\frac{\varepsilon_3 + \varepsilon_1}{(1+\nu)\bar{a}} \mp \frac{\sqrt{(\varepsilon_3 - \varepsilon_1)^2 + (\varepsilon_3 + \varepsilon_1 - 2\varepsilon_2)^2}}{\bar{b}}\right)$$

(2.2)

  where $\bar{a}$ and $\bar{b}$ are dimensionless calibration constants depending on the diameter and depth of the hole [79].

- Contour method
  The contour method for measuring residual stresses is based on the elastic superposition principle [80]. The technique involves cutting the part in two completely, and the part will deform due to the release of the stresses. By measuring the profile, or contour, of the newly created surface, the original out-of-plane residual stress can then be uniquely calculated using a finite element model in which
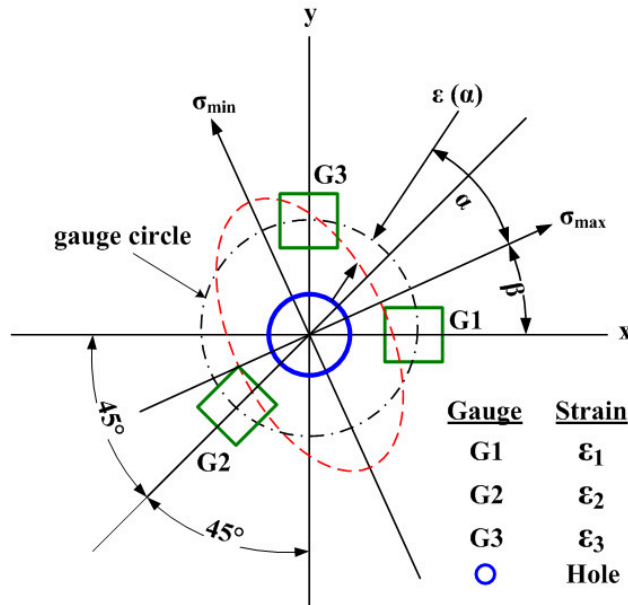
Figure 2.4: Illustration of hole drilling method.

the distorted surface is forced back into a planar state. Figure 2.5 illustrates the principle of the contour method.

- Slotting method
  The slotting method, also called the crack compliance method, generally provides a measure of the stress perpendicular to the slot and is applicable when there is little stress variation parallel to the line of the slot [81]. A slot is cut incrementally and the change in gauges located on both the top and bottom surfaces recorded [2].

Non-destructive method of determine residual stresses rely on diffraction within crystalline materials and engineering components. The crystalline lattice is used like an atomic strain gauge, and the lattice strain can be related directly to stress using appropriate elastic constants. Three main types of radiation are available with wavelength suitable for measuring atomic lattice spacing, namely, electron, X-ray photon and neutron beams. The three beams can travel very different distances into crystalline materials before attenuation becomes significant and so their uses are quite different [2]. The following non-destructive methods are often used:
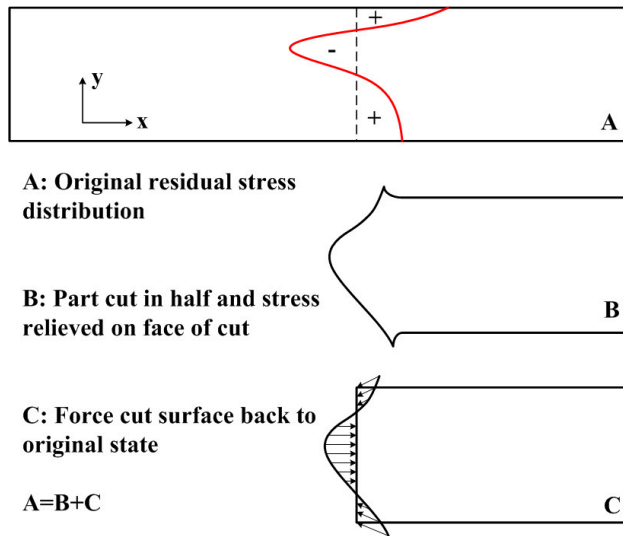
Figure 2.5: Superposition principle to calculate residual stress from surface contour measured after cutting a part in two [80].

- X-ray diffraction method
  The principle of this method is that the crystal lattice spacing of metals is proportional to elastic strain [78]. The $\sin^2 \psi$ X-ray method of stress determination has been used for over 80 years [82]. In essence, measurements are made over a range of inclination angles (ψ, illustrated in Figure 2.6) using a high scattering angle (2θ) [2]. By direct measurement of interlattice strain in terms of plane spacing, as induced by residual stress, the residual stresses can be calculated by the following equation [2]:

$$\frac{d_\psi - d_0}{d_0} = \frac{1+\nu}{E} \sigma_\phi \sin^2 \psi - \frac{\nu}{E}(\sigma_{11} + \sigma_{22}) \tag{2.3}$$

  where σ_{11} and σ_{22} are the principal in-plane stresses and σ_ϕ is the in-plane stress corresponding to $\psi = 90°$. d_ψ is the spacing of the lattice planes parallel to the welding direction at an angle ψ with the specimen surface, d_0 is the stress-free spacing of the lattice planes. The relationship predicts a linear variation in d_ψ and $\sin^2 \psi$ form which the slope can be used to determine the in-plane stress.

- Synchrotron X-ray diffraction method
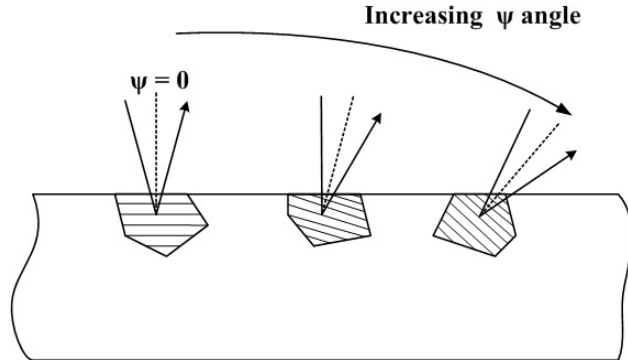
Figure 2.6: Schematic illustrating the $\sin^2\psi$ technique whereby the in-plane stress can be deduced from the variation in atomic lattice spacing as the ψ angle is increased [2].

Synchrotron, or hard X-rays, provide very intense beams of high energy X-rays [2]. There X-rays have a much higher depth penetration than the conventional X-rays, typically around 50 mm in aluminum [76]. Thus, this method is capable of providing high spatial resolution, 3D maps of the strain distribution to millimeter depths in engineering components. Another great advantage that synchrotron has is that intense narrow beams of 1mm to 10 μm in size are possible, which leads to spatial resolutions that are limited not by the instrument but by the crystallite size within the sample.

- Neutron diffraction
  Neutrons have the advantage over X-rays that for wavelengths comparable to the atomic spacing, their penetration into engineering materials is typically many centimeters [71]. With high spatial resolution, neutron diffraction can provide complete three-dimensional strain maps of engineering components [76].There are essentially two neutron diffraction techniques, namely, conventional $\theta/2\theta$ scanning and time of flight approach [71]. Compared to other diffraction techniques, the cost of neutron diffraction method is much higher and the availability is very much lower.

- Ultrasonic method
  Ultrasonic methods utilize the sensitivities of the velocity of ultrasound waves traveling through a solid to the stress level within the

solid body [76]. Changes in the speed of ultrasonic waves in a material are directly affected by the magnitude and direction of stresses present. Because the velocity changes are small and are sensitive to the material's texture, it is often more practical to measure transit times as the ultrasonic path length is usually not known to sufficiently high precision. This method has the advantage of being able to measure in the bulk of the material and are therefore well suited to routine inspection operations [71].

There are many other methods to measure the residual stresses in engineering materials. It is important to consider the characteristic length-scale of the residual stress, which can be helpful for selecting a proper measurement technique. The ability to measure and monitor the development of residual stresses during the whole material processing procedure can be helpful to manage residual stresses for different processing stages.

2.4 Numerical prediction

2.4.1 Description

The thermal and thermal-mechanical process associated with welding residual stress evolution during welding can be extremely complex [3], as illustrated in Figure 2.7. The distribution of welding residual stress depends on several main factors such as structural dimensions, material properties, restraint conditions, heat input, number of weld pass and welding sequences [83]. Due to the complexity of physical processes involved in welding, it is impossible for any experimental technique to obtain a complete mapping of the residual stress and distortion distribution in a general welded structures [84]. With advances in computer hardwares and finite element method (FEM) software, numerical simulations now play an important role in predicting residual stresses. A series of review papers on numerical modeling of welding can be found in Ref. [85–88].

There are several challenges in numerical prediction of residual stresses. Among all challenges, it is critical to formulate an accurate constitutive model that can properly describe the time-dependent properties of the materials. A unified welding constitutive model may include many internal state variables, as illustrated in Figure 2.8. The constitutive model can then
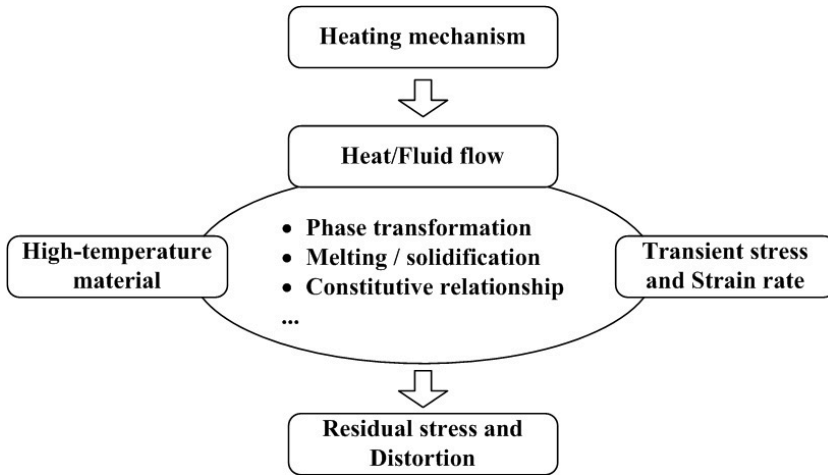
Figure 2.7: Residual stress and distortion evolution in welded joints [3].

be implemented into finite element platforms and perform the simulations of welding residual stresses. It is also very important to obtain the reliable material properties, including temperature-dependent properties, the properties of different phases and the phase-transformation temperature etc. Another important issue for the numerical simulation is the proper heat source model. In practice, for different welding methods, different heat source model should be utilized, e.g. the keyhole cylinder volumetric heat source together with a surface Gaussian heat source model is used for laser welding, and the volume Gaussian double ellipsoid heat source model can be used for arc welding.

For predicting residual stresses different types of special purpose or adapted general purpose computer codes have been applied. SYSWELD from ESI group* is the leading tool for the simulation of welding and welding assembly processes. In the RESIA project, a new platform, namely WeldsimS, for predicting the welding residual stresses and microstructures of high strength steels has been developed based on IFE's in-house FEM software package, IfeFEM.
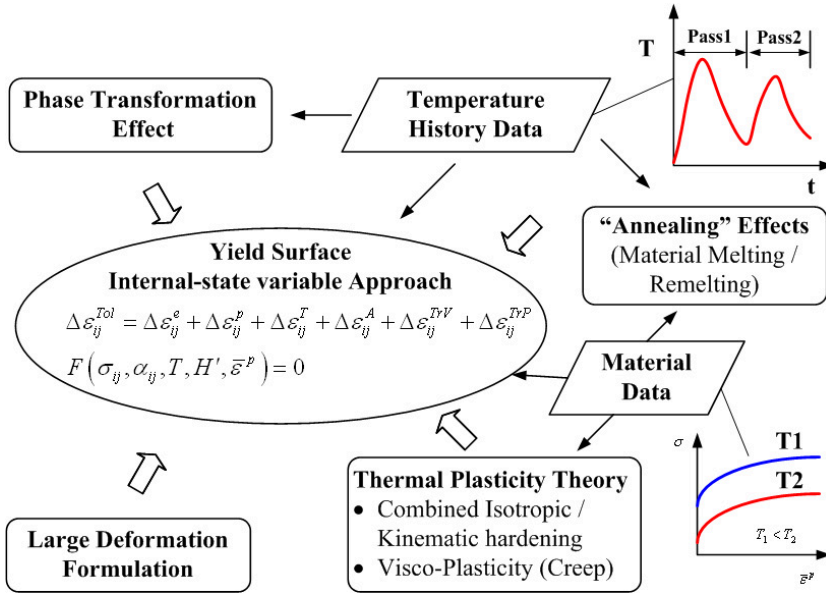
Figure 2.8: Basic elements of unified weld constitutive model [3].

2.4.2 WeldsimS

WeldsimS [89] is part of the computer programs WLEDSIM/ALSIMS developed by IFE. The main function of WeldsimS is the prediction of welding residual stresses and hydrogen diffusion as well. The codes account for a series of complex phenomena such as the moving heat source, melting and solidification, solid-state phase transformations, work hardening, strain rate sensitivity and the flow stress dependency on the specific mixture of phases appearing at the different temperatures. Specific WeldsimS features are:

- Different properties in base and weld metal can be handled.

- Build-up of fillet regions in multi-pass welding, which is simulated by pre-defined weld metal elements being successively activated for each pass.

- Adaptive mesh refinement for numerical accuracy and high spatial resolution of the stress field.

- Export of the stress field to failure assessment analyses in 3D domains or 2D cross sections

It should be noted that WeldsimS only contains the main solver, and the pre-process and post-process should be accomplished in other commercial software. Also, WeldsimS cannot perform fracture mechanics analysis now. Simulated results should be exported into ABAQUS to perform further analysis.

2.5 Effect of residual stress on failure

Residual stresses plays an important role in material failure. This study focuses on the effect of residual stresses on cleavage and ductile fracture behaviour. However, residual stresses can also have effect on other failure mechanisms. A review on this topic has been reported by Withers [2]. In the following context, the effect of residual stresses on fatigue, creep and hydrogen embrittlement will be briefly introduced.

The fatigue behaviour of structural components is a strong function of the load history. The amplitude of the applied load cycles is a primary variable influencing the fatigue lifetime, and the mean (or maximum) value of the load in each cycle is a secondary variable that can also have a major influence on fatigue [90]. Fatigue crack growth includes nucleation and propagation of crack. Fatigue nucleation life is a function of the alternating stress amplitude but not the mean stress, while the growth rates of fatigue cracks are a function of both the stress amplitude and mean stress. Thus, it implies that residual stresses have relatively little influence on fatigue crack nucleation, but potentially a significant influence on fatigue crack growth. There are two types of fatigue, i.e. low cycle fatigue (LCF) and high cycle fatigue (HCF) [91]. Residual stress often has little effect on LCF life. However, HCF is very sensitive to residual stresses [2]. To the extent that the S-N curve is driven by crack nucleation behaviour, the effects of residual stresses may be small, but to the extent that the S-N curve is driven by crack growth, including the growth of microcracks, the effects of residual stresses may be large.

Time-dependent plasticity, or "creep", is an important failure mechanism at elevated temperatures. The failure mode of creep is often characterized by the growth of cavities on grain boundaries [92]. If the accu-

mulated creep strains exhaust the creep ductility of the material, cracks will initiate. Creep strain and ultimate cracking can be driven by residual stresses, for example, as a means of thermal relaxation of weld residual stress in areas with poor material creep ductility at the operating temperature and creep deformation rate [2]. Also, a highly triaxility stress state can reduce the creep ductility relative to the uniaxial response substantially.

Hydrogen embrittlement is a general phenomenon which lowers the fracture resistance of high-strength steels, and therefore raises the failure risk of the components [93]. In the case of hydrogen induced fracture, the role of the residual stresses is potentially twofold [94]. First, the mechanical effect of residual stresses is additive to the stresses caused by applied load. In addition, the heterogeneous fields of residual stresses affect the rate of hydrogen transportation toward potential rupture sites in the components by the stress-assisted diffusion governed by the gradient of the hydrostatic component of stresses.

Chapter 3

Methodology

3.1   Problem description

This study concerns an ideal problem. A large cylinder with a weld in the center was studied. The reason for selecting such model is that it can be easily modeled by a 2D plane strain MBL model. With the MBL model, a reference case can be well established, and the constraint conditions can be easily handled by changing the remote boundary governed by the elastic *K-field* and *T-stress*. A sharp crack was embedded in the weld region. The analysis procedure, as illustrated in Figure 3.1, consists of the following steps: 1) enforce a welding procedure, which introduces a residual stress field; 2)introduce a sharp crack; 3) apply the external load. The possible contact between the upper and lower free surfaces of the crack has also been considered when the residual stress was introduced.

3.2   Modified boundary layer model

One of the basic assumptions behind the application of linear elastic fracture mechanics to elastic-plastic materials is that plastic deformation at the crack tip is governed by the intensity of the elastic stress singularity, K_I. In this case, the plastic zone size is small compared to other geometric dimensions of the problem. The crack problem can be solved by using a boundary layer approach, which assumes that the boundary value stresses of the elastic-plastic crack problem are given by the extension of the validity of the singularity term (Eq. 3.1) in the elastic stress solution to large
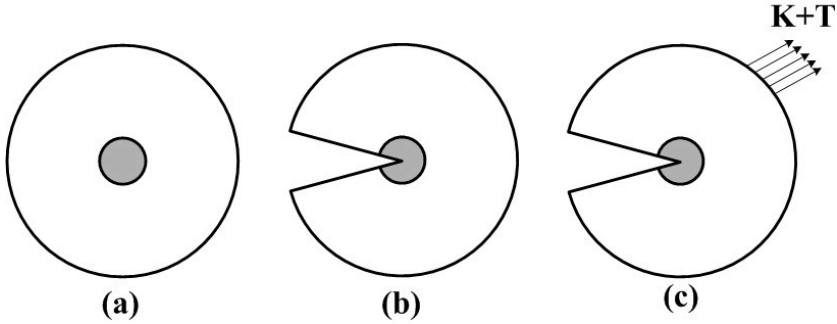
Figure 3.1: Illustration of the problem, (a) welding at the center of the round cylinder, (b) introduce a sharp crack, and (c) apply the external load.

values of r and small-scale-yielding [25]

$$\sigma_{ij} = \frac{K_I}{(2\pi r)^{1/2}} f_{ij}(\theta) \tag{3.1}$$

where r and θ are polar co-ordinates referred to the crack tip, and the function f_{ij} are given by the elastic solution.

Analytically, the stress state at the crack tip in the elastic case is given by a singular stress component and non-singular terms. As shown in Chapter 1, Williams [24] proposed an analytical expansion to represent the stress state at the crack tip, and the first two terms has the form of Eq. 1.8. It should be noted that the second term is independent of r. Larsson and Carlsson [25] demonstrated that the second term in the series was important to modify the boundary solution to fit the real crack problem, and the *T-stress* has a significant effect on the plastic zone size and shape. In this way, a modified boundary layer solution is obtained which is expected to agree with the solution for the actual geometry.

In this study, the modified boundary layer analysis was performed to study the effect of residual stresses on fracture behaviour, and the boundary conditions on the remote edges of the model is applied through a displacement field (u, v) controlled by the elastic asymptotic stress field of a plane strain mode I crack

$$u(r,\theta) = K_I \frac{1+\nu}{E} \sqrt{\frac{r}{2\pi}} \cos(\frac{1}{2}\theta)(3 - 4\nu - \cos\theta) + T\frac{1-\nu^2}{E}r\cos\theta$$

$$v(r,\theta) = K_I \frac{1+\nu}{E} \sqrt{\frac{r}{2\pi}} \sin(\frac{1}{2}\theta)(3 - 4\nu - \cos\theta) - T\frac{\nu(1+\nu)}{E}r\sin\theta$$

(3.2)

where $K_I = \sqrt{EJ/(1-\nu^2)}$ under plane strain condition; E is Young's modulus, ν is Poisson's ratio; r and θ are polar coordinates centered at the crack tip with $\theta = 0$ corresponding to the crack tip.

3.3 Complete Gurson model

The complete Gurson model has been employed to study the effect of residual stress on ductile crack growth resistance in this thesis. It seems that conventional plasticity theories lose their applicability when ductile fracture is involved [95]. Also, the ductility or fracture toughness of a material varies with the change of geometry constraint level and cannot be directly transfered from one geometry to another [49]. Thus, both the evolution of matrix stress and the material deterioration due to the damage should be considered when the full stress-strain relationship of the material is to be described.

3.3.1 Gurson model

The accuracy of the ductile fracture simulation depends on the modeling of physical behaviour of solids. Using the micro-mechanical model-based constitutive equations to predict the ductile fracture process has attracted much efforts in last decades. One of the best well-known micro-mechanical models is Gurson [96] model, which is based on the work by Rice and Tracy [97] and McClintok [98]. The Gurson model has later been modified by Tvergaard and Needleman [99–101], thus, it is most often referred to as the Gurson-Tvergaard-Needleman (GTN) model. The GTN model is in fact a void growth model. The effect of void coalescence can be considered with the introduction of a so-called critical void volume fraction, which is not a physical mechanism-based coalescence criterion. In GTN model, the softening effect due to the presence of voids was reflected

in a yielding function. By idealizing the true void distribution into a unit cell containing on spherical void and carrying out the rigid-plastic upper bound analysis, the following yield function was obtained:

$$\phi(q, \bar{\sigma}, f, \sigma_m) = \frac{q^2}{\sigma_f^2} + 2q_1 f cosh \left(\frac{3q_2\sigma_m}{2\bar{\sigma}} \right) - 1 - (q_1 f)^2 = 0 \qquad (3.3)$$

where f is the void volume fraction, σ_m is the mean macroscopic stress, q is the von Mises stress, σ_f is the flow stress, and q_1 and q_2 are parameters introduced by Tvergaard [99, 100]. Unlike many soil material models where yielding is also dependent on hydrostatic stress but yield surface is fixed in stress space, the yield surface of the Gurson model decreases with the increase of damage until the complete loss of load-carrying capacity [49]. Due to the incompressible nature of the matrix material the growth of existing voids can be expressed as:

$$df_{growth} = (1 - f)d\varepsilon^p : \mathbf{I} \qquad (3.4)$$

where ε^p is the plastic strain tensor and $\mathbf{I}$ is the second-order unit tensor. In the original Gurson model ($q_1 = q_2 = 1$), material softening with the increase of void volume fraction is a continuous process, and complete loss of load carrying capacity would occur only when the void has grown to the ultimate value $f = 100\%$, which is an unrealistic situation [49]. Even with the modification made by Tvergaard, the void volume fraction at which the Gurson model will lose load carrying capacity is still unrealistically large as $f = 1/q_1$. However, the void volume fraction is much smaller than $f = 1/q_1$ and usually less than 15% according to both experimental observations [102] and numerical analysis [103]. It thus indicates that the Gurson model can not naturally predict void coalescence and an extra void coalescence criterion should be used [49]. Then, so-called critical void volume fraction criterion for void coalescence has been proposed, which assumes that void coalescence appears when a critical void volume fraction f_c is reached. A review on the development of this criterion has been made by Zhang [104]. Once the void coalescence has been determined to occur according to a criterion, the post-coalescence deformation behaviour of the Gurson model is numerically simulated by an artificial acceleration

of void growth, as suggested by Tvergaard and Needleman [101]:

$$f^* = \begin{cases} f & \text{for} \quad f \leqslant f_c \\ f_c + \frac{f_u^* - f_c}{f_F - f_c}(f - f_c) & \text{for} \quad f > f_c \end{cases} \tag{3.5}$$

where $f_u^*=1/q_1$ and f_F is the void volume fraction at the end of void coalescence. Here, $f_F=0.15+2f_0$, where f_0 is the initial void volume fraction. When the coalescence starts and $f > f_c$, f^* replaces f in Eq.(3.3).

Before any growth, voids should be nucleated first. Void nucleation can be stress controlled or strain controlled [105]. The strain controlled nucleation can be written as:

$$df_{nucleation} = f_\varepsilon(\varepsilon^p)d\varepsilon^p \tag{3.6}$$

where f_ε is the void nucleation intensity, and ε^p is the equivalent plastic strain. Two types of void nucleation models may be used for engineering materials, the cluster nucleation model and continuous void nucleation model. The detailed description of such models can be found in Ref. [105].

3.3.2 Thomason's coalescence criterion

As described in Section 1.2.4, the fracture of ductile material displays two distinct phases, the homogeneous phase and localized phase. Thomason developed a so-called dual dilatational constitutive equation theory for ductile fracture [106–108], and argued that two fracture phases are in competition for a void-containing material, as shown in Figure 3.2.

Both deformation modes are dilatational, by which plastic deformation will result in change of material volume and the material will always follow the deformation mode which needs less energy. In the early stage of deformation, the voids are small and it is easier to follow the homogeneous deformation mode (the stress required for going to homogeneous deformation is less than the stress required for going to a localized deformation mode), and with the advance of plastic deformation and increase of void volume fraction, the stress required for localized deformation decreases [105]. When the stress for localized deformation is equal to the stress for homogeneous deformation, the void coalescence occurs. The plastic limit criterion by Thomason states that no coalescence will occur as long as the following conditions is satisfied [108, 109]:
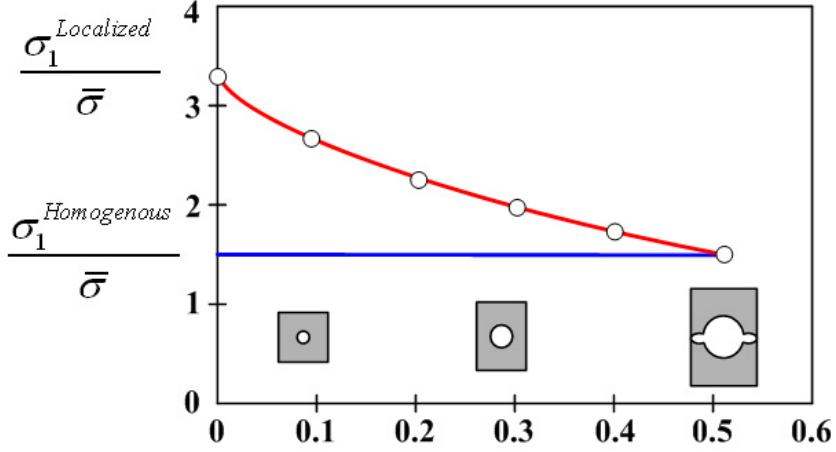
Figure 3.2: The competition of the two deformation modes in the Thomason theory [49]

$$\frac{\sigma_1}{\bar{\sigma}} < \left(\alpha \left(\frac{1}{r} - 1 \right)^2 + \frac{\beta}{\sqrt{r}} \right) (1 - \pi r^2) \qquad (3.7)$$

Coalescence will first happen when the left-hand side becomes equal to the right-hand side in Eq. 3.7, and the void volume fraction at coalescence will be taken as the f_c. In Eq. 3.7, σ_1 is the current maximum principal stress, r is the void space ratio, $r = \sqrt[3]{(3f/4\pi)e^{\varepsilon_1 + \varepsilon_2 + \varepsilon_3}} / (\sqrt{e^{\varepsilon_2 + \varepsilon_3}}/2)$ and ε_1 is the maximum principal strain, ε_2 and ε_3 are the two other principal strains, $\alpha=0.1$ and $\beta=1.2$ are constants fitted by Thomason [108]. For plane strain problem, Eq. 3.7 can still be used, but with $\varepsilon_3=0$. This work has been later improved by Pardoen and Hutchinson [110] and Zhang et al. [105] to take the effect of hardening into account and the following relation has been found:

$$\alpha(n) = 0.12 + 1.68n \qquad (3.8)$$

where n is the hardening exponent, improves the prediction of coalescence.

3.3.3 Complete Gurson model

By combining the GTN model for void growth and Thomason's plastic limit load model for coalescence a so-called "complete Gurson model" has been proposed by Zhang et al. [105], with which the complete process of ductile fracture can be simulated. The complete Gurson model has been verified [49] for non-hardening material against the finite element results by Koplik and Needleman [103]. It was found that the complete Gurson model was very accurate, in particular, for small initial void volume fraction cases [105]. By using the complete Gurson model, ductile fracture is exclusively linked to the void nucleation parameters and the mesh size.

Because the yield surface of the Gurson model is changing with the increase of damage, the computer implementation of the Gurson model is complicated, especially for the finite element programs which use implicit algorithms [49]. Zhang and Niemi [111], Zhang [112, 113] performed the numerical treatment of the Gurson model and a family of the generalized-midpoint algorithms has been proposed. The complete Gurson model is then implemented into ABAQUS [114] using the algorithms developed by Zhang via the material user subroutine UMAT.

3.4 Cohesive zone model

Linear elastic fracture mechanics (LEFM) has been proven a useful tool for solving fracture problems provided a crack-like notch or flaw exists in the body and the nonlinear zone ahead of the crack tip is negligible. However, an important issue when considering failure is the observation that most engineering materials are not perfectly in the Griffith sense, but display some ductility after reaching the strength limit [115]. The nonlinear zone due to plasticity or microcracking for ductile metals or cementitious materials is not negligible in comparison with other dimensions of the cracked geometry [116], and small-scale-yielding, micro-cracking and void initiation, growth and coalescence may take place. A proper process zone model is then needed to characterize the fracture process and describe the local fracture behaviour. Among the various process models, the cohesive zone model seems particularly attractive for practical application since it is applicable to a wide range of materials and fracture mechanisms [117].
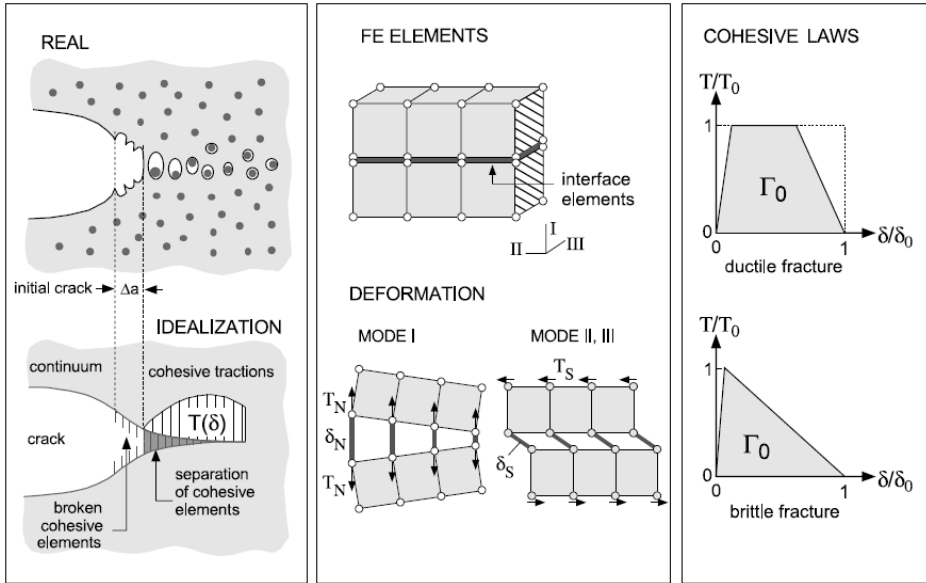
Figure 3.3: Schematic plot of the concept of cohesive zone model [117].

3.4.1   Concept

The cohesive zone model was introduced by Barenblatt [118] and Dug-
dale [119] for elastic-plastic fracture in ductile metals and for quasi-brittle
materials by Hillerborg et al. [120] under the name of fictitious crack model.
The fundamental concept of the cohesive zone model is a so-called *traction-
separation-law* (TSL), which is a function described by the cohesive stress
(σ) and separation (δ) [121]. The area under the traction-separation rela-
tion represents the cohesive energy Γ_0. The basic parameters necessary
to describe the traction-separation-law are two among the critical traction
σ_{max}, the critical separation δ_c and the cohesive energy Γ_0 [122]. The basic
concept of the cohesive zone model is shown in Figure 3.3.

3.4.2   Traction-separation-law

One of the key problems in the application of the cohesive zone model
is the choice of the TSL within the cohesive zone. Needleman first pro-
posed a polynomial law [123], and later an exponential law was intro-
duced by Xu and Needleman [124]. Tvergaard and Hutchinson [122] pro-
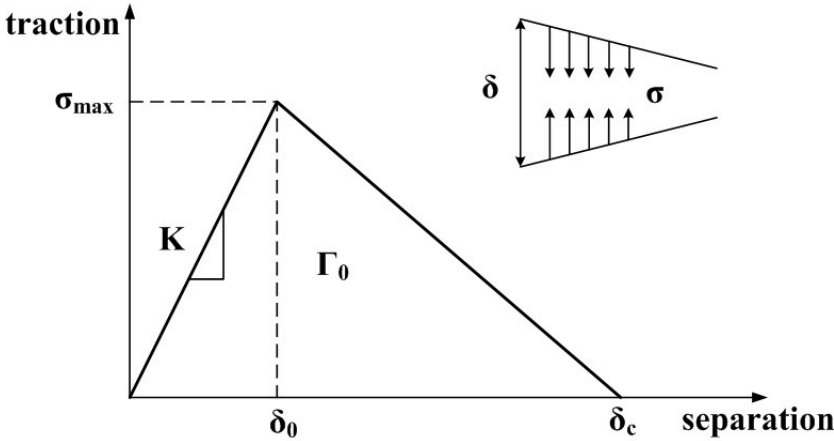
Figure 3.4: Schematic plot of the traction-separation-law used in the analysis.

posed a trapezoidal law for ductile fracture. The traction-separation-law used in this paper is a bilinear relationship between the traction and the separation, which is characteristic of brittle materials [117]. The traction-separation-law used in this thesis is a bilinear relationship between the traction and the separation, as shown in Figure 3.4, which is characteristic of brittle materials [117]. The dominant parameters are cohesive energy Γ_0 and the maximum cohesive stress σ_{max}.

When a cohesive zone model is employed to simulate the cracking behaviour of a brittle thin interface, the softening part of the TSL may cause some problems to the solution algorithm. A snap-back instability can occur depending on interface thickness, stiffness and the length of the elements adjacent to the cohesive zone [125]. If a discontinuity of the response occurs, the simulation can stop. A possible solution is the viscous regularization method proposed by Chaboche et al. [125], which introduces a fictitious viscosity parameter in the constitutive equation of the cohesive elements. In turn, the convergence of the solution can be achieved by dissipating excess energy; but the value of the viscosity parameter should be small enough to not affect the results. Pezzotta and Zhang [126] demonstrated that when the viscosity value $v \leq$ 1.0E-5 the predicted failure becomes independent of the viscosity parameter when other parameters are fixed. Thus, the value v=1.0E-5 was used for all the calculations in this study.

3.5   Eigenstrain method

The complete Gurson model and the cohesive zone model are constitutive models to describe the fracture mechanisms. In this thesis, the eigenstrain method was utilized to introduce the residual stresses into the MBL model. The eigenstrain method will be further investigated and described in this section. The background regarding the nature of residual stress and a formulation of eigenstrain approach to residual stress determination will be described. Then, the application of the eigenstrain method in this thesis will be discussed.

3.5.1   Description

Generally, the stress contained in a self-balanced body is called residual stress. In the body, the source of residual stress is an incompatible strain field. The incompatible strain field could be produced by plastic deformation, thermal strain, phase-transformation, or other means. Ueda et al. [127] refers to the sum total of all such possible causes of incompatible strain as the "inherent strain" presented in the body. In this study, we adopt Mura's [74] terminology in calling the incompatible strain as "eigenstrain".

When a body contains residual stress, cutting the body along an arbitrary plane will alter the stress. This fact is problematic for many stress measurement techniques, but is employed by the present method. If we have an ideal cutting process, the eigenstrain in each piece of the original body will not be altered by the process. Sectioning of the body changes the distribution of residual stress, but not that of eigenstrain. By measuring the stress change when the body is sectioned, the eigenstrain can be determined. Further, it need not be assumed that residual stress is entirely relieved by the cutting process in applying this method [78]. When certain assumptions about the spatial distribution of the source of residual stress can be made, estimates of residual stress can be generated for locations which are remote from strain measurement points. Thus, the eigenstrain method is basically a hybrid experimental/analytical method.

In the welding procedure, elastic-plastic phenomena of the material essentially occur, and eigenstrain always generates in the body. Therefore, the elastic response equations are generally derived as the relationships between the vectors of eigenstrain ε^*, elastic strain ε^e, and stress σ. These

vectors are related as follows [128, 129]:

$$\varepsilon^e = [H^*]\varepsilon^* \tag{3.9}$$

$$\boldsymbol{\sigma} = [D]\varepsilon^e = [D][H^*]\varepsilon^* \tag{3.10}$$

where $[H^*]$ is the matrix relating elastic strain to eigenstrain, and $[D]$ is the matrix relating elastic stress to strain. The matrix $[H^*]$ links the overall fields of eigenstrain to the overall fields of elastic strain, and depends on the domain occupied by the body and its boundary conditions.

When the vectors of inherent strain ε^* are known, the residual stress can be obtained by elastic analysis without calculating $[H^*]$ corresponding to the initial body through

$$\boldsymbol{\sigma} = [D](\varepsilon - \varepsilon^*) \tag{3.11}$$

where ε is total strain and can be expressed as the sum of the eigenstrain and the elastic strain ε^e. The magnitude of eigenstrain depends on the welding conditions and configurations of the welded joints.

3.5.2   Simplification

The analytical and experimental requirements of the eigenstrain method make its application expensive. Some efforts have been made to improve the applicability of this method, e.g. localized eigenstrain technique [78], which allows residual stress estimates to be made inside a small region of interest near the weld bead. By using this technique, the experimental effort required is reduced by up to five times relative to Ueda's method. Also, this new method was verified by numerical simulation and shown to be as accurate as the original Ueda's method.

Another approach was introduced by Mochizuki et al. [128] to simplify the distribution of the eigenstrain in complicated weld structures and residual stresses can be calculated based on such distribution. The eigenstrain of various welded joints with shapes were shown to have trapezoidal distributions in three vertical paths around the weld metal, and shear components near zero. The width and magnitude of the eigenstrain distribution depend on the kind of material, heat input, and the configuration of the joint. An example of pipe penetrating the thick plate was show in Figure 3.5, and the calculated residual stresses were compared
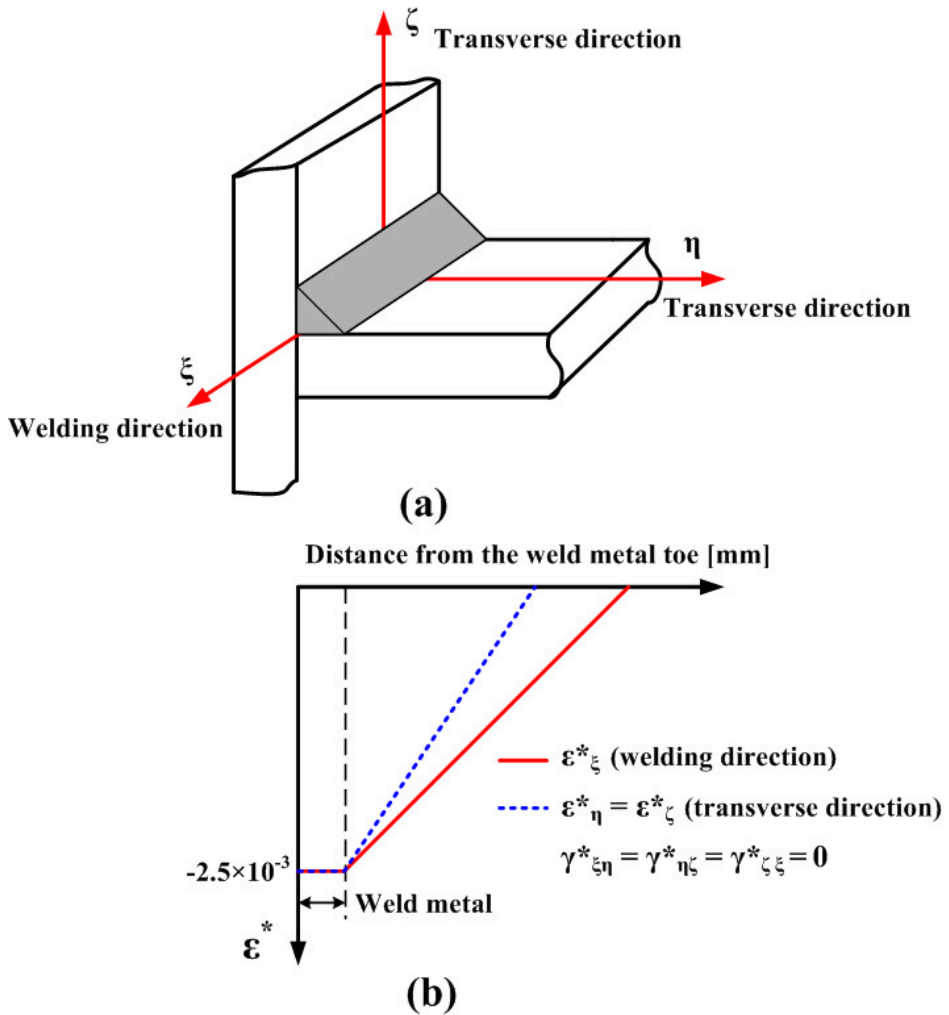
Figure 3.5: Illustration of the simplified eigenstrain method, (a) definition of the direction around weld metal, and (b) assumed eigenstrain and their distribution zone [128].
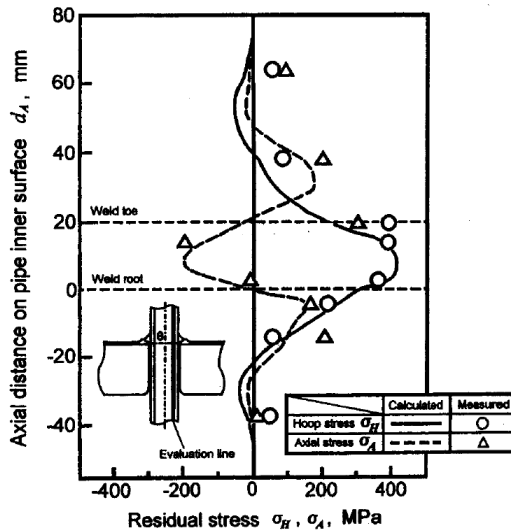
Figure 3.6: Residual stress on pipe inner surface for perpendicular welded joint ($\theta = 90deg$) [128].

with the experimental measurement stress in Figure 3.6. It can be seen that the distribution from the eigenstrain analysis agrees well with the direct measurement values in both circumferential and axial direction.

3.5.3   Application

The main objective of this thesis is to investigate the effect of residual stresses on crack-tip constraint and failure mechanisms, and to obtain the accurate distribution of the residual stresses is out of the scope. Therefore, a simplified method was utilized to introduce residual stress fields into the finite element model.

Residual stress field was introduced by the eigenstrain method through the following steps:

- Assume different eigenstrain distribution in base metal and weld metal respectively. Set the eigenstrain values equal to the thermal expansion coefficients of different regions.

- Load the model by a unit temperature change.

- Insert the crack and residual stress redistributes.

Chapter 4

Effect of residual stress on crack-tip constraint

Transferability of test data from small specimen to predicting fracture behaviour of large scale components is alway a main concerning factor when applying traditional fracture mechanics approaches. It has been well recognized that crack-tip constraint due to geometry, mismatch, pre-strain and residual stress affect the distribution of stresses around a crack and consequently preclude the use of a single parameter characterization of the crack tip stress field [44]. In this chapter, the effect of residual stress on crack-tip constraint will be investigated.

4.1   Problem description

The modified boundary layer (MBL) model consisting a weld metal region located in the center of the model and an outer base metal region was utilized to study the problem under Mode I plane strain conditions. The load was applied to the remote edges of the model through a displacement field (u,v) controlled by the elastic asymptotic stress field, as shown in Eq. 3.2. Only the upper-half plane was modeled because of symmetry. The crack is assumed to be a sharp crack without initial radius and the radius of the MBL model was taken as 1000 mm to ensure that the small-scale-yielding condition is fulfilled. The model was meshed by standard eight-node elements with reduced integration, CPE8R, with a finer mesh in the crack-tip region and the interface between the weld metal region
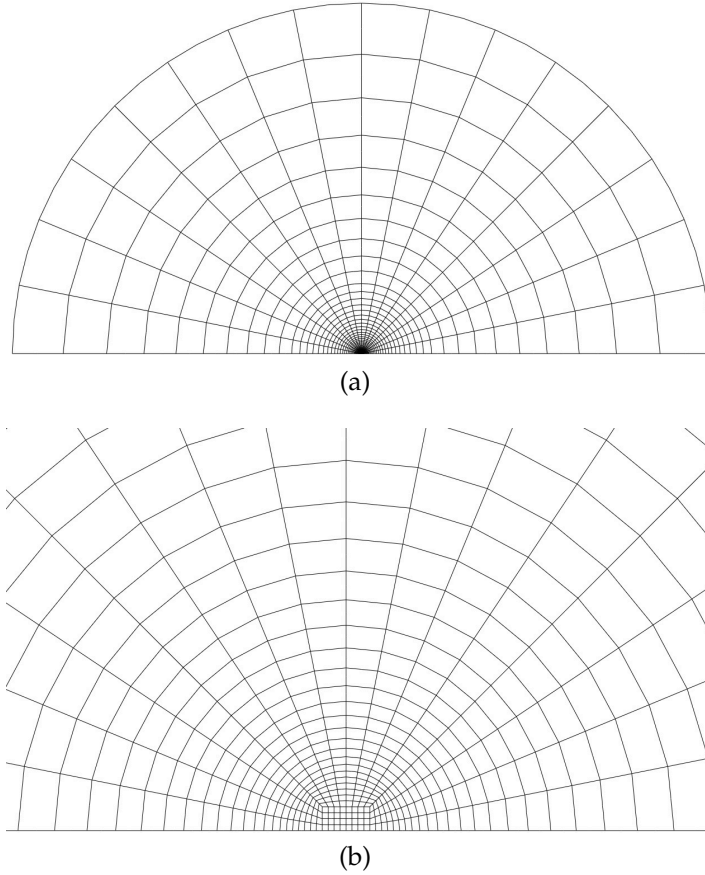
Figure 4.1: Modified boundary layer model, (a) global mesh; (b) crack-tip mesh.

and the base metal region. The size of smallest elements near the crack tip is 0.1 mm. The finite element model has 1408 elements and the meshes are shown in Figure 4.1.

The weld metal and base metal were assumed to have the same elastic properties (E=2$\times$10^5 MPa, ν=0.3) and plastic properties. The rate independent power law strain hardening materials were assumed to have the form of

$$\sigma_f = \sigma_0(1 + \frac{\bar{\varepsilon}^p}{\varepsilon_0})^n \tag{4.1}$$

where σ_f is the flow stress; $\bar{\varepsilon}^p$ is the equivalent plastic strain, σ_0=400 MPa the yield stress, $\varepsilon_0 = \sigma_0/E$ the yield strain and n is the plastic strain

hardening exponent. Different thermal expansion coefficients for the base metal (α_b) and weld metal (α_w) are assumed to introduce the residual stresses into the model by eigenstrain method. It should be noted that the thermal expansion coefficients here are not physical thermal coefficients, but are just used to introduce the residual stress into the computational model.

4.2   Residual stress field

The eigenstrain method was employed to introduce residual stress into the FE model, in which a "spot" weld with a round shape located in the center of the model was assumed. The eigenstrain for the base metal was assumed to be zero, and isotropic non-zero value for the weld was assigned. The size of the weld region was described by radius c, and three different sizes were investigated. Figure 4.2 shows the redistributed residual stress after the crack was introduced for the case with α_w=0.003 and α_b=0. The stress components were normalized by the yield stress, and the distance from the crack tip was normalized by c.

It can be seen that the residual stresses along both the parallel and opening directions have a sharp turning point at the interface between the base metal and weld metal. The reason for this sharp turning point is that the assumption of eigenstrain distribution is not continuous between the two regions. It can also be observed that the normalized residual stress fields collapse into one curve for different weld regions. Both the parallel and opening residual stress components in the weld metal are tensile and the peak values are approximately 1000 MPa and 1520 MPa, respectively. In the base metal region, the residual stress parallel to the crack plane is also tensile in a large range while the opening residual stress component is compressive to counter balance the tensile stress in the weld. The effect of the biaxial residual stress on the crack-tip constraint will be investigated in the following by using the residual stress field with weld size c=20 mm.

4.3   Results

The J-integral is adopted by the majority of the integrity assessment procedures currently used as the elastic-plastic fracture parameter. But for
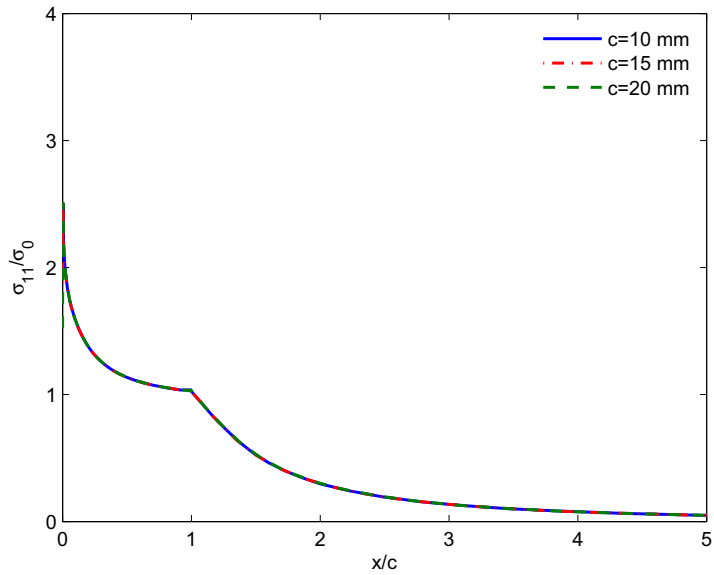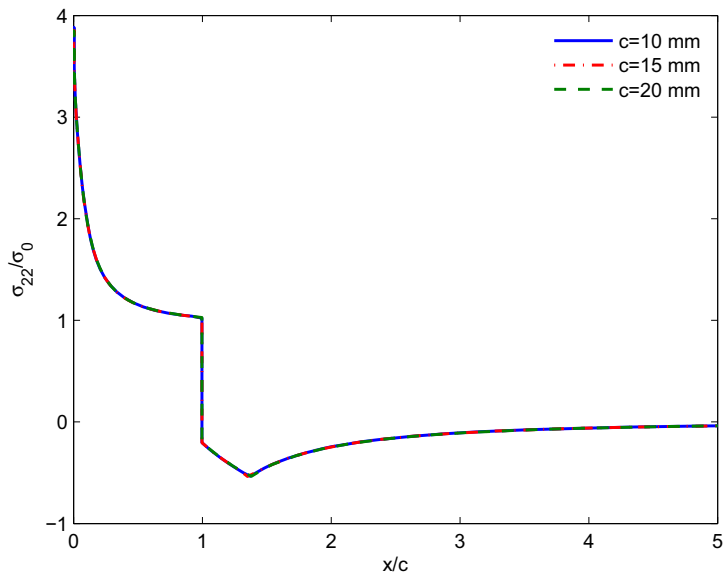
Figure 4.2: The redistribution of the residual stress fields after the crack was introduced. (a)σ_{11}^R; (b)σ_{22}^R. E/σ_0=500, ν=0.3, n=0.1; α_w=0.003 and α_b=0.

a crack in a residual stress field or the combination of mechanical and residual stresses a general path-independent J-integral appears to be path-dependent [11]. In our study, the computed J-integral by ABAQUS [114] has been investigated and compared with the applied J-integral (external loading) to the MBL model. Residual stresses as an additional stress field induce an initial J-integral, which is about 0.04% of the final J-integral caused by the combination of residual stress and external load. The residual stress was found to have significant effect on the path independence at the early stage of loading, while the path dependence becomes less severe with the increase of external loading. We also found that the J-integral in both the cases with and without residual stress loses path independence in the finite strain region, beyond which the J-integral are practically path-independent. The difference between the computed J-integral and applied J-integral is 0.2% $\sim$ 2.78% when a residual stress is present with applied J-integral from 200 N/mm to 600 N/mm, and it is 1.1% $\sim$ 3.25% for the case without residual stresses. The calculated J-integral has been used in the calculation of the stress field, J in the following means the computed J-integral.

4.3.1   Reference solution and Q field

The reference solution is important for studying the crack-tip constraint. The stress field distribution according to the HRR singularity or the small scale yielding solution (SSY) from MBL analysis is generally considered as the reference field. The difference between the HRR singularity and SSY solution was found to be very small. Dodds et al. [130] showed that the choice of HRR field or SSY solution as reference field does not result in significant difference. But, applying SSY solution as the reference field can extend the applicability of the approach to a much broader range of materials, because the HRR singularity is limited to deformation plasticity.

In this study, we used a homogeneous SSY solution without residual stresses and the *T-stress* as the reference field. Small scale yielding conditions are enforced by not allowing the plastic zone size r_p to exceed 0.2 times the radius of the MBL model. The stress distribution obtained from the small strain analysis for T=0 under different loading levels is presented in Figure 4.3.

Here, opening stresses are normalized by the yield stress σ_0; r is the
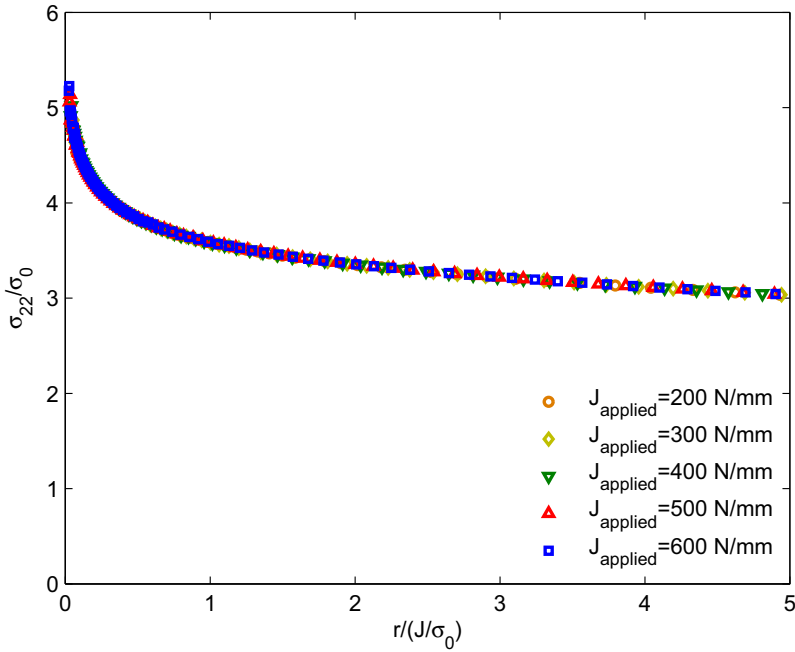
Figure 4.3: Small scale yielding solution without residual stresses and the *T-stress*. $E/\sigma_0 = 500$, *n*=0.1, *v*=0.3.

radial distance of the material in the undeformed state measured from the crack tip and normalized by J/σ_0. As shown in Figure 4.3, the opening stresses for different external loadings collapsed into a single curve. In other words, the reference field is independent of applied load. In this study, solution with $J_{applied}$=200 N/mm was taken as the reference one.

In order to better understand the effect of residual stresses on the crack-tip constraint, the *Q-field* is revisited. The *Q* value in the *J-Q* theory [30, 31] represents the crack-tip constraint induced by specimen geometry, crack size or loading mode. The small scale yielding solution was used as the reference solution to measure the *Q* value. Fields of different crack-tip constraint levels were induced by applying different combinations of *K* and *T*. Bilby et al. [131] showed that the near-tip stress distribution depends on *T*, but is independent of *K*. Therefore, the *K-field* was fixed in this section, but the *T-stress* varied in the range of -1<T/σ_0<1. The effect of loading path will be further investigated in Section 4.3.6. The opening stresses of the
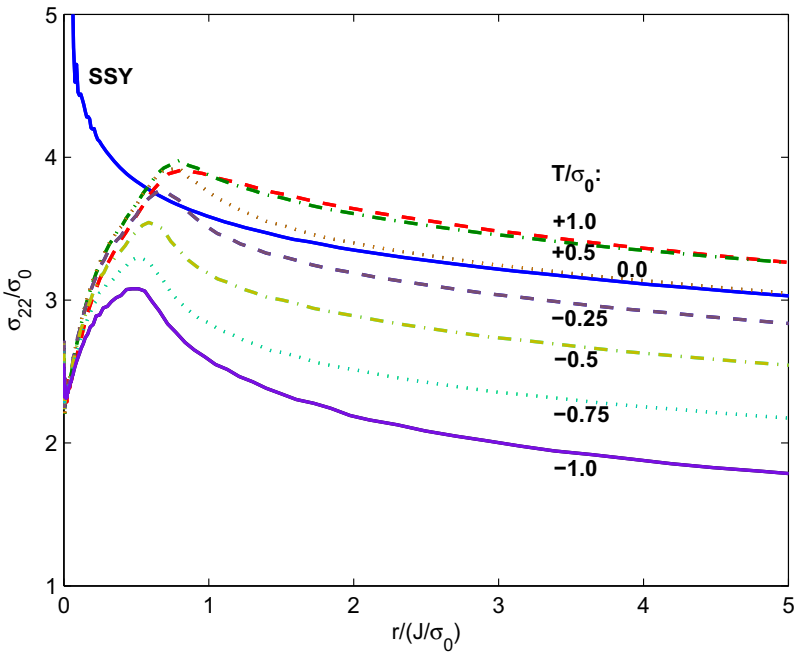
Figure 4.4: Opening stresses at different *T-stress*. $E/\sigma_0 = 500$, n=0.1, ν=0.3.

case with different T are showed in Figure 4.4.

It can be seen that the finite-strain effect is significant in the range $r/(J/\sigma_0)<1$, beyond which the stress field shows similarity. The stress distribution of T/σ_0=0 corresponds to the SSY solution and the stress distribution for T/σ_0=0.5 and 1 are almost identical. The reason for this is that the crack-tip field will approach full plasticity and a further increase of *T-stress* does not change the crack-tip field anymore when T/σ_0 is greater than certain value, as was shown by Du and Hancock [26]. However, negative T/σ_0 values cause a significant downward shift of the stress field.

O'Dowd and Shih [31] have demonstrated that there was a one-to-one correspondence between T and Q under the conditions that the remote stress field is given by the first two terms of the small-displacement-gradient linear elastic solution, in which the applied load and geometry affect Q only through T. i.e.

$$Q = F(T/\sigma_0; n) \tag{4.2}$$
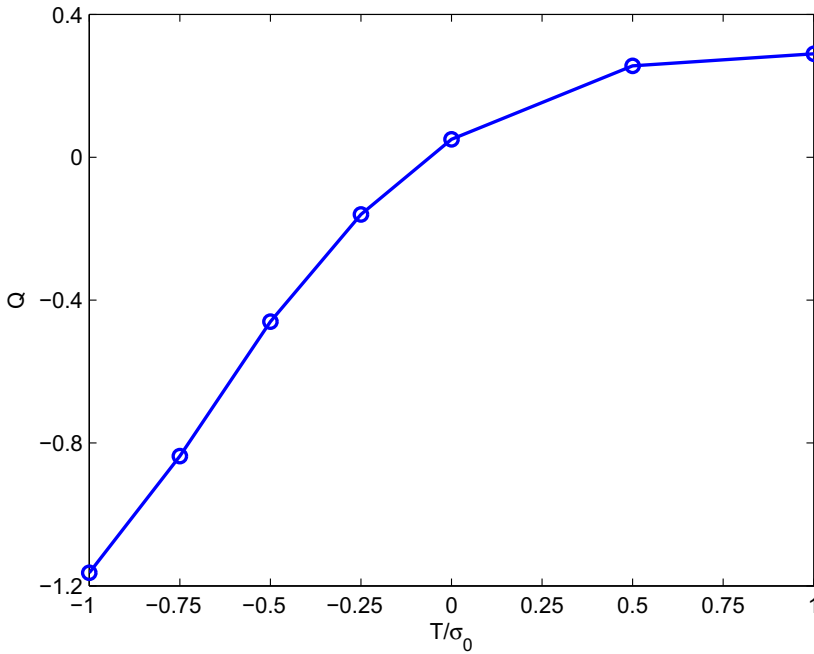
Figure 4.5: Relationship between Q and T. The Q value was taken out at $r/(J/\sigma_0) = 2$. $E/\sigma_0 = 500$, n=0.1,ν=0.3.

Here, Q also depends on the material hardening exponent n, but the dependence is weak. The relationship between Q and T in this study is showed in Figure 4.5.

4.3.2   Definition of R-parameter

To quantify the effect of residual stresses on crack-tip constraint is a interesting topic. In order to investigate the effect of residual stress fields on crack-tip constraint, different biaxial residual stress fields (see Figure 4.2) were introduced by varying the eigenstrain values under the same external loading ($J_{applied}$=200 N/mm) controlled by the *K-field*. The stress distributions including residual stresses are compared with the reference SSY field in Figure 4.6. Here, the stress components along the crack line (θ=0) were shown in range $0<r/(J/\sigma_0)<5$.

It can be seen that the presence of residual stresses elevates the stress
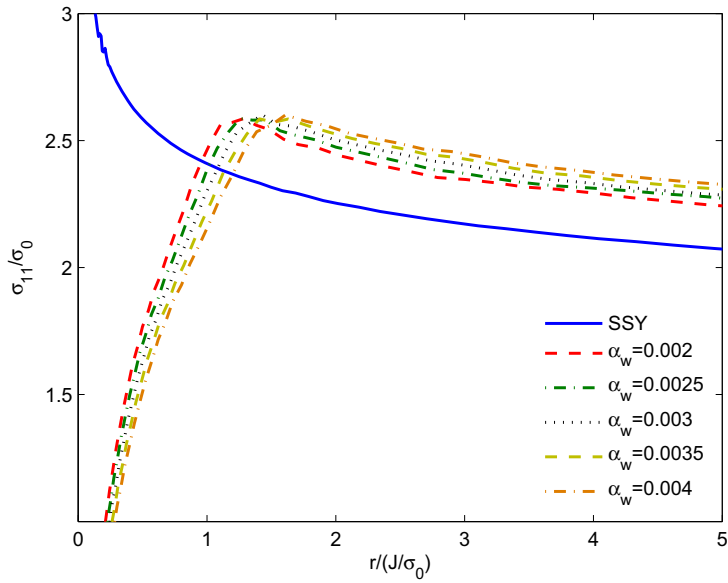
(a)
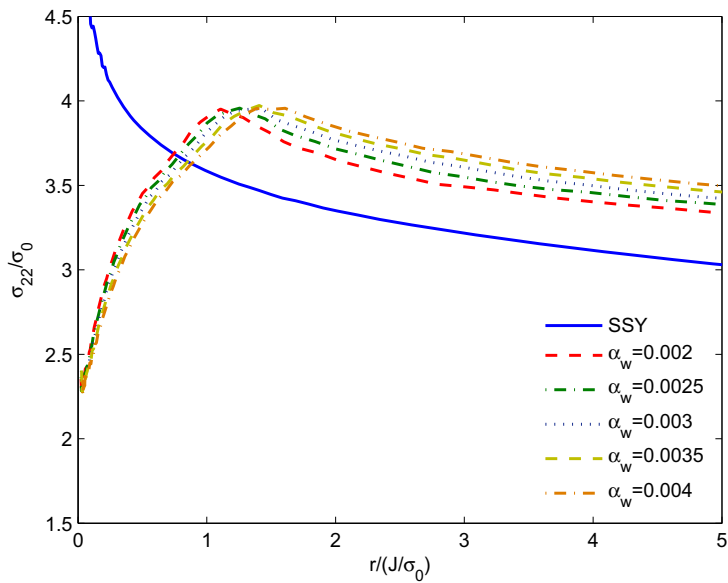
(b)

Figure 4.6: Comparison of the reference field and the stress field including residual stresses along θ=0, $J_{applied}$=200 N/mm. n=0.1, $E/\sigma_0 = 500$, ν=0.3. (a) σ_{11}; (b) σ_{22}.
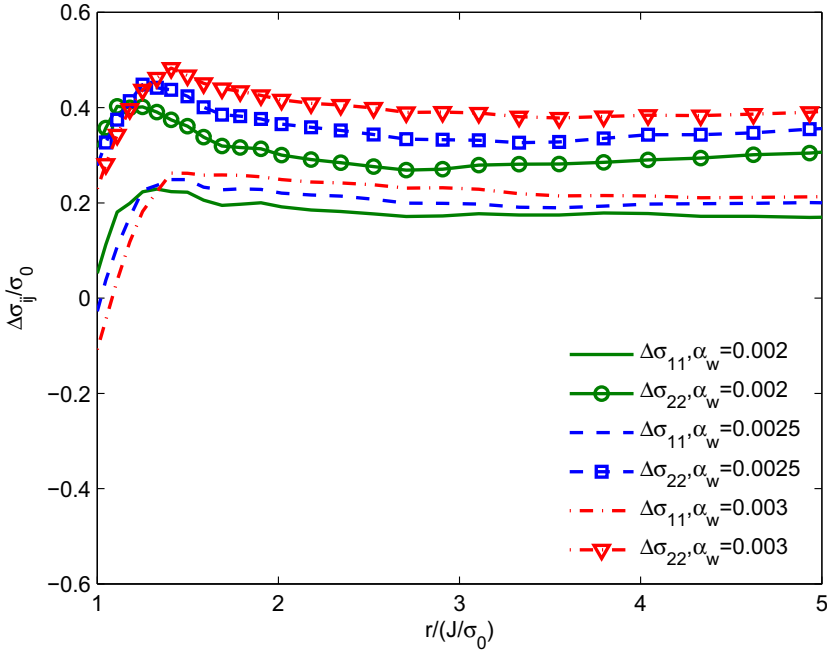
Figure 4.7: Difference stress between the full stress field and reference field along θ=0 with T=0. n=0.1, $E/\sigma_0 = 500$, ν=0.3.

level compared with reference solution, and the elevation of the stress level increases with the increase of the eigenstrain level. It can be observed that the finite-strain effects are significant in the range $r/(J/\sigma_0) < 1.5$, beyond which the stress distributions seem to be parallel to each other. It should be noted that the magnitudes of normalized opening stress are greater than that of the stress component parallel to the crack flank. Due to the symmetrical condition, the shear stress component is zero.

A difference stress field has been calculated between the full stress field with residual stresses and the reference solution ($\triangle\sigma_{ij} = \sigma_{ij}^{with} - \sigma_{ij}^{ref}$, where σ_{ij}^{with} is the stress field with residual stresses and σ_{ij}^{ref} is reference SSY solution). The difference fields for the three eigenstrain levels α_w=0.002, 0.0025 and 0.003 are shown in Figure 4.7. In our earlier work, Liu et al. [44] showed that the residual stress-induced difference field could be approximated by a hydrostatic stress with both principle components
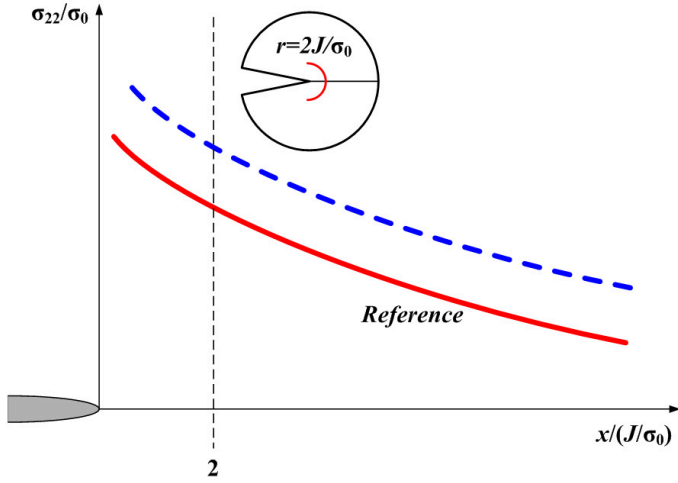
Figure 4.8: Illustration of the definition of parameter R.

almost identical and shear component zero. However, as shown in Figure 4.7, $\triangle\sigma_{11}$ and $\triangle\sigma_{22}$ are different for the same eigenstrain level. With the increase in the eigenstrain level, the difference between $\triangle\sigma_{11}$ and $\triangle\sigma_{22}$ increases. It should be noted that uniaxial residual stresses perpendicular to the crack flank were used in [44] while biaxial residual stress fields were introduced in this study. The difference between the present results and the results in [44] may be explained by the different residual stress components. Biaxial residual stresses tend to have more significant effects on the crack-tip constraint than uniaxial ones. Similar features have also been reported by Xu and Burdekin [43].

It is known that the cleavage fracture is controlled by the critical levels of the opening stress acting over a microstructurally significant distance ahead of the crack tip [130]. In order to quantify the effect of residual stresses on the crack-tip constraint, a parameter R can be defined based on the difference in the opening stresses. The same reference stress used in the previous section was used here. The definition of R is illustrated in Figure 4.8, and has the form as Eq. 4.3.

$$R = \frac{\sigma_{22} - (\sigma_{22})_{SSY,T=0}}{\sigma_0} \quad at \quad r = 2J/\sigma_0 \qquad (4.3)$$

The distance $r/(J/\sigma_0) = 2$ is chosen so that R is evaluated outside
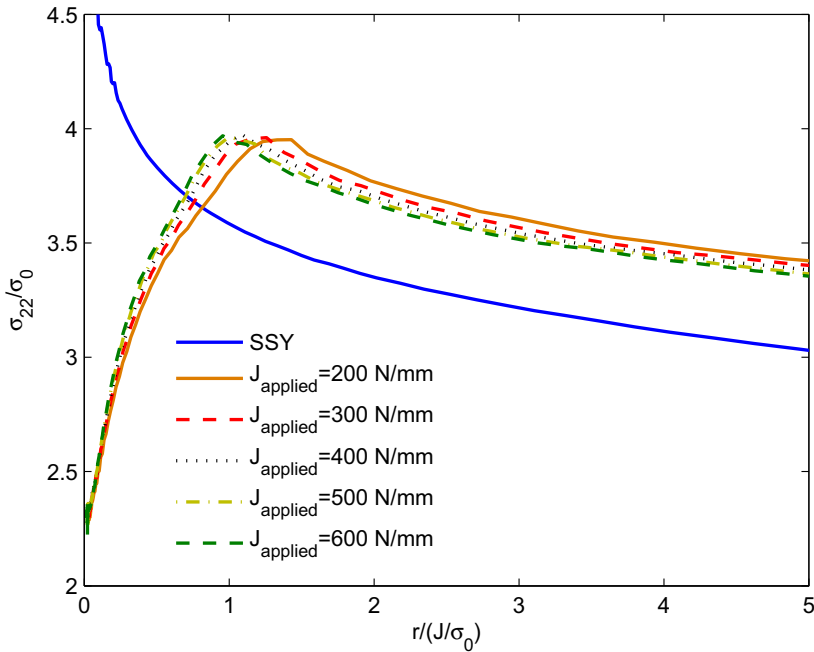
Figure 4.9: Comparison of reference field with stress field combining external loading and residual stresses along $\theta = 0$ with $T=0$. $E/\sigma_0 = 500$, $\nu=0.3$.

the finite-strain region. It can also be seen that the difference between the finite strain solution with $T=0$ and reference small scale yielding solution is negligible when the distance is greater than $r/(J/\sigma_0) = 2$.

4.3.3   Effect of external load on R

Welded structures with residual stresses are subject to various service loading conditions. It is interesting to investigate the effects of external loading on the crack-tip constraint induced by residual stresses. A residual stress field with eigenstrain value $\alpha_b=0$, $\alpha_w=0.003$ was introduced into the MBL model, and the crack-tip constraint was investigated under five external loading levels ($J_{applied}$=200, 300, 400, 500 and 600 N/mm). The opening stresses of combined external loading and residual stresses are shown in Figure 4.9 together with the reference solution.

Figure 4.9 shows that in the presence of residual stresses the crack-tip opening stresses exceed the reference solution for all the loading levels considered. However, the opening stress decreases with the increase of external loading. The difference between the opening stresses and reference solution are plotted in Figure 4.10(a). The R values quantifying the residual stress-induced crack-tip constraint have been calculated using Eq. 4.3 and are plotted as a function of the external load in Figure 4.10(b).

It can be seen from Figure 4.10(a) that different stresses under the various external loading levels are parallel to each other to a large extent when $r/(J/\sigma_0) > 1.5$. The residual stress-induced constraint R decreases with the increase in the external loading, as shown in Figure 4.10(b). Liu et al. [44] observed a similar trend in their studies. The behaviour is in agreement with common knowledge that the external loading and plasticity can reduce the effects of residual stresses. It is also interesting to note that R is different to the mismatch-induced constraint parameter M that depends on the material properties but is independent of external loading and geometry constraint [18, 39, 40]. The above results indicate that the residual stress as an additional stress field has interaction with the applied stress fields and depends strongly on the residual stress field itself.

4.3.4   Interaction of R and Q

It has been demonstrated that the specimen geometry, crack size and loading mode influence the crack-tip constraint and the geometry constraint can be characterized by the Q parameter [30, 31]. Liu et al. [44] recently demonstrated that the residual stress induced constraint in the tensile specimen is in general higher than that in the bending specimen. It is known that for the same geometry and crack size, the bending specimen displays a higher geometry constraint than the tensile specimen. Thus, it is interesting to study how the geometry constraint interacts with the residual stress-induced constraint.

In a boundary layer formulation, the normalized crack-tip stress fields depend on the remote *T-stress* but are supposed to be independent of the *K-field*. By changing the *T-stress*, different geometry constraint levels can be obtained. In the following, the near-tip stress field in the presence of both a residual stress field and *T-stress* has been investigated. The residual stress is fixed with eigenstrain value α_b=0, α_w=0.003, and T/σ_0=-1, -0.75, -
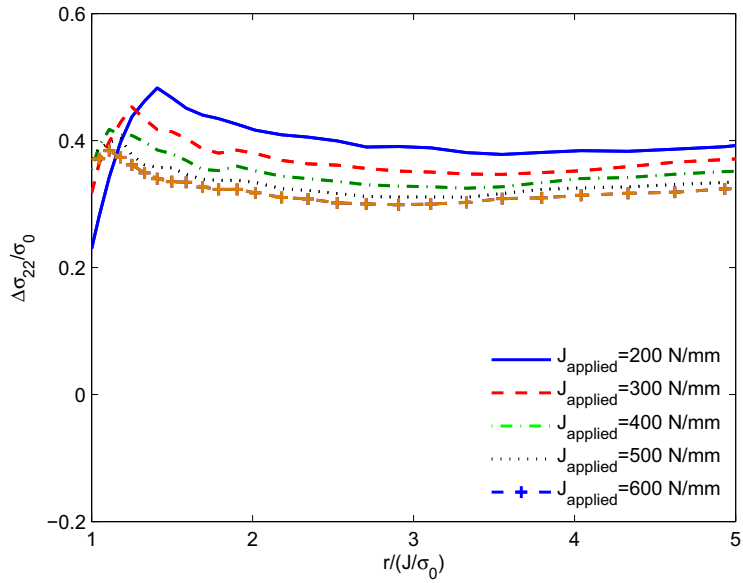
(a)
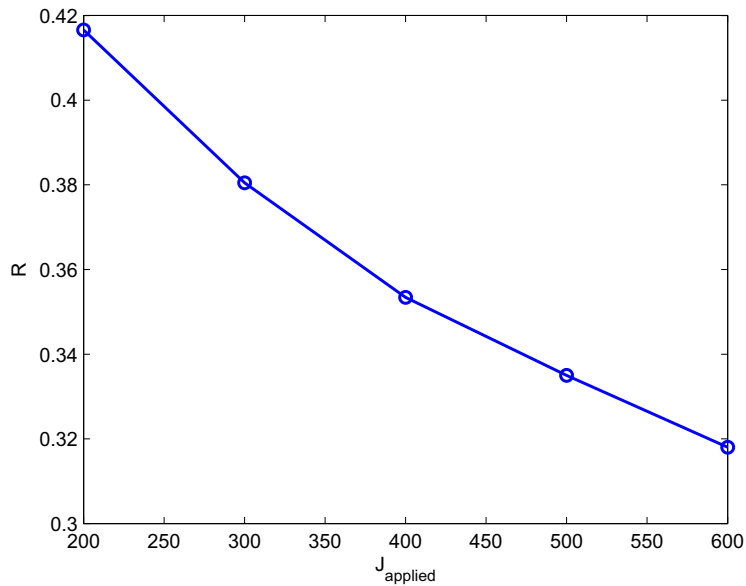
(b)

Figure 4.10: Effect of external loading. (a) different opening stress fields along θ=0; (b) R as a function of external loading. T=0, n=0.1, $E/\sigma_0 = 500$, ν=0.3.
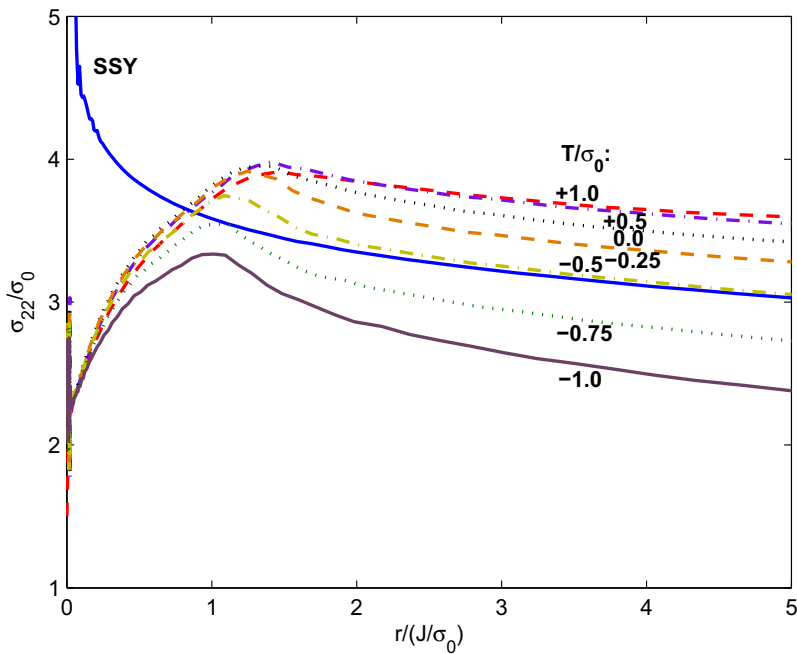
Figure 4.11: Comparison of reference solution with stress field including residual stress and geometry effects along $\theta=0$. $n=0.1$, $E/\sigma_0 = 500$, $\nu=0.3$.

0.5, -0.25, 0, 0.25, 0.5 and 1 have been considered. The normalized opening stresses at $J_{applied}$=200 N/mm are shown in Figure 4.11.

Figure 4.11 shows that the stress field was shifted up and down by different *T-stresses* compared with the reference solution. It can be seen that the compressive *T-stress* affects the stress field more significantly than the tensile *T-stress*.

In order to investigate the interaction between R and Q, R was calculated according to Eq. 4.3 for different *T-stresses* and compared with Q. Here, it should be noted that R defined in Eq. 4.3 represents the crack-tip constraint induced purely by the residual stress. However, the R value here (designated as R_Q) includes both the residual stress-induced constraint and geometry constraint, i.e. $R_Q = R + Q$. The comparison of R_Q and Q with different T is plotted in Figure 4.12.
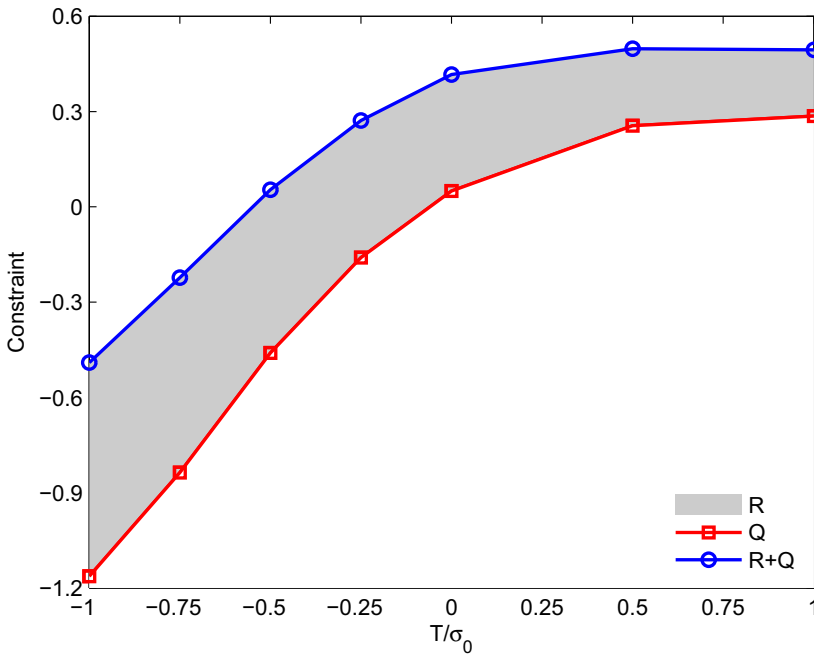
Figure 4.12: Comparison of R and Q. n=0.1, E/σ_0=500, ν=0.3, α_b=0, α_w=0.003.

The difference between R_Q and Q is the constraint induced by the residual stress, i.e. R showed by the shaded area in Figure 4.12. It can be seen that the difference between R_Q and Q decreases with the increase of T/σ_0, which indicates that the higher the geometry constraint, the weaker the residual stress effect on the crack-tip constraint. *T-stress* was applied as a uniaxial tension or compression parallel to the crack flank to change the crack-tip stress triaxiality in the boundary layer formulation. In this study, the *T-stress* which generates different Q stresses was designated as T^Q. The biaxial residual stress component parallel to the crack flank can also be considered as a *T-stress* component, designated as T^R. Thus, the interaction between R and Q can be explained as the interaction of T^R and T^Q. As shown in Figure 4.2, the residual stress component parallel to the crack flank is mainly tensile. Therefore, the superposition of T^Q and T^R enhances the total *T-stress* that results in a higher crack-tip constraint. A
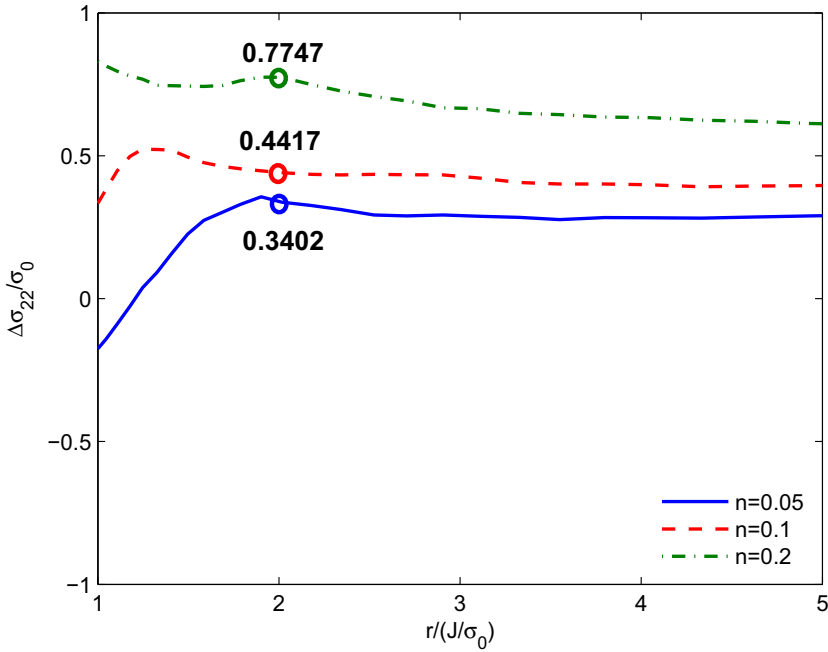
Figure 4.13: Difference opening stress for the stress fields with residual stresses and the corresponding reference solution with $n=$ 0.05, 0.1, and 0.2 along $\theta=0$. $E/\sigma_0=500$, $\nu=0.3$

positive T^R can reduce the constraint loss significantly when T^Q is compressive while it has a weak effect on the crack-tip constraint when T^Q is positive. However, when the crack-tip achieved the full plasticity, a further increase in tensile *T-stress* does not have any significant effect.

4.3.5 Effect of material hardening on R

Finally, it is interesting to investigate the influence of material properties on the residual stress-induced constraint. The same residual stress field generated by eigenstrain values $\alpha_b=0$ and $\alpha_w=0.003$ was introduced and the same external loading $J_{applied}=200$ N/mm was applied for three hardening components. Figure 4.13 shows the difference in the opening stress between the case with residual stresses and the corresponding reference solution. The values of R for different n were marked by circles.

Figure 4.13 shows that the difference in the opening stresses increases with the increase of the strain hardening exponent. R is also higher for the case with stronger strain hardening. For the materials with weak hardening, the crack tip can easily develop full plasticity. Thus, for the same residual stress field, its effect on the crack-tip constraint is smaller for weaker hardening materials. It should also be noted that the finite strain effect becomes more significant for a material with weaker strain hardening.

4.3.6   Effect of loading path on R and Q

For the same external displacement field applied at the outer boundary of the MBL model, different loading path may induce a different crack-tip constraint, which was generally neglected by most of the work in the literature. There are generally two loading paths to apply to remote displacements: the proportional loading path controlled by fixing the ratio of *K/T* (Path I); and the sequent loading path by applying the *T-field* first and then the *K-field* (Path II). In this study, the effect of the loading path on the crack-tip constraint was investigated both with and without residual stress cases. T/σ_0=-0.5 and *K-field* with $J_{applied}$=200,300,400,500 and 600 N/mm were studied and the same reference field was used. Figure 4.14(a) and (b) show the effect of the loading path on Q and R, respectively.

It can be seen that proportional loading path can generate a higher crack-tip constraint than the sequent loading path both with and without the residual stress cases. It should be noted that the compressive *T-stress* represents the loss of crack-tip constraint. Thus, the lower crack-tip constraint induced by loading path II indicates that the *T-stress* applied as an additional field affects the crack-tip constraint. We also observed that the effect of the loading path on R is stronger than the effect on Q for the same external loading. This indicates that the effect of residual stresses on the crack-tip constraint can be regarded as the superposition of components parallel to the crack flank and the additional *T-field*. It was also found that under the same geometry constraint level ($T/\sigma_0 = -0.5$), the effect of residual stresses decreases with the increase in external loading, as shown in Figure 4.14(b).
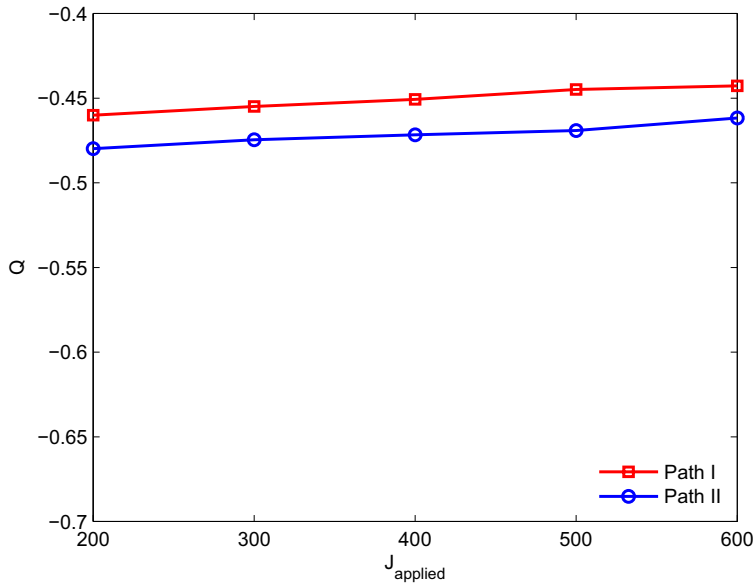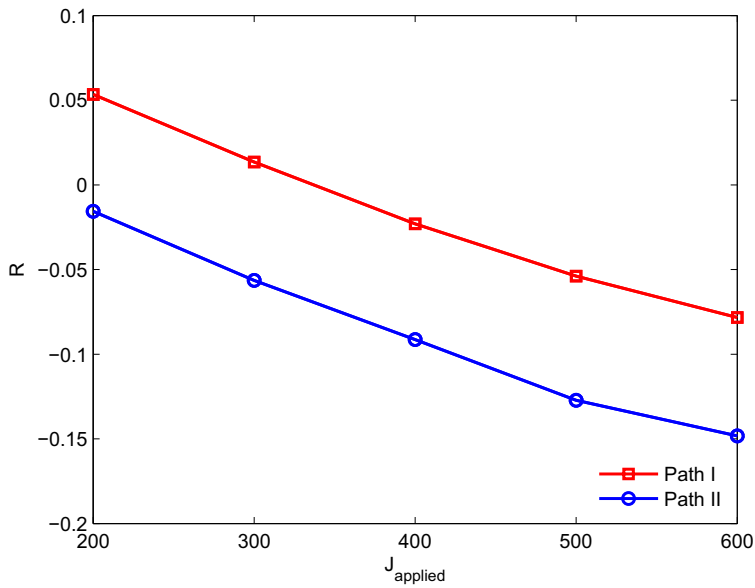
Figure 4.14: Effect of the loading path on the crack-tip constraint with T=-0.5, n=0.1, $E/\sigma_0 = 500$, ν=0.3. (a) effect on Q; (b) effect on R. α_b=0, α_w=0.003.

4.4 Conclusions

Welding residual stresses are unavoidable and play a crucial role in the integrity assessment procedure. Residual stresses affect both the crack driving force and the crack-tip constraint. This study has focused on the latter effect by using a new parameter to quantify its effect. The modified boundary layer model with a remote displacement field controlled by the *K-field* and *T-stress* was used. A two-dimensional residual stress field was introduced into the model by the eigenstrain method. A small scale yielding solution without residual stress and geometry constraint ($T/\sigma_0=0$) was taken as the reference field.

It has been shown that the difference in the stress fields between the full stress field with residual stresses and the reference solution show similarity. Unlike previous findings, we found that the stress components of the difference fields parallel and perpendicular to the crack flank are not equal. Thus, parameter R is not a hydrostatic term for the cases examined. Since the cleavage fracture is more sensitive to the opening stress, a parameter R was defined based on the opening stress difference to quantify the welding residual stress-induced constraint.

The results showed that external loading can remedy the residual stress-induced constraint R that decreases with the increase in the external loading. R is different to the mismatch-induced constraint parameter M which is independent of the external loading.

The results also indicate that the geometry constraint interacts with the constraint induced by the residual stresses. For a higher geometry constraint, the effect of the residual stresses becomes weaker. This could be explained by the fact that the residual stress components parallel to the crack flank interact with the remote *T-stress*.

The study also indicates that a sequential loading path with the *T-field* taken as an additional field will result in lower crack-tip constraint. The loading path effect is stronger for the cases with residual stresses.

The residual stress-induced constraint depends on the material hardening exponent as well. R increases with the increase of the hardening, in which the near-tip plasticity plays an important role. Full plasticity is easier to cover the crack tip for the weaker hardening material and then the residual stresses have a smaller effect on the crack-tip constraint.

The present work is concerned with the residual stress-induced crack-tip constraint. The parameter R was defined to quantify the residual stress-

induced crack-tip constraint. The parameter R can be constructed as [132]:

$$R = F(\varepsilon^*, n, Q, P) \tag{4.4}$$

where ε^* represents the eigenstrain; n is the hardening exponent; Q measures the geometry constraint, and P characterizes the external loading.

Chapter 5

Effect of residual stress on cleavage fracture

Cleavage fracture featured with negligible plastic tearing before final failure is often the most dangerous failure mode. It occurs by the unstable propagation of microcracks formed within grain boundary particles by twinning or slip dislocation pile-ups and then grows into the ferrite matrix under the action of tensile stress [41]. The cleavage fracture toughness exhibits sensitivity to the local stress and deformation fields due to its highly localized character of the failure mechanism [133]. Understanding how residual stresses influence the cleavage fracture behaviour becomes more and more important when high strength steels are increasingly utilized in offshore industry.

5.1   Problem description

This chapter presents the effect of residual stresses on cleavage fracture toughness by using the cohesive zone model under Mode I, plane stain conditions. Modified boundary layer simulations were performed with the remote boundary conditions governed by the elastic *K-field* and *T-stress*. The eigenstrain method was used to introduce residual stresses into the finite element model. A layer of cohesive elements was deployed ahead of the crack tip to simulate the fracture process zone. A bilinear traction-separation-law (see Figure 3.4) was used to characterize the behaviour of the cohesive elements. It was assumed that the initiation of the
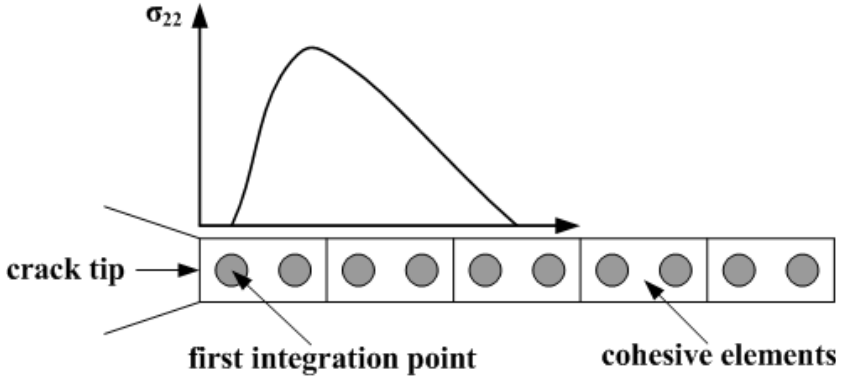
Figure 5.1: Schematic plot of the assumption made in the study.

crack occurs when the opening stress drops to zero at the first integration point of the first cohesive element ahead of the crack tip, as illustrated in Figure 5.1.

The finite element computations were performed using ABAQUS [114]. The radius of the MBL model was taken as 200 mm. A layer of uniform-sized cohesive elements was deployed along the central line ahead of the crack tip to simulate the fracture process. The length of the cohesive element layer is 20 mm, and the size of the uniform cohesive element l_c is 0.1 mm. The thickness of the cohesive elements is 2.5×10^{-4} mm. The weld metal and base metal region of the model was meshed by standard full integration 4-node 2D plane strain elements. The cohesive elements are standard cohesive element COH2D4. The finite element model has 4992 elements and the meshes are shown in Figure 5.2.

5.2　Residual stress field

Te eigenstrain method was used to introduce residual stresses into the finite element model. A rectangular weld region was constructed in the center of the MBL model, as illustrated in Figure 5.2(b). The thermal expansion coefficient of the base metal α_b was assumed to be zero, and it was assumed to be orthogonal and represented by α_{11} and α_{22} for weld metal. The ratio α_{11}/α_{22} was fixed to be 2, and by setting α_{22}= -0.0005, 0.0005, 0.001 and 0.002, four residual stress fields were generated and

(a)

crack tip

cohesive elements

9.6 mm
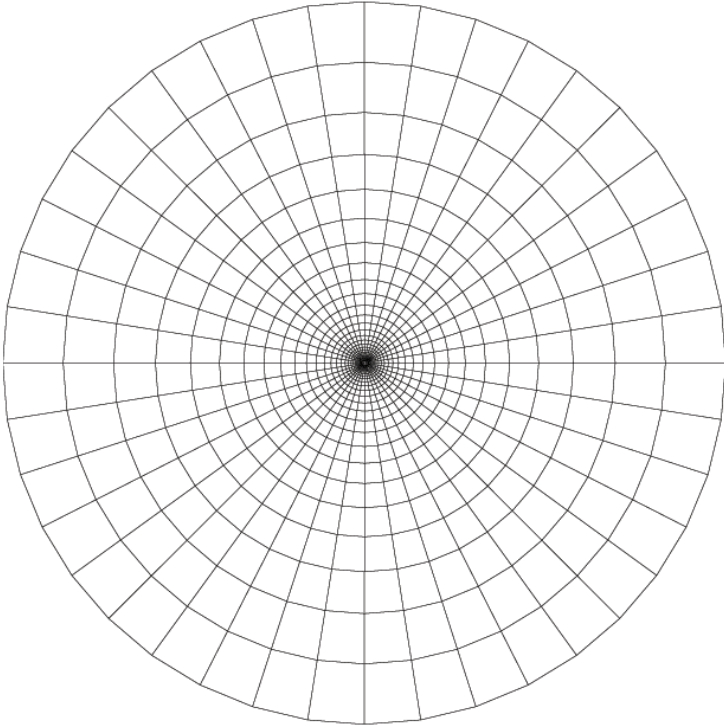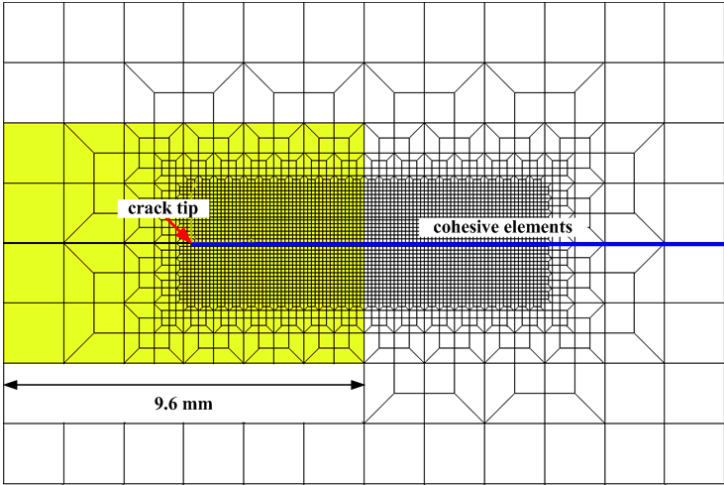
(b)

Figure 5.2: Finite element meshes for the modified boundary layer model, (a) global view; (b) crack-tip region and the illustration of the weld region.

designated as RsField0, RsField1, RsField2 and RsField3 respectively, as shown in Figure 5.3. It should be noted that the eigenstrain values selected here are taken from the experimental measurement results in literature [129, 134]. The residual stress fields generated by these values have similar distribution to that showed in Ref. [135]. To obtain accurate distribution of the residual stress fields by eigenstrain method, one should carry out the experiments to measure the distribution of the eigenstrain. However, the main objective of this study is to investigate the effect of the residual stresses, the prediction of the real distribution of the residual stress field is outside the scope. Note that the stress components are normalized by the yield stress, and the distance from the crack tip x is normalized by the size of the uniform element size l_c.

It can be seen that the negative eigenstrain value introduces the compressive residual stress at the weld region while the positive ones generate tensile residual stresses. Both tensile and compressive residual stresses parallel to the crack front converge to zero far from the crack tip. The opening residual stresses are self-balanced ahead of the crack tip. There is a sharp turning point in the distribution of the opening residual stresses, which is the region where eigenstrain discontinuities have been introduced into the FE model, namely a weld metal-base metal boundary. The tensile residual stresses also show similarity, and the level of the tensile residual stress increases with the increase of α_{22}. Due to the crack-tip singularity, σ_{11} is about 960 MPa and σ_{22} is about 1380 MPa at the crack tip for RsField3.

5.3   Results

Cleavage fracture toughness exhibits a strong sensitivity to the local stress and deformation fields due to its highly localized character. Residual stresses affect both the crack driving forces and crack tip constraint [11, 17, 41, 44], which may further influence the cleavage fracture toughness. Therefore, the effect of residual stresses on cleavage fracture toughness was investigated in this study. The contour *J*-integral [8] was utilized as the measure of the cleavage fracture toughness. Lei et al. [11] and Lei [12] showed that the *J*-integral shows path-dependent with the presence of the residual stresses. In our study, the computed *far-field J*-integral by ABAQUS shows practically path-independence beyond the large strain
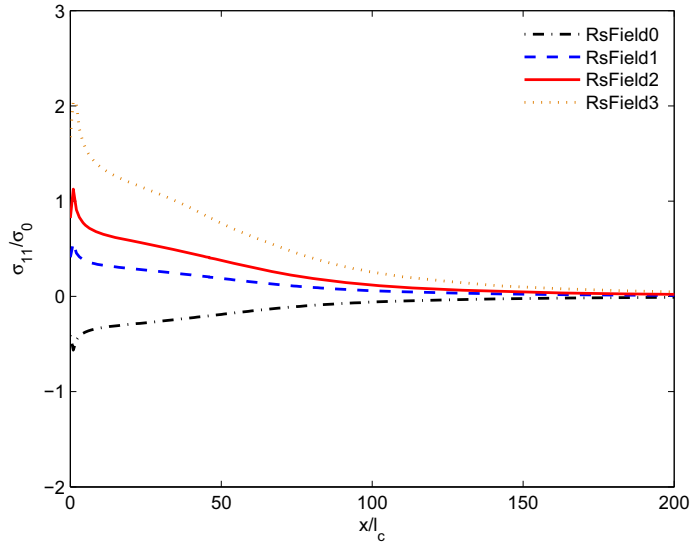
(a)
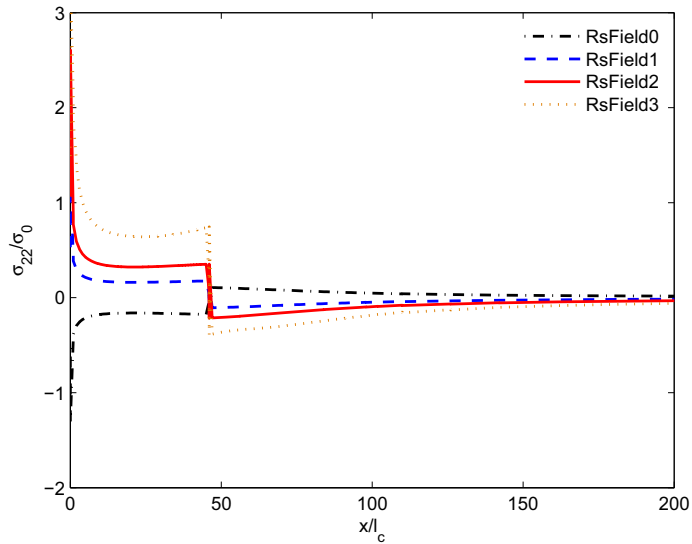
(b)

Figure 5.3: Residual stress distribution in MBL model, (a) components parallel to the crack plane; (b) normal to the crack plane. Four different residual stress cases were considered, where RsField0 is compressive and the remaining 3 are tensile. $\alpha_{11}/\alpha_{22}=2$, $\alpha_{22}=-0.0005$ is for RsField0, $\alpha_{22}=0.0005$, 0.001 and 0.002 for RsField1, RsField2 and Rsfield3 respectively.
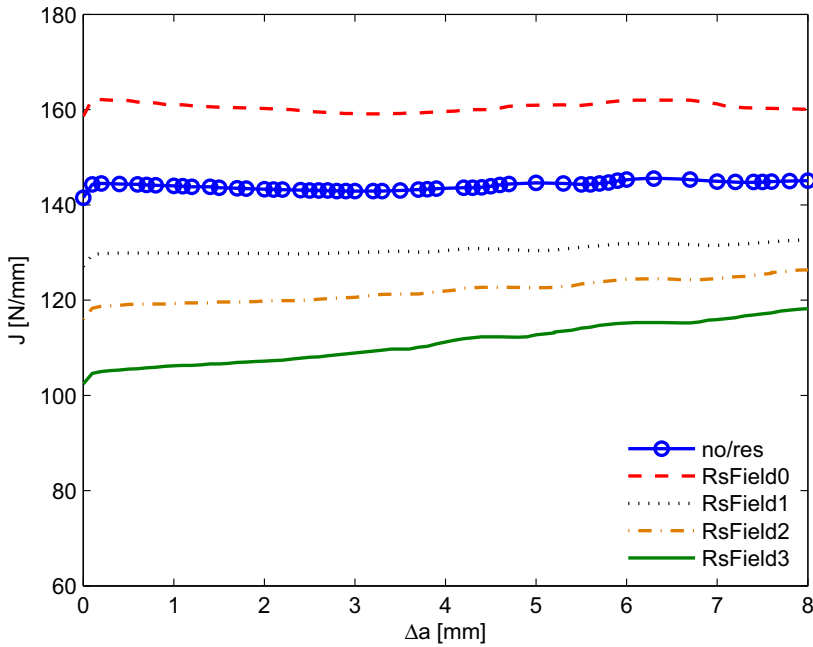
Figure 5.4: Cleavage toughness as the function of crack growth length when the incremental plasticity model is used for surrounding materials. E/σ_0=450, ν=0.3; n=0.1; $\Gamma_0 = 100$ N/mm, $\sigma_{max} = 3\sigma_0$.

region for the cases investigated. The *J*-integral in the following means the calculated *J*-integral.

5.3.1 Effect on cleavage toughness

Cleavage fracture is a crucial failure mode in practice, and understanding how residual stresses affect the cleavage fracture is very important. The effect of residual stresses, i.e. Figure 5.3, on cleavage fracture toughness was investigated in this section. Cohesive parameters Γ_0=100 N/mm was selected and the maximum cohesive stress σ_{max} was set to be $3\sigma_0$. The cleavage toughness was plotted as the function of crack growth length in Figure 5.4.

It can be seen that the crack growth resistances are almost flat for both with and without residual stress cases. Figure 5.4 also indicates that the
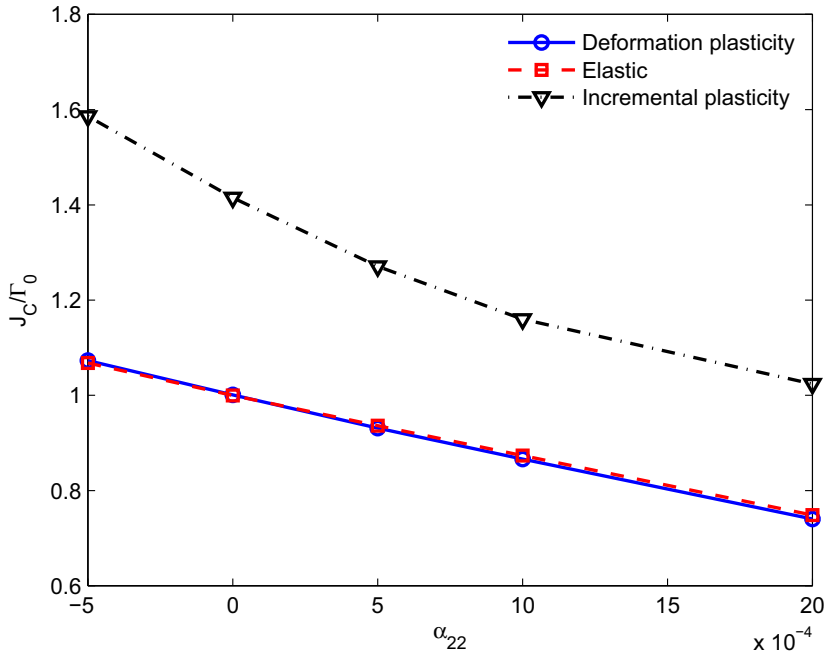
Figure 5.5: Cleavage fracture toughness as the function of α_{22}. n=0.1; $\Gamma_0 =$ $100N/mm$, $\sigma_{max} = 3\sigma_0$.

cohesive zone model with bilinear traction-separation-law is applicable to predict the cleavage fracture toughness. In the following context, the initiation fracture toughness (J_C) predicted according to the assumption made in Section 5.1 will be investigated. Residual stresses may influence both the fracture process zone and plasticity of surrounding materials. Therefore, three different constitutive models, i.e. incremental plasticity, deformation plasticity and elastic, were employed to characterize different behaviour of surrounding materials. The relationship between J_C and the eigenstrain value α_{22} was showed in Figure 5.5. It should be noted that α_{22}=0 represents the reference case without residual stresses.

As shown in Figure 5.5, the compressive residual stress ($\alpha_{22} < 0$) increases the cleavage fracture toughness while the tensile residual stresses decrease the cleavage fracture toughness. With the increase of tensile residual stress, the cleavage fracture toughness decreases. Also observe that the effect of residual stress on fracture toughness is almost the same for elastic

and deformation plasticity surrounding materials. However, the cleavage fracture toughness for surrounding materials predicted with incremental plasticity is significantly larger than other cases. When the surrounding material is elastic or characterized by deformation plasticity model, the cleavage fracture toughness without residual stress ($\alpha_{22} = 0$) equals to cohesive energy Γ_0, which represents energy needed to advance the crack in the absence of plasticity. For incremental plasticity material model, it can be seen that cleavage fracture toughness is larger than 1. For elastic and deformation plasticity model, the deformation can return back to the original state when the load is removed. However, when an incremental plasticity model is used and unloading occurs, the plastic deformation will be retained and the energy will be dissipated, which in turn increases the fracture toughness. In the following, the incremental plasticity model has been used for the study. In order to better understand the contribution of plasticity of surrounding material, the effect of different σ_0 on cleavage fracture toughness in the absence of residual stresses was investigated. Figure 5.6 shows the relationship between cleavage fracture toughness and σ_0/E.

It can be seen that with the increase of yield stress, the cleavage fracture toughness decreases and approaches to Γ_0, which indicates that the decreasing of the plastic zone size of surrounding materials. When residual stress is present, it may influence the plastic deformation of the surrounding materials. Figure 5.7 shows the plastic zone size when cleavage fracture occurs for different residual stresses.

Figure 5.7 shows that the compressive residual stress field, i.e. RsField0, both enlarges the maximum radius of the plastic zone and causes plastic zone to swing forward. In contrast, tensile residual stress fields cause the plastic zone to decrease in size and rotate backward. Similar behaviour has been reported by Du and Hancock [26] who investigated the effect of *T-stress* on the crack-tip constraint. Negative *T-stress* indicates loss of the crack-tip constraint while the positive *T-stress* has the opposite effect. Thus, we may conclude that the compressive residual stress reduces the crack-tip constraint and enlarges the plastic zone, which in turn enhances the cleavage fracture toughness significantly. Unlike the compressive residual stress, tensile residual stresses increased the crack-tip constraint and reduced the cleavage toughness. Also, we can conclude that the effect of residual stress on the cleavage fracture toughness mainly comes from the contribution of the plasticity of the surrounding materials.
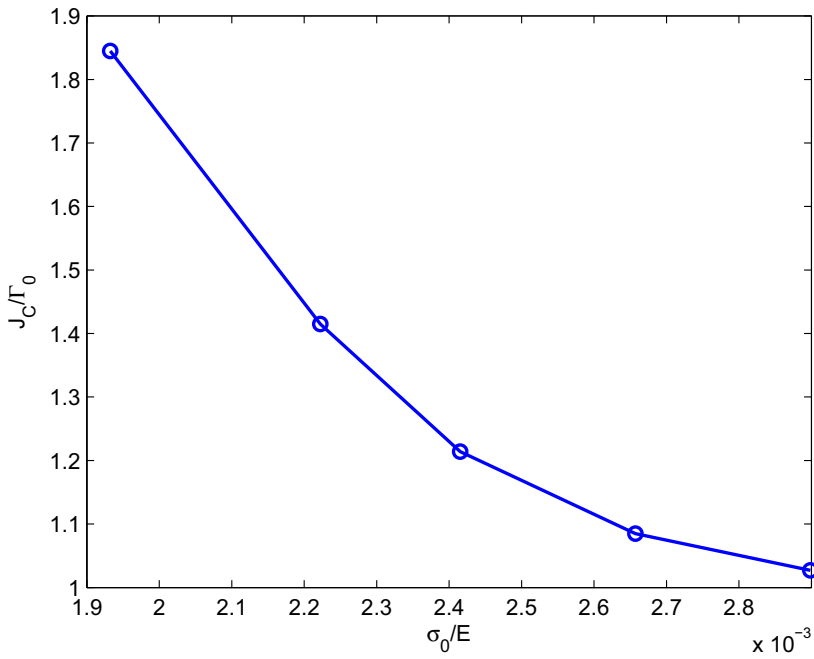
Figure 5.6: Plasticity contribution from the surrounding materials at the crack initiation. n=0.1; $\Gamma_0 = 100N/mm$, $\sigma_{max} = 3\sigma_0$
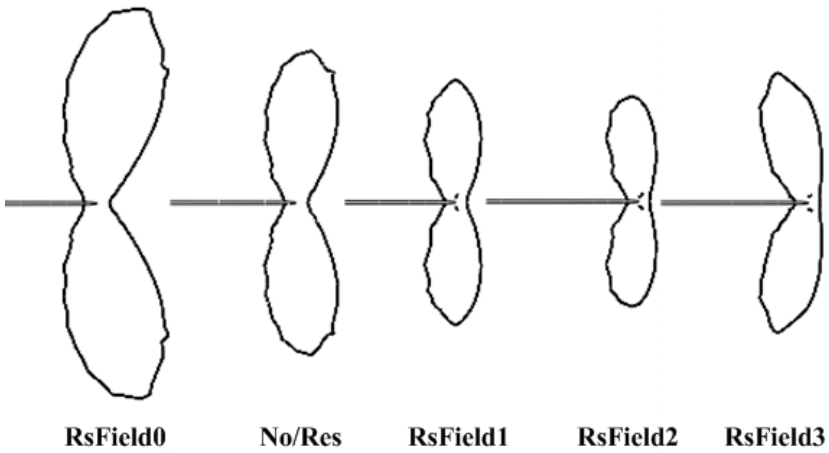
Figure 5.7: Plastic zone size when cleavage fracture occurs, ε^p=1%. E/σ_0=450, ν=0.3; n=0.1; $\Gamma_0 = 100$ N/mm, $\sigma_{max} = 3\sigma_0$.
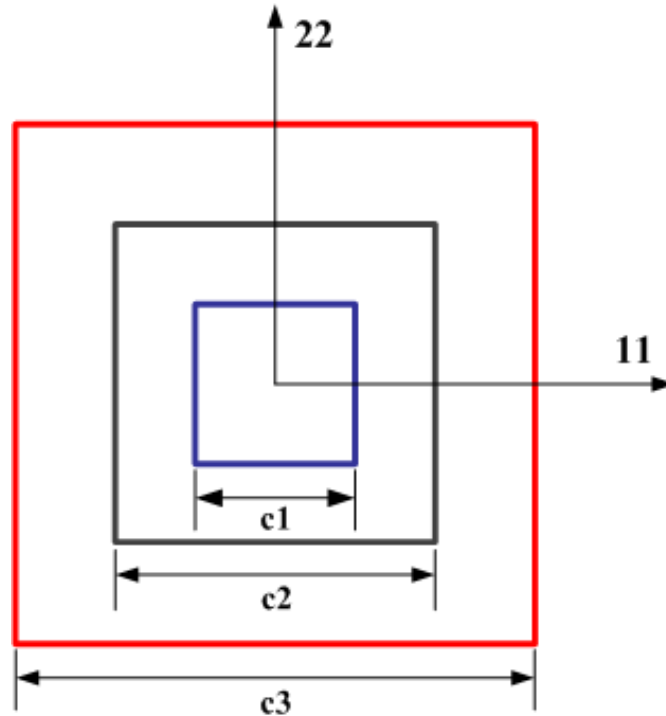
Figure 5.8: Schematic plot of different weld zone sizes considered in the study.

5.3.2   Effect of weld zone size

The length scale of residual stress field may play an important role on the effect of residual stress on cleavage fracture toughness. To better demonstrate this, three geometrically similar rectangular weld regions were constructed, as shown in Figure 5.8. The size of the weld is designated as c. Eigenstrain values α_{11}=0.004 and α_{22}=0.002 have been used to generate residual stress field for all welds. Residual stress fields represented by Size1, Size2 and Size3 respectively are showed in Figure 5.9, in which residual stresses are normalized by the yield stress and the distance from the crack tip is normalized by l_c. Residual stresses are tensile in the weld metal and show similar feature as the previous residual stresses showed in Figure 5.3. With the increase of the weld zone size, residual stress components parallel to the crack plane increases, and the size of the tensile dominated region of opening stress also increases.
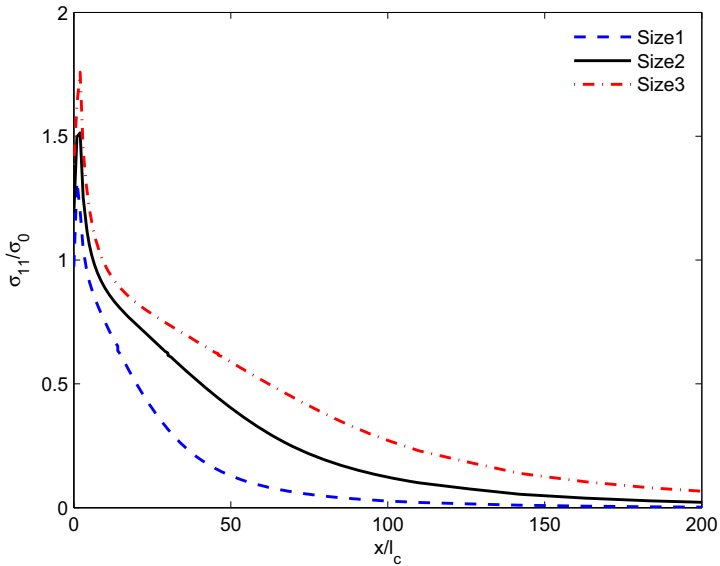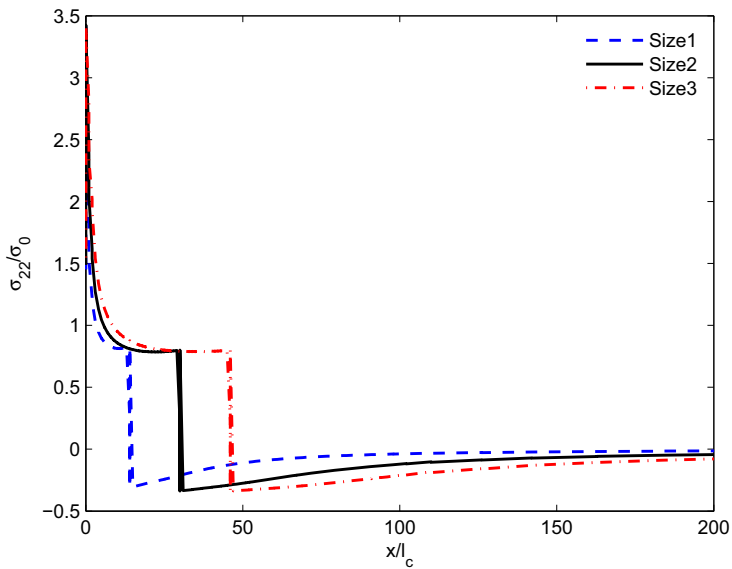
Figure 5.9: Residual stress distribution in MBL model for different weld zone sizes, (a) components parallel to the crack plane, and (b) normal to the crack plane. l_c is the uniform element size close to the crack tip. E/σ_0=450, ν=0.3; n=0.1; Γ_0 = 100 N/mm, σ_{max} = $3\sigma_0$; α_{11}=0.004, α_{22}=0.002.
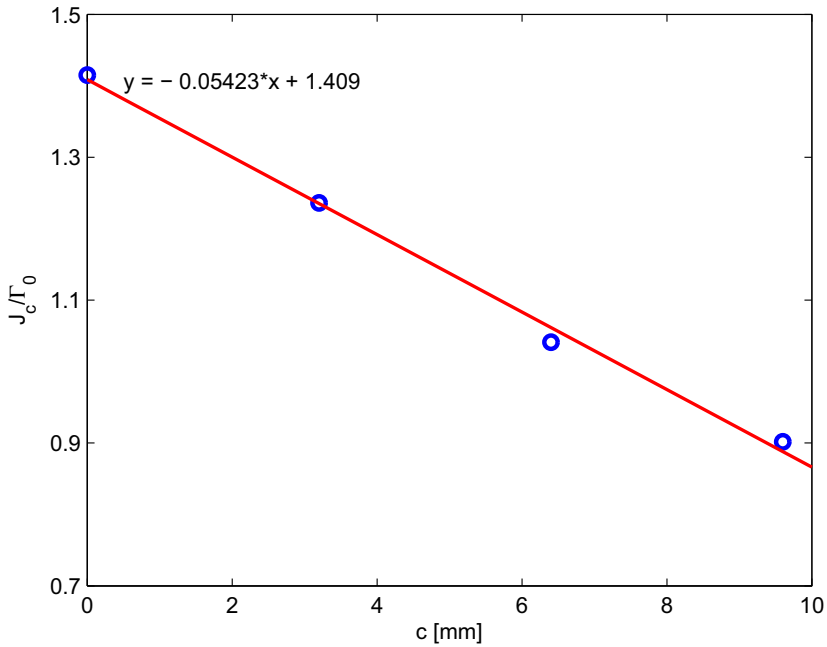
Figure 5.10: Effect of weld zone size on cleavage fracture toughness. E/σ_0=450, ν=0.3; n=0.1; $\Gamma_0 = 100N/mm$, $\sigma_{max} = 3\sigma_0$; α_{11}=0.004, α_{22}=0.002.

Figure 5.10 shows that the cleavage fracture toughness decreases with the increase of the weld region size c, which can be expected because both the residual stress level and tensile dominated residual stress region increases with the increase of the weld zone size. Furthermore, it is interesting to observe that the relationship between the cleavage fracture toughness and the weld zone size can be fitted by a linear function, i.e. $y = -0.05432x + 1.409$, which can possibly be used to predict the effect of residual stress on the cleavage fracture toughness for geometrically similar welds.

5.3.3   Effect of material hardening

In this study, the effect of the residual stress on the cleavage fracture toughness was investigated for three hardening exponents, i.e. n=0.05, 0.1 and 0.2. Residual stress field with α_{11}=0.004 and α_{22}=0.002, i.e. RsField3, was
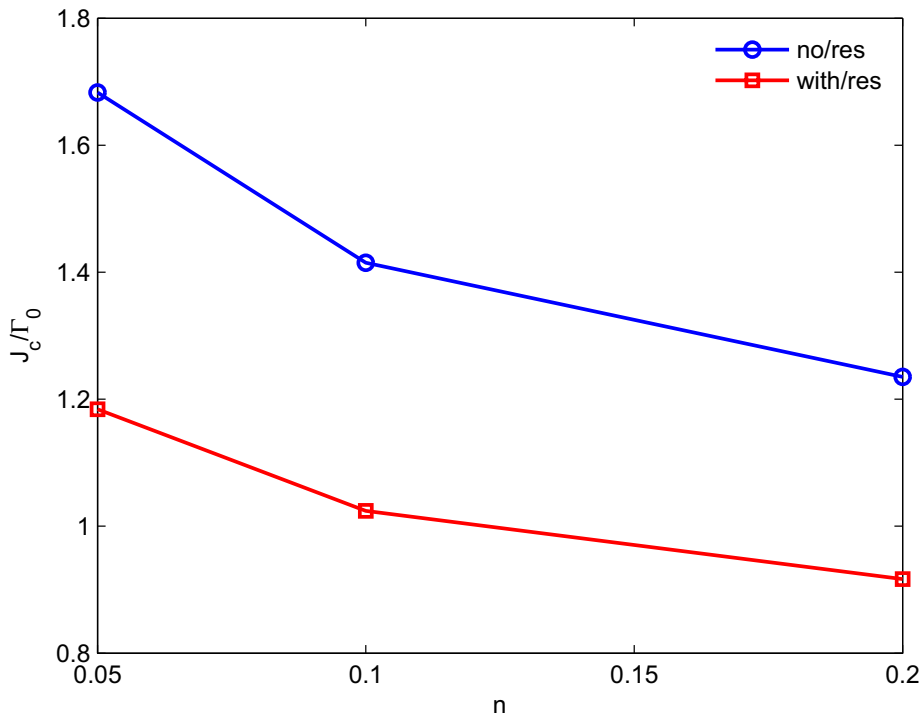
Figure 5.11: Effect of residual stress on cleavage fracture toughness for different hardening. E/σ_0=450, ν=0.3; Γ_0=100 N/mm; $\sigma_{max} = 3\sigma_0$; α_{11}=0.004, α_{22}=0.002.

introduced for study. The relationship between the cleavage fracture toughness and the hardening exponent for both with and without residual stress are showed in Figure 5.11, and the difference between two curves represents the effect of residual stress.

As shown in Figure 5.11, the existence of residual stress reduces the cleavage fracture toughness for all the cases analyzed. However, the effect of the residual stress decreases with the increase of material hardening. As it is known, fully developed plastic zone is easier to be achieved for weaker hardening material. Hence, the effect of plastic dissipation becomes significant, and a larger reduction of the cleavage fracture toughness can be expected.
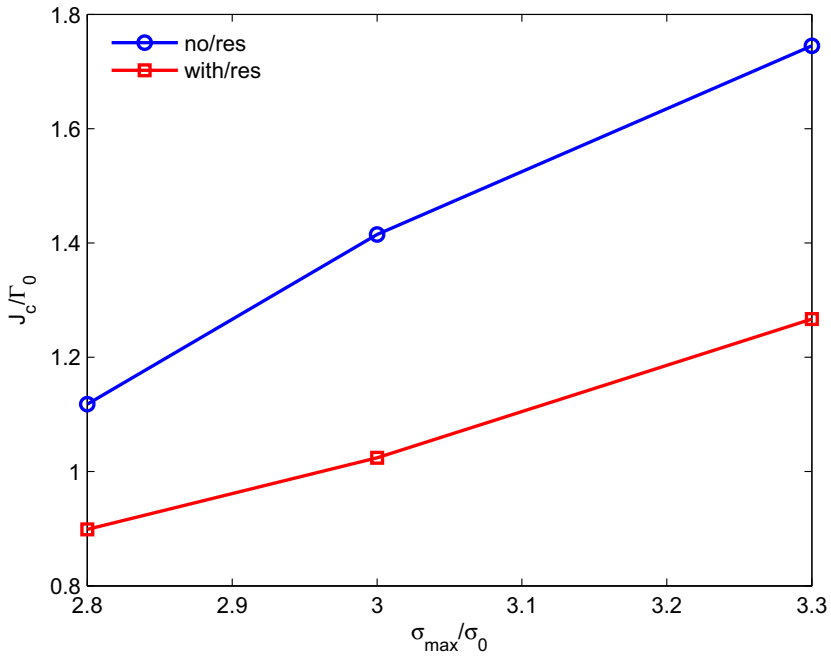
Figure 5.12: Cleavage fracture toughness as a function of maximum cohesive stress for both with and without residual stress cases. E/σ_0=450, ν=0.3; n=0.1; Γ_0=100 N/mm; α_{11}=0.004, α_{22}=0.002.

5.3.4 Effect of damage parameters

The cohesive energy Γ_0 and the maximum cohesive stress σ_{max} are two dominant parameters of the traction-separation-law. The effect of the residual stress on the cleavage fracture toughness may vary for different cohesive zone parameters. In present study, the effect of residual stress on the cleavage fracture toughness for three maximum cohesive stresses, i.e. $\sigma_{max}/\sigma_0 = 2.8$, 3.0 and 3.3 were studied firstly. Residual stress field with α_{11}=0.004 and α_{22}=0.002, i.e. RsField3, was used. Cohesive energy Γ_0 was fixed to be 100 N/mm. The relationship between the cleavage fracture toughness and the maximum cohesive stress is showed in Figure 5.12.

It can be seen that with the increase of σ_{max}, the reduction of cleavage fracture toughness due to residual stress increases. When the maximum cohesive stress is smaller, the energy needed to initiate a crack is less, and

a fully developed plastic zone cannot be formed. It has been shown that plastic dissipation only becomes significant compared to Γ_0 when fully developed plastic zone can form [122]. Thus, a stronger effect of residual stress on the cleavage fracture toughness can be expected for higher σ_{max}.

Γ_0 is another important parameter in cohesive zone model. In this study, the effect of the residual stress on the cleavage fracture toughness for different Γ_0 with same σ_{max} has also been investigated. Residual stress field with α_{11}=0.004 and α_{22}=0.002, i.e. RsField3, was introduced for the study. Figure 5.13 shows the comparison of the cleavage fracture toughness J_C for both with and without residual stress as the function of cohesive energy.

It can be seen that with the increase of the cohesive energy Γ_0, the cleavage fracture toughness increases for both with and without residual stresses, as shown in Figure 5.13(a). Figure 5.13(b) shows that the normalized cleavage fracture toughness tends to converge to the case without residual stress with increasing Γ_0. Note that the cleavage fracture toughness with residual stress was normalized by the toughness without residual stress effect. Figure 5.14 shows the effect of the residual stress on the plastic zone for different Γ_0, and the length of the fracture process zone (FPZ), which measures the distance between the point where all traction is lost and where the peak stress is first attained [122].

As shown in Figure 5.14(a) the residual stress increases the length of FPZ when Γ_0<150 N/mm, beyond which the residual stress does not affect the FPZ for the cases studied. However, the tensile residual stress both reduces the size of the plastic zone and rotates the plastic zone backward for all Γ_0, as shown in Figure 5.14(b). We can also observe that with the increase of Γ_0, the plastic zone size increases for both with and without residual stress cases, which can explain the increasing cleavage fracture toughness showed in Figure 5.13(a).

5.3.5   Effect of *T-stress*

In this study, no real structural component was considered. It is thus interesting to investigate the effect of residual stress on the cleavage fracture toughness for different geometry constraint levels characterized by *T-stress*. The outer boundary condition for the MBL model is governed by the elastic *K-field* and a *T-stress* under small-scale-yielding condition. For
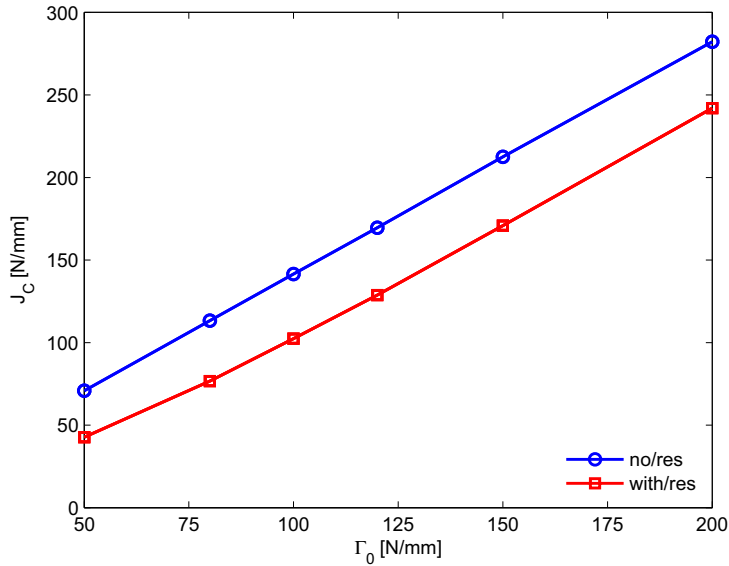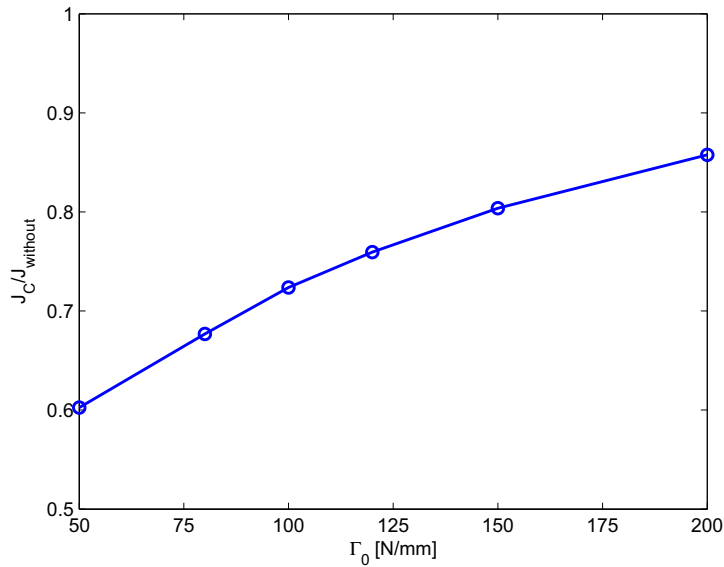
Figure 5.13: Relationship between the fracture toughness and cohesive energy, (a) absolute difference between the case with and without residual stress, and (b) normalized values. E/σ_0=450, ν=0.3; n=0.1; $\sigma_{max} = 3\sigma_0$; α_{11}=0.004, α_{22}=0.002.

(a)

(b)
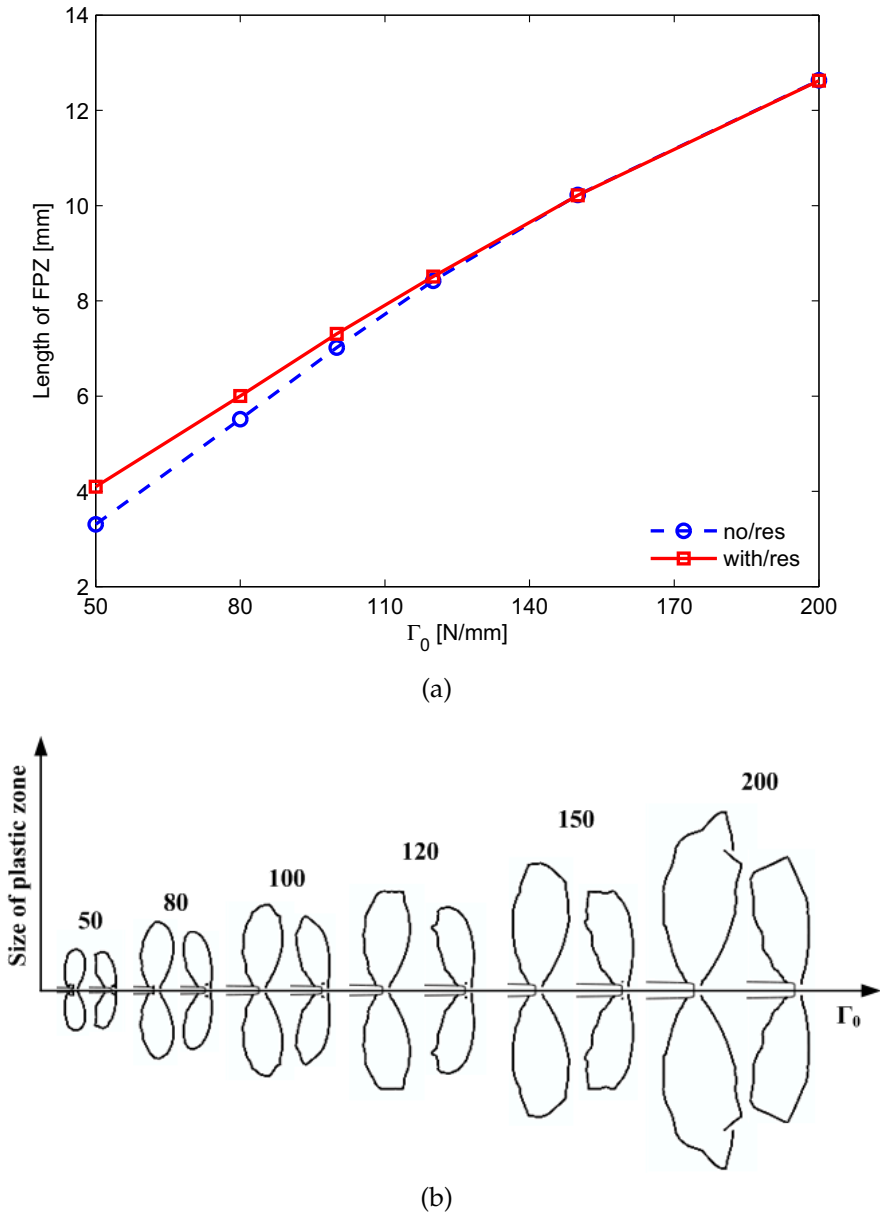
Figure 5.14: Effect of the residual stress on (a) the fracture process zone, and (b) plastic zone size of surrounding materials for ε^p=1%. E/σ_0=450, ν=0.3; n=0.1; $\sigma_{max} = 3\sigma_0$; α_{11}=0.004, α_{22}=0.002.
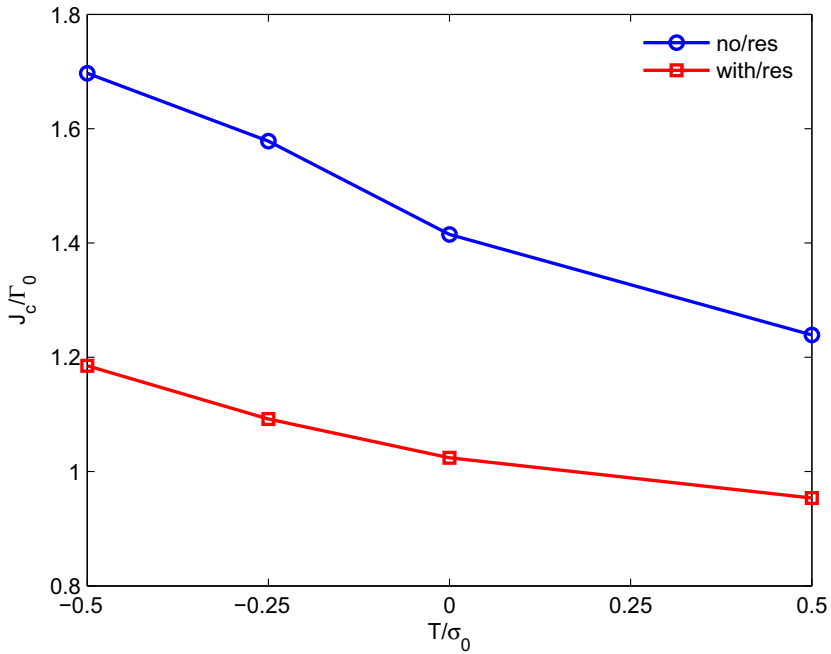
Figure 5.15: Effect of residual stresses on the cleavage fracture toughness for different T/σ_0. E/σ_0=450, ν=0.3; n=0.1; Γ_0=100 N/mm, $\sigma_{max} = 3\sigma_0$; α_{11}=0.004, α_{22}=0.002.

Mode I loading, K is the amplitude of the singular stress field, while the T is a non-singular stress term, acting parallel to the crack plane. Geometry constraint effects on fracture behaviour can be investigated by utilizing the *T-stress* [136]. In current study, *T-stress* with the value of T/σ_0= -0.5, -0.25, 0, and 0.5 was studied. The same residual stress field as previous with α_{11}=0.004 and α_{22}, i.e. RsField3, was used. The cleavage fracture toughness was plotted as the function of T/σ_0 in Figure 5.15.

It can be seen that with the increase of the *T-stress*, the cleavage fracture toughness decreases for both with and without residual stresses. As expected, with the increase of the *T-stress* the crack-tip constraint increases and thus the plastic zone shrinks. Similar results were also reported by Tvergaard and Hutchinson [137] in their study on the effect of *T-stress* on Mode I crack growth resistance in a ductile solid. It is interesting to observe that with the increase of the *T-stress* the effect of the residual stress
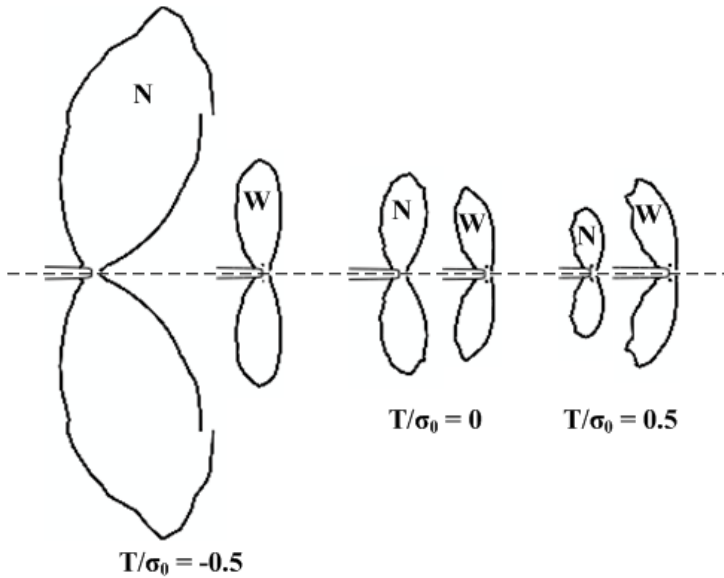
Figure 5.16: Effect of residual stress on size of plastic zone for different geometry constraint when ε^p=1% at initiation. E/σ_0=450, v=0.3; n=0.1; Γ_0=100 N/mm, $\sigma_{max} = 3\sigma_0$; α_{11}=0.004, α_{22}=0.002. "N" represents the case without residual stress; "W" denotes the case with residual stress.

decreases. Figure 5.16 shows the effect of the residual stress on plastic zone size for different *T-stress*.

It can be seen that the negative *T-stress* enlarges the plastic zone. However, the presence of tensile residual stress significantly decreases the size of the plastic zone and rotates the plastic zone backward slightly. The positive *T-stress* shrinks the plastic zone, and the residual stress further rotates the plastic zone backward. We thus can conclude that the tensile residual stress influences the cleavage fracture toughness similar way as the positive *T-stress*.

5.4 Conclusions

In this paper the effect of residual stresses on cleavage fracture toughness has been investigated. The damage mechanics-based cohesive zone model was utilized to simulate the fracture process zone. The modified boundary layer model simulations were performed under Mode I, plane strain

conditions, and the remote boundary conditions of the model is governed by elastic *K-field* and *T-stress*. Residual stresses were introduced into the FE model by the eigenstrain method. Cleavage fracture was assumed to occur when the opening stress of the first integration point of the first cohesive element ahead of the crack tip dropped to zero. *Far-field* contour *J*-integral has been employed to quantify the cleavage fracture toughness.

Cohesive zone model with a bilinear traction-separation-law was employed to study the effect of residual stresses on cleavage fracture behaviour. The introduction of a small fictitious viscosity in the traction-separation-law in combination with the use of a small step-increment in the simulations, improved the convergence rate, and its effect on the results is negligible.

Results show that residual stresses affect both the length of the fracture process zone and surrounding plasticity. Local compressive residual stress enhances the cleavage fracture toughness while positive residual stresses have opposite influences. The compressive residual stress enlarges the plastic zone significantly while tensile residual stresses shrink the plastic zone and shift the plastic zone backward. When the welds are geometrically similar, the effect of residual stresses on the cleavage fracture toughness is a linear function of the size of the weld. The dominant cohesive parameters Γ_0 and σ_{max} also play an important role on the effect of residual stresses on the cleavage fracture toughness. With the increase of cohesive energy, the effect of residual stresses on the cleavage toughness decreases. The reduction of the toughness caused by the residual stress increases with the increase of the maximum cohesive stress.

The effect of residual stresses on the cleavage fracture toughness becomes weaker for higher geometry constraint configuration. It has been found that residual stresses show similar behaviour as the *T-stress*. When combining the residual stresses with *T-stress*, the superposition principle can be applied. For higher geometry constraint configuration, the effect of tensile residual stress becomes smaller. However, for lower geometry constraint case, the combined effect can induce a significant reduction of the cleavage fracture toughness.

Chapter 6

Effect of residual stress on ductile fracture

Ductile crack growth plays an important role in the analysis of the fracture behaviour of structures [109]. Crack extension reduces the load-bearing ligament and will influence the capacity of the structures. Ductile crack growth may also change the near-tip stress/strain fields and promote the transition to unstable cleavage fracture. The mechanism of ductile fracture in metallic materials may be considered as a three-stage process: nucleation, growth and coalescence of microvoids. The ductile fracture process is influenced by the local conditions of stress triaxiality and plastic strain within the vicinity of a stress concentrator such as a notch or a crack-tip [51]. Liu et al. [44] and Ren et al. [17] have demonstrated that residual stresses can induce an additional crack-tip constraint, and a parameter R was defined based on the difference between the full stress field and the reference field to quantify the residual stress-induced crack-tip constraint. It is thus interesting to further investigate how residual stresses influence the local failure mechanisms and global ductile crack resistance.

6.1 Problem description

The present analyses were carried out for the conditions of small-scale-yielding. The MBL model used for this study consists of a weld region located in the center of the model, an outer base metal region, and a sharp crack in the center of weld. The load was applied to the remote edges of

(a)

(b)
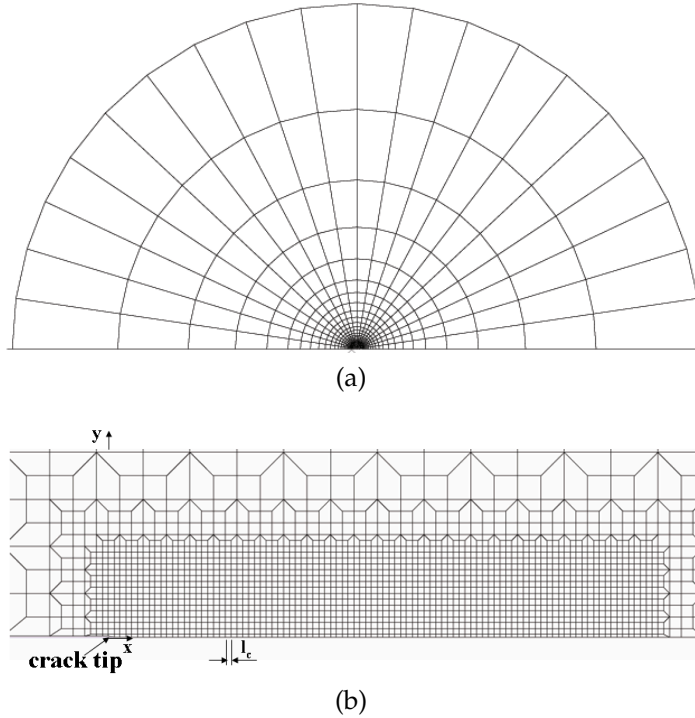
Figure 6.1: Modified boundary layer model, (a) global view; (b) crack-tip mesh.

the model through a displacement field (u, v), as shown in Eq. 3.2. The finite element computations were performed using ABAQUS [114]. Due to symmetry, only the upper half of the geometry is modeled. The mesh is shown in Figure 6.1. The radius of the MBL model is taken as 1000 mm to ensure the small-scale-yielding condition is fulfilled. Close to the crack tip, there is a rectangular region (9.4 mm ahead of the initial crack tip and 1.6 above the symmetry line) with uniform mesh sizes of 0.1×0.05 mm for the first layer and 0.1×0.1 mm for the rest of the layers are created. Full integration 4-node 2D plane strain elements are used. The finite element model has 2616 elements. Nonlinear geometry effects (NLGEOM in ABAQUS) are accounted for in the analyses. An initial opening of 0.02 mm is applied for the upper half model. When the residual stresses are introduced into the model, the crack faces can be partly closed. Thus, a rigid analytical plane is defined in the model to simulate the contact of the crack surfaces.

Two scenarios have been considered to study the effect of the residual stresses on the crack growth resistance in this thesis. Firstly, the effect of residual stresses on ductile crack resistance in a large round weld region was investigated. In such a way, the final crack growth length still locates in weld region. Secondary, a much smaller rectangular weld region was constructed, where the crack can propagate through the whole weld region. The effect of the weld zone size was also taken into account and studied. In addition, the effects of initial void volume fraction and material hardening have also been studied.

6.2   Residual stress field

The eigenstrain method was used to introduce residual stresses into the finite element model. A round weld region was introduced in the center of the model, as illustrated in Figure 6.2. According to the eigenstrain method, the thermal expansion coefficients of both the weld metal (α_w) and base metal (α_b) were assumed to be isotropic and equal to the eigenstrain values respectively. In this section, we assume α_b=0. Four residual stress fields were generated by setting α_w= -0.001, 0.001, 0.002 and 0.003 and designated as RsField0, RsField1, RsField2 and RsField3 respectively. Figure 6.3 shows the distribution of the residual stresses both before and after the crack was inserted. Note that the stresses are normalized by the yield stress, and the distance from the crack tip x is normalized by the size of the uniform element, i.e. l_c.

It can be seen that the negative eigenstrain value introduces the compressive residual stress at the weld region while the positive ones generate tensile residual stresses. Both tensile and compressive residual stresses parallel to the crack front converge to zero far from the crack tip. The opening residual stresses are self-balanced ahead of the crack tip. There is a sharp turning point in the distribution of the opening residual stresses, which is the region where eigenstrain discontinuities have been introduced into the FE model, namely the weld metal-base metal boundary. The tensile residual stresses also show similarity, and the level of the tensile residual stress increases with the increasing α_w. Due to the singularity, σ_{11} is about 800 MPa and σ_{22} is about 1200 MPa at the crack tip for RsField2. Figure 4 also shows that residual stress components are smaller than the yield stress before the crack was inserted.
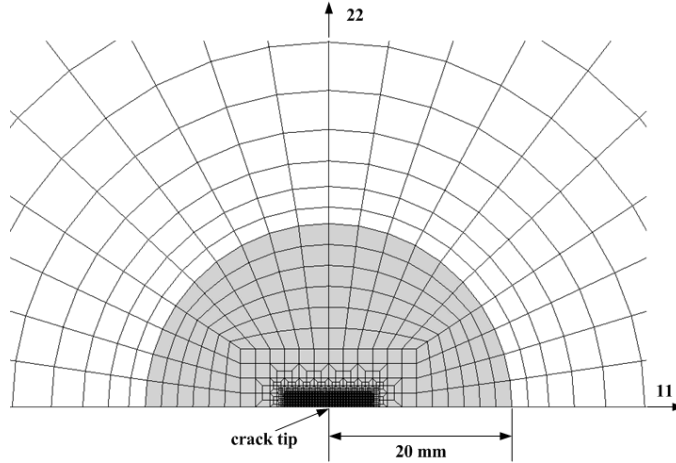
Figure 6.2: Illustration of the weld region (gray area). The radius of the weld is 20 mm.

6.3 Results

In fracture mechanics, the J-integral [8] or Crack Tip Opening Displacement (δ, CTOD) are used to characterize the crack-tip driving force of a cracked body made of an elastic-plastic material. The J-integral is a path-independent integral based on the assumption that the strain energy density is a single-valued function of the strain (or stress) [12]. However, non-proportional loading may occur in the region where the J-integral is evaluated and lead to path-dependence, for example, in the case of ductile crack growth [109], or in the presence of a residual stress field [11]. In this study, the J-integral is evaluated on contours far away from the zone of highly non-proportional loading, and displays practically path independence in both cases with and without residual stresses. J in the following context thus represents *far-field J*-integral.

6.3.1 Effect on ductile crack growth resistance

Ductile crack growth resistance is important for structural integrity assessment, and it is interesting to investigate the effect of residual stresses on it. In this section, effects of residual stress fields on the crack growth resistance were studied. The initial void volume fraction f_0 is fixed to be
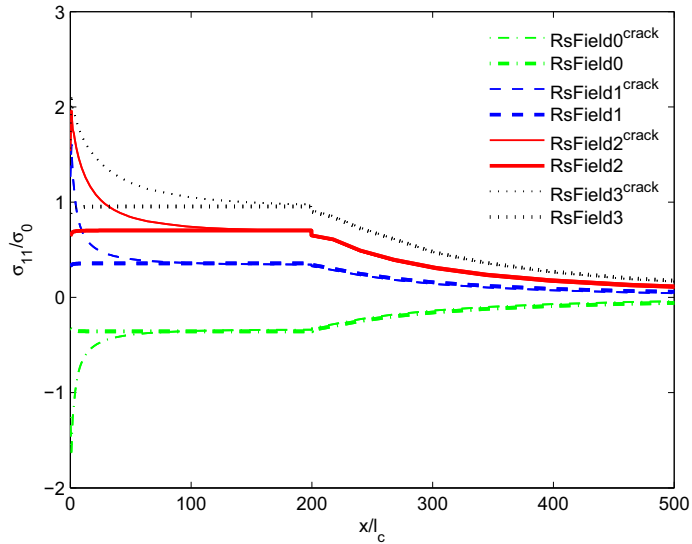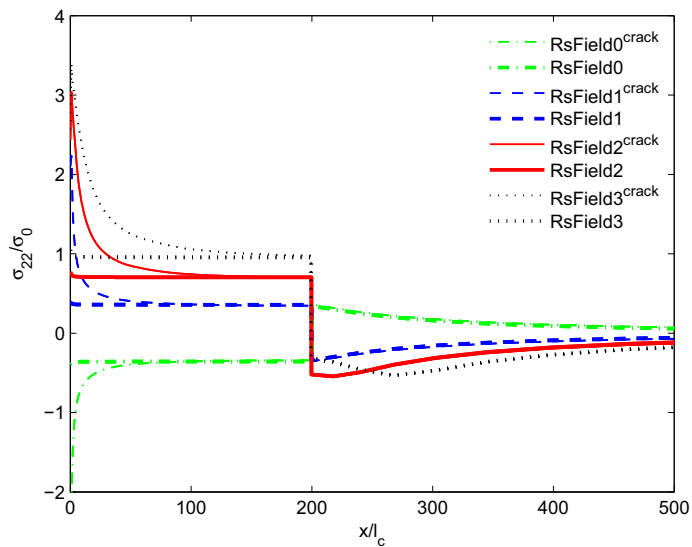
Figure 6.3: Comparison of the residual stress distribution in MBL model with a large round weld before (bold line) and after (thin line) the crack was inserted, (a) components parallel to the crack plane, and (b) normal to the crack plane. Four different residual stress cases were considered, where RsField0 is compressive and the remaining 3 are tensile. α_b=0, α_w=-0.001, 0.001, 0.002 and 0.003.

0.1% and the strain hardening exponent n equals to 0.1. The crack growth resistance described by the J-integral is showed in Figure 6.4.

For the cases chosen, the residual stresses seem to have significant effects on the ductile crack growth resistance. Figure 6.4(a) shows that the compressive residual stress enhances the crack growth resistance while the tensile residual stresses have the opposite effect. With the increase of tensile residual stress, the crack growth resistance decreases. The absolute difference between the case with and without residual stress increases with the increase of crack growth. Figure 6.4(b) presents the normalized crack growth resistance. The resistances with residual stresses were normalized by the resistance at the same crack growth without residual stresses. The distance from the original crack tip was normalized by l_c. It can be seen that the tensile residual stresses significantly decrease the initiation toughness while the compressive residual stress increase it. With advancing crack growth, the effect of the residual stresses decreases and approaches to a constant value. Note that the current crack grows only to 3 mm, which is very small compared to the size of the residual stress dominant length scale shown in Figure 6.3. As shown in Figure 6.3, beyond the singularity affected zone ($x/l_c > 30$, i.e. 3 mm), the residual stress fields approach a hydrostatic stress state. Thus, the residual stresses cannot be easily released by the crack growth, and the effect of residual stresses retains.

In order to better understand the effect of residual stress on crack growth resistance, a smaller rectangular weld region was constructed, as illustrated in Figure 6.5. In this section, α_b=0, and α_w was assumed to be orthogonal and characterized by α_{11} and α_{22} in following context. The ratio α_{11}/α_{22} was fixed to be 2. Four residual stress fields with α_{22}=-0.001, 0.001, 0.002 and 0.003 were generated and represented by RsField0, RsField1, RsField2 and RsField3 respectively, as shown in Figure 6.6. It should be noted that the eigenstrain values selected here are taken from experimental measurement results in literature [129, 134].

The absolute and normalized crack growth resistances are shown in Figure 6.7. It can be seen that the compressive residual stress increases the crack growth resistance while tensile residual stresses decrease the crack growth resistance, as shown in Figure 6.7(a). Figure 6.7(b) shows that the reduction of the crack growth resistance converges with crack growth to the case without residual stress. As known, the quantity σ_m/σ_e defines a convenient measure of triaxiality linked to the growth rate of micro-scale voids consistent with the subsequently introduced damage measures
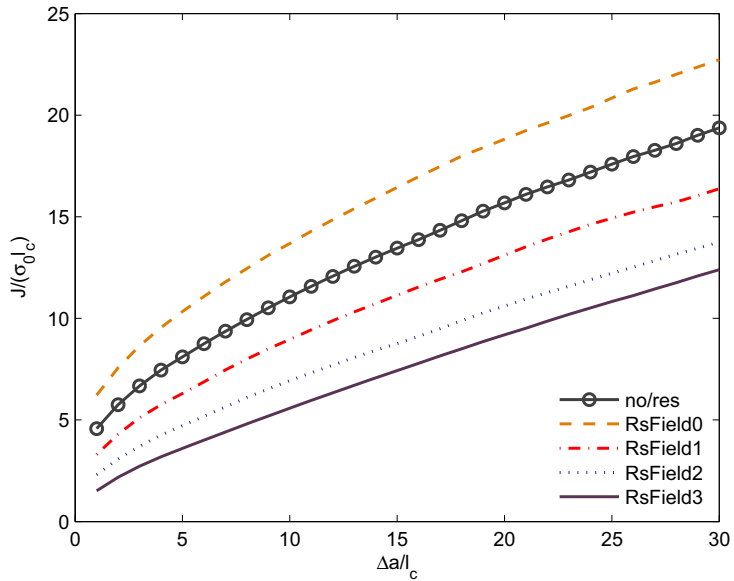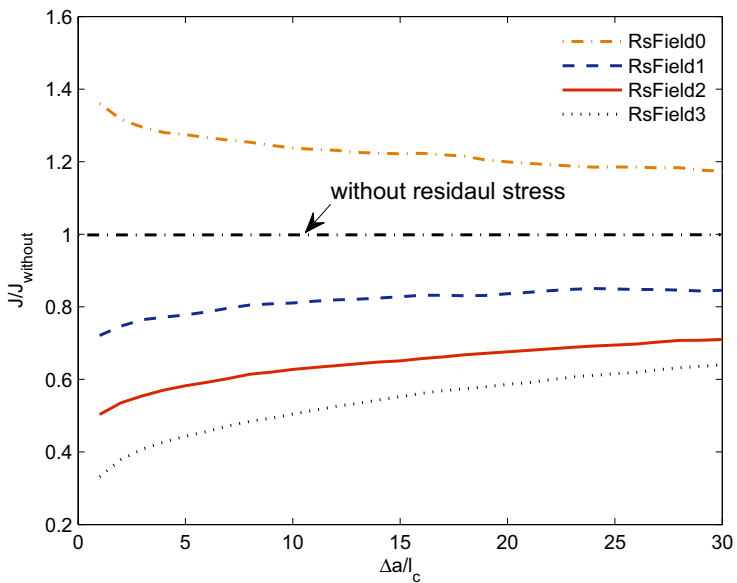
Figure 6.4: Effect of residual stresses on crack growth resistance, (a) absolute crack resistance curves; (b) normalized crack resistance curves. f_0=0.1%; n=0.1; E/σ_0=500.
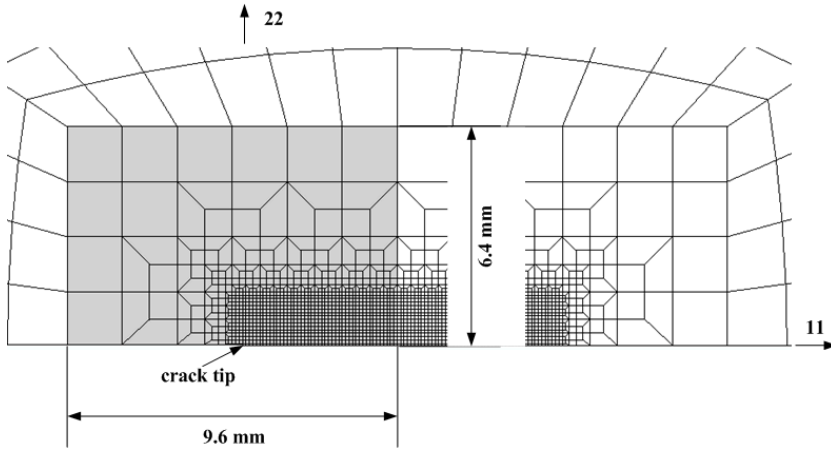
Figure 6.5: Illustration of the weld region (gray area). The length of the weld region along the "11" direction is 9.6 mm, and the length along the "22" direction is 6.4 mm .

[138]. Therefore, we investigated the distribution of triaxiality ahead of the crack tip. Figure 6.8 presents the triaxiality values on the ligament ahead of the original crack tip for different crack growth. The distance from the original crack tip are scaled by J/σ_0, or equivalently $(K_I/\sigma_0)^2$, which defines approximately the value of crack-tip opening displacement and provides a physical meaningful length-scale for normalization.

It can be seen that tensile residual stresses enhance the triaxiality values while the compressive residual stress reduce the triaxiality value at the crack initiation, see Figure 6.8(a), which corresponds to our previous findings [17, 44]. However, the effect of residual stress on triaxiality tend to be negligible when the crack advanced to 3.5 mm, as shown in Figure 6.8(b). Higher stress triaxility corresponds to a smaller plastic zone. Thus, the energy dissipated by the plastic deformation is smaller, which in turn result in a lower crack growth resistance.

6.3.2   Effect of weld zone size

The length scale of the residual stress field may play an important role on the effect of residual stress on ductile crack growth resistance, as shown in Section 6.3.1. To better demonstrate this, four geometrically similar rectangular weld regions were constructed, as illustrated in Figure 6.9. The
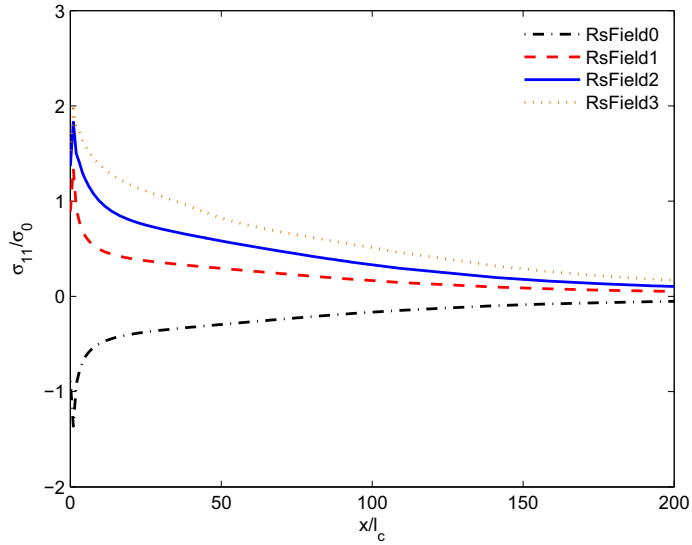
(a)
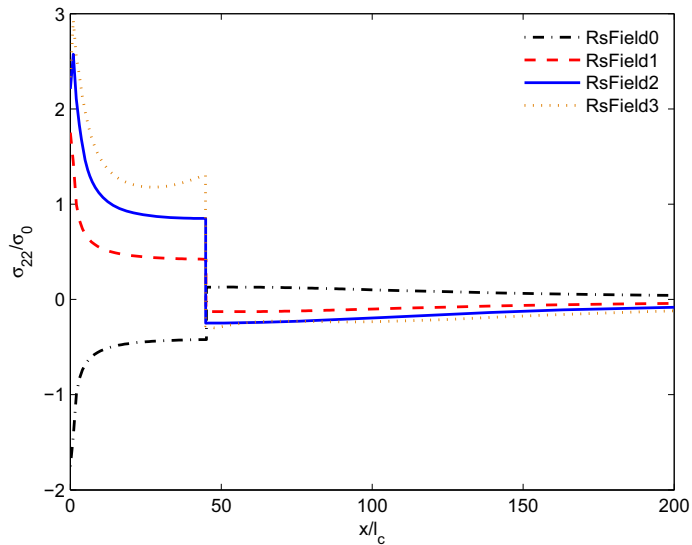
(b)

Figure 6.6: Residual stress distribution in MBL model with a rectangular weld after the crack was inserted, (a) components parallel to the crack plane, and (b) normal to the crack plane. Four different residual stress cases were considered, where RsField0 is compressive and the remaining 3 are tensile. $\alpha_{11}/\alpha_{22}=2$, α_{22}=-0.001, 0.001, 0.002 and 0.003.
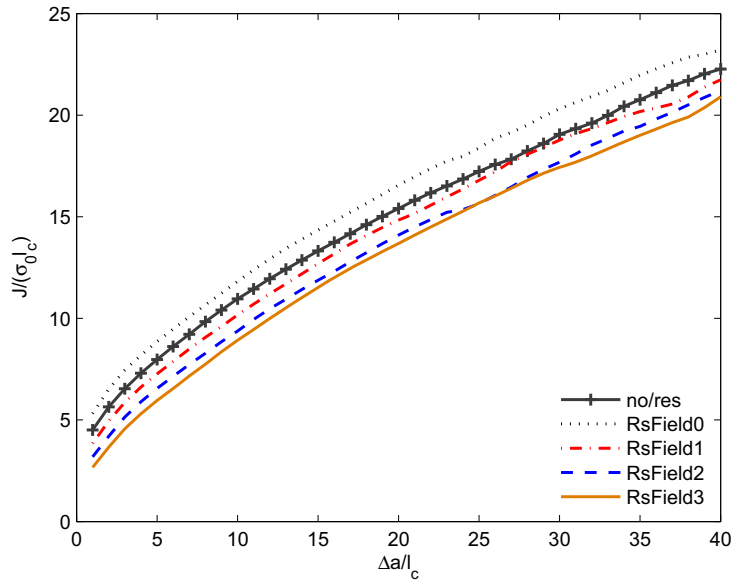
(a)
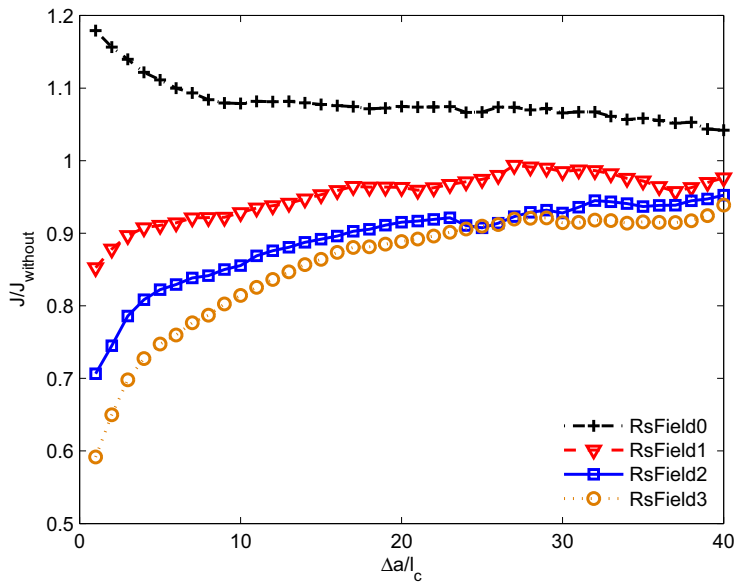
(b)

Figure 6.7: Effect of residual stresses on crack growth resistance, (a) absolute crack resistance curves; (b) normalized crack resistance curves. f_0=0.1%; n=0.1; E/σ_0=500.
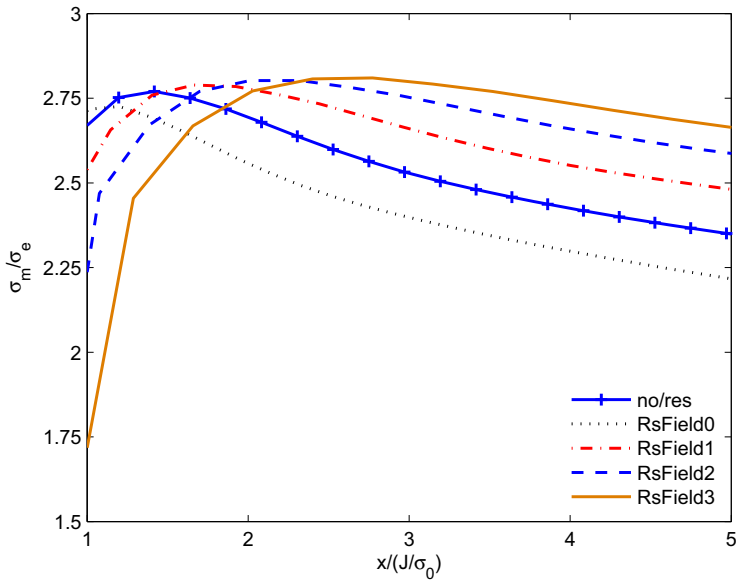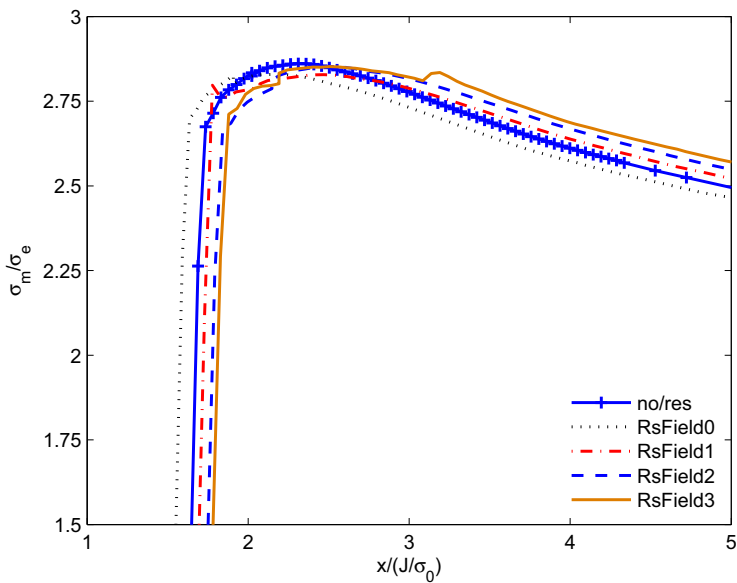
Figure 6.8: Triaxiality values ahead the crack tip for different crack propagation, (a) Δa=0.1 mm; (b) Δa=3.5 mm. f_0=0.1%; n=0.1; E/σ_0=500.
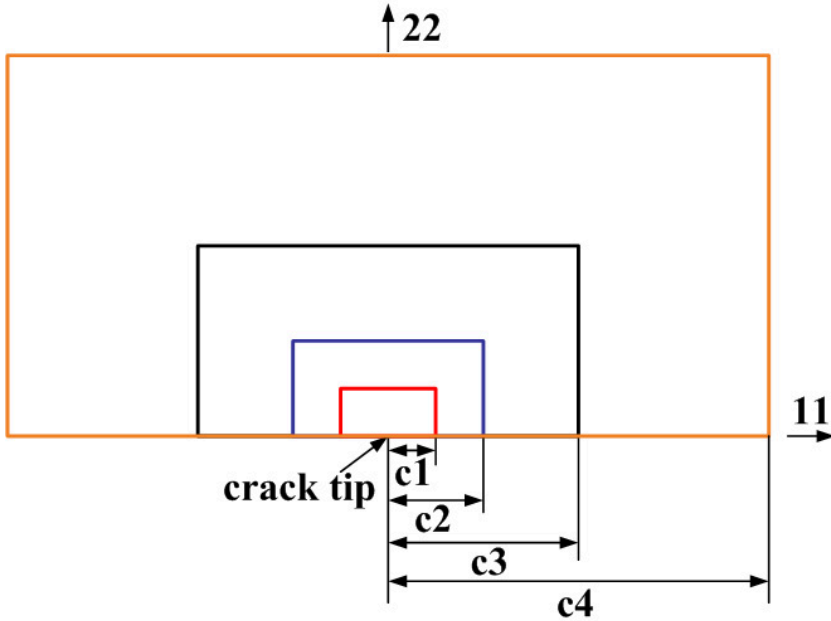
Figure 6.9: Illustration of weld size. The size increases by a scale of 2.

size of the weld is designated as c. The orthogonal thermal expansion co-efficient was used with a value of α_{11}=0.004 and α_{22}=0.002 for all welds. The residual stress fields designated as Size1, Size2, Size3 and Size4 respectively are showed in Figure 6.10. The residual stresses are tensile in the weld metal and show similar features as the previous residual stresses shown in Figure 6.6. With increasing weld size, the residual stresses parallel to the crack plane increase; and the size of tensile dominated region of the opening stress also increases.

Figure 6.11(a) presents the absolute crack growth resistance. In Figure 6.11(b), crack growth length was normalized by l_c. It can be seen that the residual stresses generated in the larger welds influence more significantly the crack growth resistance. With increasing crack growth, the effect of the residual stresses on the crack growth resistance converges to the case without residual stresses. However, an interesting pattern emerges when normalizing the crack growth length by the weld zone size c, as shown in Figure 6.12. Surprisingly, the normalized crack growth resistances collapse into one curve, which indicates that the effect of the residual stresses on the crack growth resistance is nearly independent of the weld zone size.
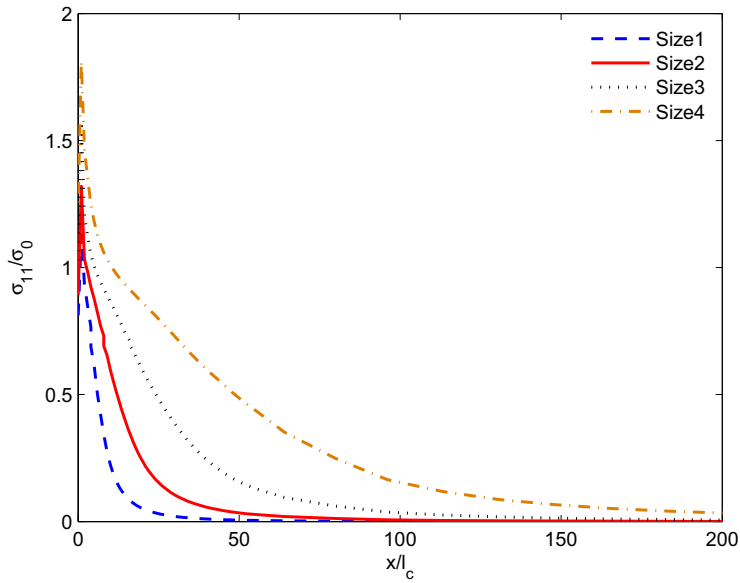
(a)
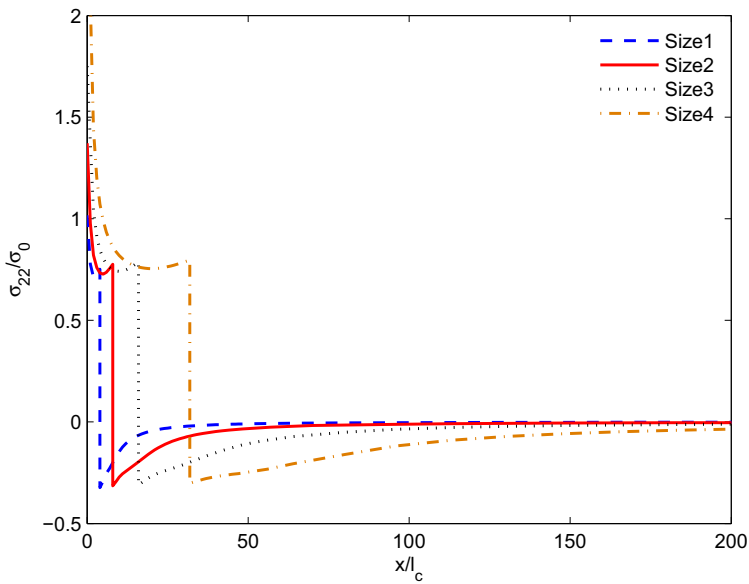
(b)

Figure 6.10: Residual stress distribution in MBL model with geometrically similar welds after the crack was inserted, (a) components parallel to the crack plane; (b) normal to the crack plane. α_{11}=0.004, α_{22}=0.002.
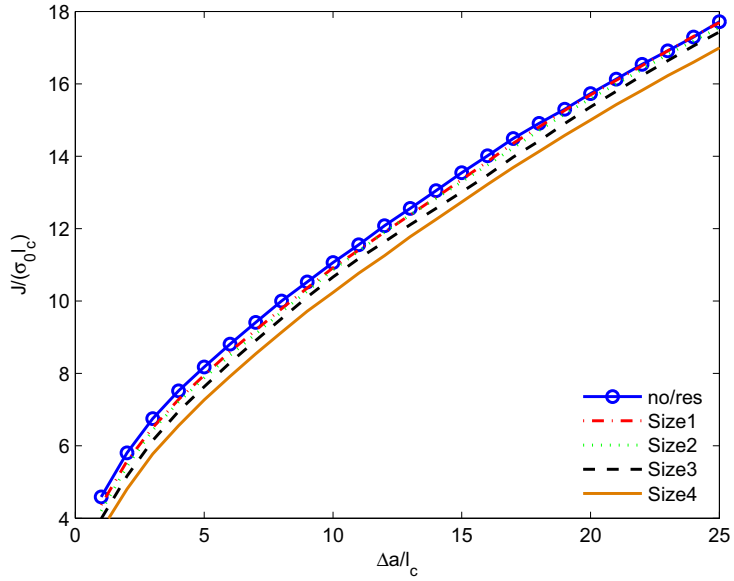
(a)
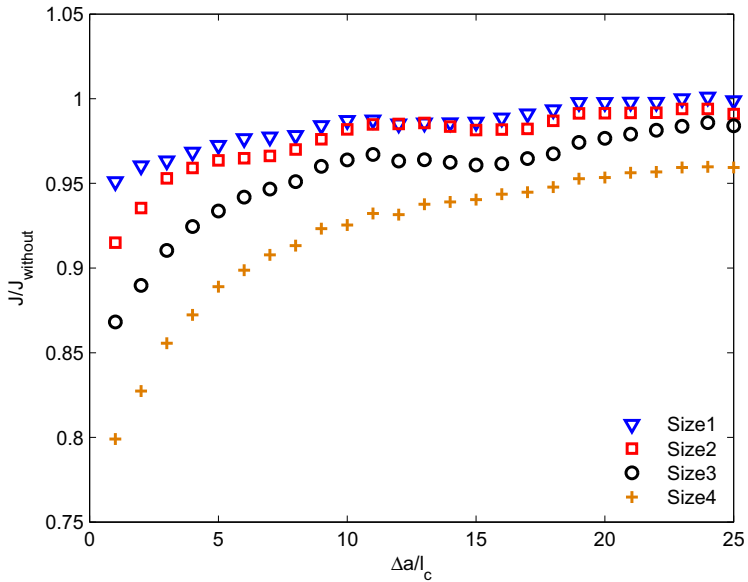
(b)

Figure 6.11: Effect of weld size on crack growth resistance, (a) absolute crack growth resistance, and (b) crack growth resistance normalized by l_c. f_0=0.1%; n=0.1; $E.\sigma_0$=500.
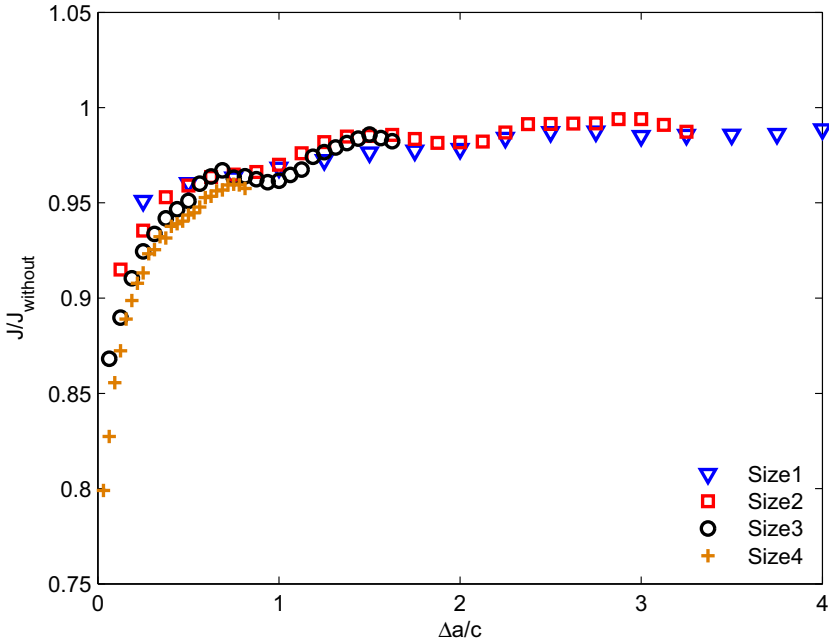
Figure 6.12: "Mater" curve obtained by normalizing the crack growth resistance by the weld zone size c.

For the cases specified in this section, when the crack grows approximately to 3 times of c, the effect of residual stresses can be neglected. For geometrically similar welds, the uniform curve can be used to roughly predict the length scale of residual stress-affected region beyond which the effect of the residual stress can be neglected. To better demonstrate our finding, residual stress fields were presented by normalizing the distance from the crack tip by weld zone size, as shown in Figure 6.13.

It can be seen that residual stress field collapse into a uniform field, which can explain the results showed in Figure 6.12. In our previous study [17], residual stress fields generated in three larger round weld regions respectively can also be normalized by the weld size and collapsed into a uniform field. Thus, a "master" curve similar as the curve shown in Figure 6.12 can also be expected.
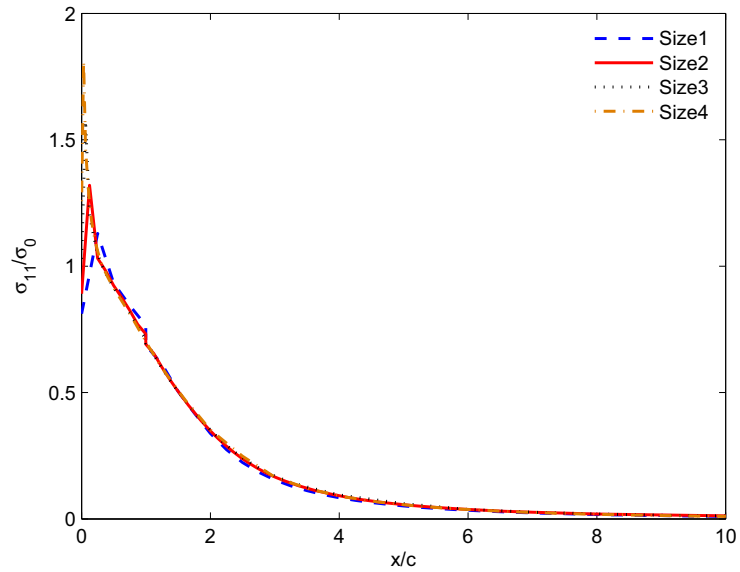
(a)
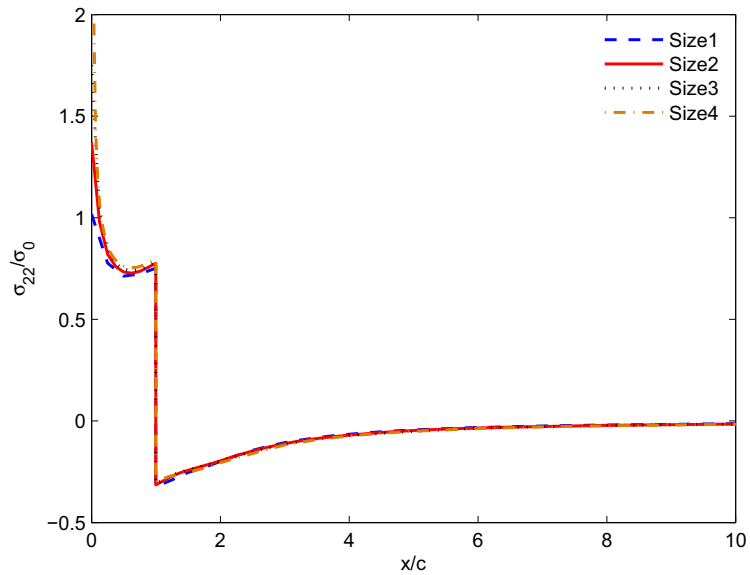
(b)

Figure 6.13: Residual stress distribution normalized by the weld zone size after the crack was inserted, (a) components parallel to the crack plane; (b) normal to the crack plane.

6.3.3 Effect of material hardening

It has been shown that the effect of strain hardening on the ductile crack resistance is not fully understood. Xia and Shih [139] demonstrated that the ductile resistance increases with increasing hardening capacity. However, Eikrem et al. [140] and Østby et al. [109, 141] reported that decreasing the hardening exponent will significantly raise the resistance curve. In this study, the effect of strain hardening on the crack growth resistance was investigated for cases both with and without residual stress. It should be noted that in this particular study, the initial volume fraction f_0 was fixed to be 0.05%, and the residual stress field was introduced by the rectangular weld with orthogonal thermal expansion coefficient α_{11}=0.004 and α_{22}=0.002, i.e. RsField2 in Figure 6.6. The crack growth resistance was plotted as a function of hardening exponent n in Figure 6.14.

Figure 6.14(a) shows that with decreasing hardening exponent the crack growth resistance increases for both with and without residual stress cases, which corresponds to the results demonstrated in Ref. [109, 140, 141]. For a given hardening exponent, residual stresses reduce both the initial toughness and crack growth resistance. Also, the effect of residual stress on the ductile resistance becomes stronger for stronger hardening material, as shown in Figure 6.14(b). With increasing crack growth, the reduction of the crack growth resistance decreases and tends to converge to the case without residual stress. Residual stresses reduce the equivalent plastic strain significantly at crack initiation, which indicates smaller plastic deformation. Hence, lower crack growth resistance curves can be expected. With the crack growth, the effect of residual stresses on the equivalent plastic strain becomes negligible for different hardening exponents.

6.3.4 Effect of initial void volume fraction

The initial void volume fraction f_0 represents the degree of damage in the material. The larger the initial void volume fraction is, the larger damage the material has. In this section, the effect of residual stress fields on crack growth resistance was investigated for three initial void volume fractions, $f_0 = 0.05\%, 0.1\%$ and 0.2%. The residual stress was introduced into a rectangular weld with α_{11}=0.004 and α_{22}=0.002, i.e. RsField2 in Figure 6.6. The crack growth resistance curves are shown in Figure 6.15.

As shown in Figure 6.15(a), for both with and without residual stress
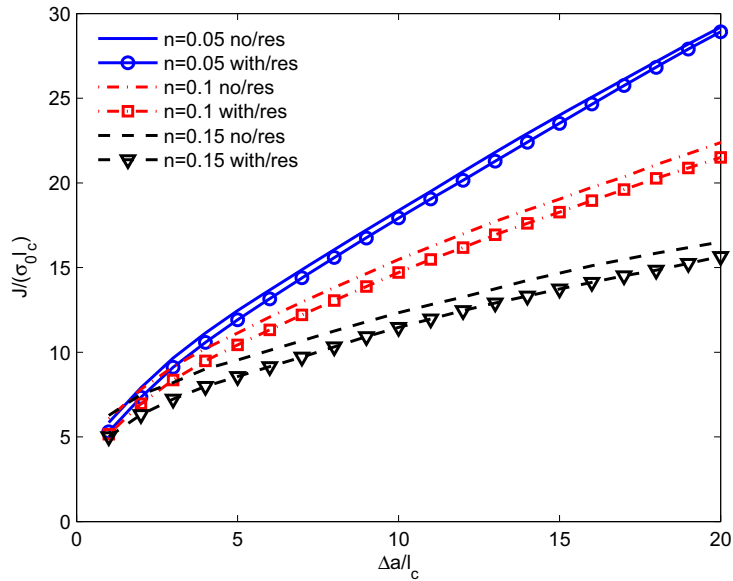
(a)
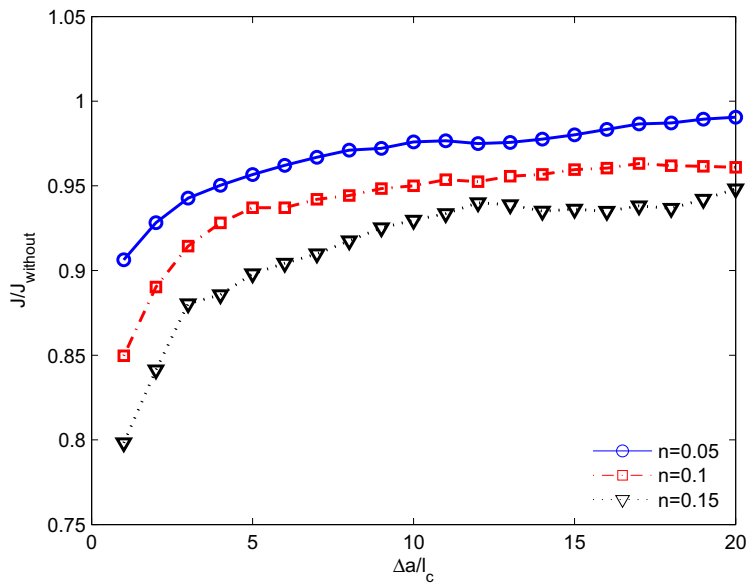
(b)

Figure 6.14: Effect of residual stresses on crack growth resistance for different hardening, (a) absolute crack growth resistance curves; (b) normalized crack resistance curves. α_{11}=0.004, α_{22}=0.002; f_0=0.05%; E/σ_0=500.

(a)

(b)

Figure 6.15: Effect of residual stresses on crack growth resistance for different initial void volume fraction, (a) absolute crack growth resistance curves; (b) normalized crack resistance curves. $\alpha_{11}=0.004$, $\alpha_{22}=0.002$; n=0.1; $E/\sigma_0=500$.

cases, the crack growth resistance increases with the decrease of f_0, which can be expected because the ductility becomes better when initial void volume fraction decreases. Also, it can be observed that the residual stress reduces the crack growth resistance for fixed f_0. Normalized crack resistance curves shown in Figure 6.15(b) indicate that with increasing crack growth, the effects of residual stresses decrease and become less dependent on f_0. The residual stress enhances the opening stress beyond the larger strain effect region compared with the case without residual stress at crack initiation, which induces an increase of crack-tip constraint [17, 44], and a lower fracture toughness can then be expected. However, it has been found that the effect of the residual stress on opening stress becomes negligible when crack growth becomes larger.

6.3.5 Effect of T-stress

Crack-tip constraint effects on fracture toughness have received considerable attention recently. In our earlier work [17], we have found that the residual stress-induced crack-tip constraint is lower for a higher geometric constraint. Xia and Shih [139], Tvergaard and Hutchinson [137] studied the effect of *T-stress* on the crack growth resistance and showed that a negative *T-stress* results in a rapidly rising resistance curve while the positive *T-stress* lowers the fracture resistance. It is thus interesting to investigate how residual stress combined with varying *T-stress* affect the crack growth resistance. In this work, T/σ_0=-0.5, 0 and 0.5 were studied. The initial void volume fraction is fixed to be 0.1%, and the residual stress with α_{11}=0.004 and α_{22}=0.002, i.e. RsField2 in Figure 6.6, was introduced. The absolute and normalized resistance curves are shown in Figure 6.16.

It can be seen that the tensile residual stress reduces the crack growth resistance for all T/σ_0 cases, as shown in Figure 6.16(a). Figure 6.16(b) shows that the normalized crack growth resistance is lower for smaller *T-stress*. However, the differences between the normalized crack growth resistances are insignificant. It should be noted that a relatively small initial void fraction was used in this study, i.e. f_0=0.1%. With increasing crack growth, the effect of residual stresses on crack growth resistance tends to be independent of the *T-stress*. The positive residual stresses reduce the plastic strain compared to the case without residual stresses. Lower equivalent plastic strain indicates a smaller plastic zone and thus the en-
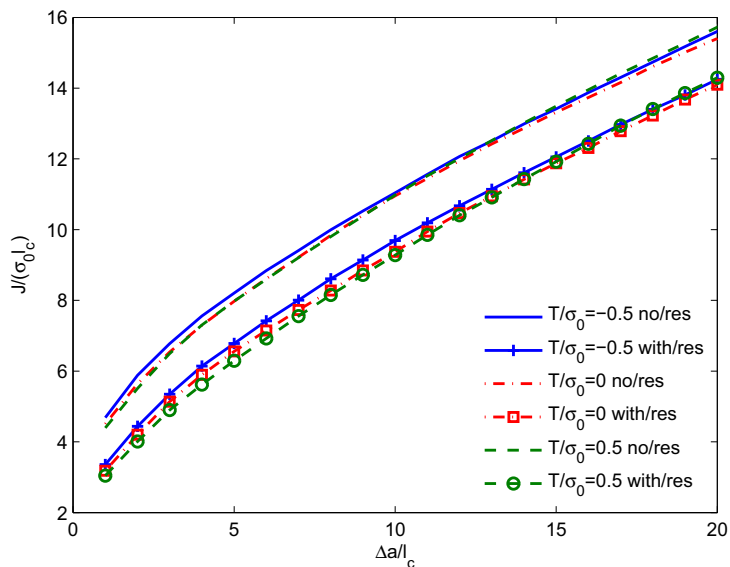
(a)
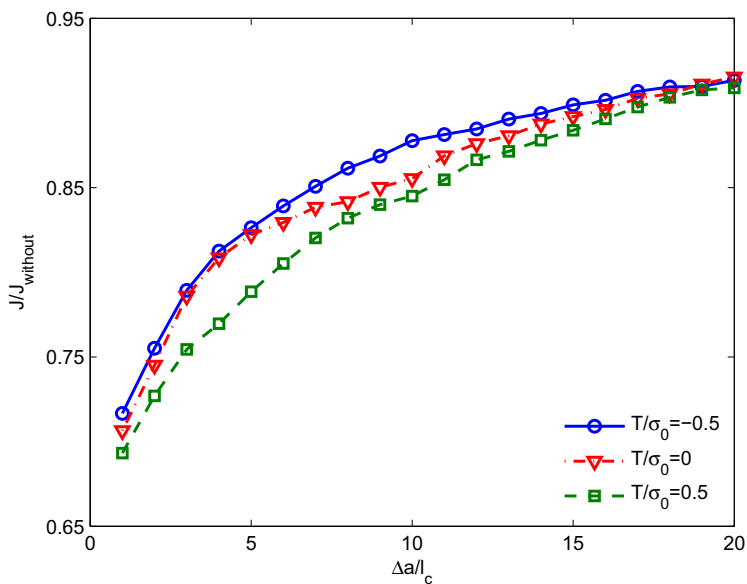
(b)

Figure 6.16: Effect of the residual stress on normalized crack growth resistances for different T/σ_0, (a) absolute crack growth resistance curves; (b) normalized crack resistance curves. α_{11}=0.004, α_{22}=0.002; f_0=0.1%; n=0.1; E/σ_0=500.

ergy dissipated by the plastic deformation decreases. In turn, the ductile crack toughness decreases. When the crack growth becomes larger, the effect of residual stresses on the equivalent plastic strain becomes negligible.

6.4 Conclusions

This study describes a systematic computational investigation of the effect of residual stresses on ductile crack growth resistance. 2D plane strain finite element analysis have been carried out in a modified boundary layer model with the remote boundary condition governed by *K-field* and *T-stress*. The large strain effect was taken into account in the analysis. The complete Gurson model was utilized to predict the crack growth resistance for both with and without residual stress situations. Residual stresses were generated by the eigenstrain method and introduced into the FE model. Both the tensile and compressive residual stress fields were introduced. However, tensile residual stress was known to be detrimental for the fracture. Thus, the effect of the tensile residual stress on crack growth resistance was mainly presented. Residual stresses as an additional field do not alter the material constitutive relation, however, the residual stress may influence the near-tip stress state and enhance the level of damage along the ligament ahead of an advancing crack tip. The following conclusions can be made:

1. Tensile residual stresses reduce the crack growth resistance while compressive residual stress can enhance the crack growth resistance. With the increase of crack growth, the effect of residual stresses decreases and converges to the case without residual stress. The initial damage of the ligament elements caused by the residual stress is negligible for the cases studied.

2. Under certain circumstances, the effect of the residual stresses on ductile crack growth resistance can be normalized by the size of the geometrically similar weld, and the normalized crack growth resistance curves collapse into a single curve. One can use this curve to evaluate the effect of the residual stress on the structural integrity and simplify the assessment procedure. It can also be used to predict the length scale of the residual stress-affected range beyond which the effect of the residual stresses can be neglected. For the cases specified in this study, when the crack grows to a length of $3c$ the effect of the residual stresses can be neglected.

3. The reduction of the crack growth resistance caused by residual stresses is smaller for weaker hardening materials, and the influence of the residual stresses decreases with crack propagation.

4. Residual stress reduces the crack growth resistance more significantly for the materials with larger initial void volume. The influence of the residual stresses decreases with the crack growth and becomes independent of f_0.

5. The reduction of the crack growth resistance induced by the residual stress increases with increasing T/σ_0 at the early stage of crack growth and then tend to be negligible when the crack growth is larger. The results are in line with our earlier findings that the effect of residual stress on the crack-tip constraint becomes weaker for higher T/σ_0.

The present study indicates that residual stress as an additional stress field can alter the stress state near the crack tip and further influence the ductile crack growth resistance. Triaxility or crack-tip constraint was shown to play an important role in the ductile fracture behaviour. Therefore, the residual stress-induced crack-tip constraint is a very important factor to consider in structural integrity assessment. In Chapter 4, we have defined a parameter R to quantify the residual stress-induced crack-tip constraint. However, the effect of residual stress on the ductile crack resistance has not been linked with R by a quantitative way in this chapter. The reason for this is that the residual stress field in reality is very complicated, hence one should find an efficient way to standardize the distribution of the residual stresses for typical weld joints. To reduce the conservatism of current integrity assessments, a proper description of the residual stress field is very important. Once a proper description of the residual stress is obtained, the "master" curve, though obtained from the MBL model, can be applied to real engineering structures and components that contain similar residual stress fields under small-scale-yielding conditions. The transferability of the results from MBL studies to real structures should be verified in further studies.

Chapter 7

Summary

Welding is a very important technique in material processing engineering, and welding residual stress is always a critical issue that should be taken into account. With the rapid development of oil and gas industry, welding and repair of pipelines and platforms under crucial conditions, e.g. deep water with the depth over 300 meter, and the arctic region with very low temperature, become more and more urgent. Meanwhile, the safety and integrity of welded components is a stringent issue for the industry as well as the whole society. It has been shown that welding residual stress can have significant effect on the structural integrity, which originally motivated this study. The research presented in this thesis has advanced the fundamental understanding of the effect of residual stress on structural integrity assessment from the fracture mechanics point of view. The main focuses are the effect of residual stresses on crack-tip constraint, cleavage fracture toughness and ductile crack growth resistance. Since tensile residual stress is detrimental for the fracture, the study mainly concerns the effect of tensile residual stress on fracture behaviour.

A series of numerical analyses were carried out to investigate the problem. The problem was simplified as an ideal modified boundary layer problem under Mode I loading and plane strain conditions. The eigenstrain method was utilized to introduce residual stresses into the finite element model. The cohesive zone model and complete Gurson model were employed to study the effect of residual stresses on cleavage and ductile fracture behaviour, respectively. The main findings of the thesis are listed below.

Main findings

- For given crack tip driving force, tensile residual stress enhances the near tip stresses compared with the reference field without residual stress while the compressive residual stress has the opposite effect. Thus, tensile residual stress can increase the crack-tip constraint.

- Based on the observation that near tip stress fields show similarity, a parameter R was defined to quantify the residual stress-induced crack-tip constraint. Parameter R is defined based on the opening stress difference between the full field including the residual stress and the reference field.

- Results of the cases investigated suggest that the defined parameter R is a non-hydrostatic parameter, which is the function of the residual stress field, external loading, material hardening, loading path and geometry constraint. For the cases with higher geometry constraint, the effect of residual stress on crack-tip constraint becomes smaller.

- It has been found that the compressive residual stress enhance the cleavage fracture toughness while positive residual stresses have the opposite effect. For elastic-plastic materials, residual stress affects both the fracture process zone size and surrounding material plasticity, and the latter effect is more important.

- Compressive residual stress enlarges the plastic zone significantly while tensile residual stress compresses the plastic zone and shifts the plastic zone backward. Residual stress shows similar effect as *T-stress* on plastic zone.

- The effect of residual stresses on the cleavage fracture toughness is dependent on the traction-separation-law parameters. With the increase of Γ_0, the effect of the residual stress on cleavage toughness decreases; the effect of residual stresses increases with the increase of the maximum cohesive stress.

- Effect of residual stress on the cleavage fracture toughness is weaker for higher geometry constraint configuration. When combining the effect of residual stresses with *T-stress*, the superposition principle

can be applied. Thus, for higher geometry constraint configuration, the effect of tensile residual stress is smaller. However, for lower geometry constraint case, the coupled effect can induce a significant reduction of the cleavage fracture toughness.

- Tensile residual stress reduces the crack growth resistance while compressive residual stress can enhance the crack growth resistance. The effect of residual stresses is dependent on the amount of crack growth. With the increase of crack growth, the effect of residual stresses decreases and converges to the case without residual stress.

- The reduction of the crack growth resistance caused by residual stress is smaller for weaker hardening materials, and the influence of the residual stress decreases with crack propagation. With the increase of the material hardening, the effect of residual stress on cleavage fracture toughness decreases.

- Residual stress reduces the crack growth resistance more significantly for the materials with larger initial void volume. The influence of the residual stress decreases with the crack growth and becomes independent of f_0. The reduction of the crack growth resistance induced by the residual stress increases with increasing T/σ_0 at the early stage of crack growth and then tend to be negligible when the crack growth becomes larger.

- When the welds are geometrically similar, the effect of residual stress on the cleavage fracture toughness is a linear function of the size of the weld. However, the effect of the residual stresses on ductile crack growth resistance can be normalized by the size of the geometrically similar weld, and the normalized crack growth resistance curves collapse into a single curve.

Chapter 8

Future work

This work focused on the fundamental understanding of the effect of residual stresses on the crack-tip constraint, cleavage and ductile fracture behaviour. However, some important work has not been carried out according to the objectives of the PhD work and RESIA project. The following work can be carried out in future:

- Experimental verification of parameter R is important to further incorporate this parameter into the structural integrity assessment procedure. A efficient and reproducible method to introduce a realistic residual stress into the test specimen should be developed.

- To obtain the accurate and whole map of the distribution of residual stresses are critical to assess their effect on fracture. Thus, both the experimental measurement techniques and numerical prediction method should be further developed.

- In integrity assessment procedure, the length scale of residual stress should be properly defined, and the standardization of distribution of residual stress can be depicted for various welding joints.

- It is also important to verify the effect of residual stresses on cleavage fracture toughness and ductile crack growth resistance by experiments. It is interesting to link the effect of residual stress on failure mechanisms to parameter R.

- It have been shown in literature that residual stresses may also play an important role in fatigue, hydrogen pick-up and diffusion, creep

and so on. Thus, both the numerical simulation and experimental verification of such topics are important.

- Effect of residual stresses on the crack driving force should be further investigated either in theoretical or other approaches. A more general and accurate crack driving force parameter should be developed to include the effect of residual stress, and it should be friendly applicable for industry and structural integrity assessment.

- A improved integrity assessment procedure, which includes the effect of residual stresses on the crack driving force, crack-tip constraint, different failure mechanisms should be developed.

Bibliography

[1] R. A. Ainsworth, J. K. Sharples, and S. D. Smith. Effects of residual stresses on fracture behaviour-experimental results and assessment methods. *Journal of Strain Analysis for Engineering Design*, 35(4):307–316, 2000.

[2] P. J. Withers. Residual stress and its role in failure. *Reports on Progress in Physics*, 70(12):2211–2264, 2007.

[3] P. Dong and F. W. Brust. Welding residual stresses and effects on fracture in pressure vessel and piping components: A millennium review and beyond. *Journal of Pressure Vessel Technology*, 122(3):329–338, 2000.

[4] Project description- Residual Stress Simulation and Integrity Assessment (RESIA).

[5] http://www.sintef.no/projectweb/resia/work-packages/.

[6] T.L. Anderson. *Fracture mechanics: fundamentals and applications*. CRC press, 2005.

[7] A. A. Wells. Unstable crack propagation in metals: cleavage and fast fracture. In *Proceedings of the Crack Propagation Symposium*, volume 1. College of Aeronautics, 1962.

[8] J. R. Rice. A path independent integral and the approximate analysis of strain concentration by notches and cracks. *Journal of Applied Mechanics*, 35:379–386, 1968.

[9] C. F. Shih. Relationships between the J-integral and the crack opening displacement for stationary and extending cracks. *Journal of the Mechanics and Physics of Solids*, 29(4):305–326, 1981.

[10] C. F. Shih, B. Moran, and T. Nakamura. Energy release rate along a three-dimensional crack front in a thermally stressed body. *International Journal of Fracture*, 30(2):79–102, 1986.

[11] Y. Lei, N.P.O'Dowd, and G.A.Webster. Fracture mechanics analysis of a crack in a residual stress field. *International Journal of Fracture*, 106:195–216, 2000.

[12] Y. Lei. J-integral evaluation for cases involving non-proportional stressing. *Engineering Fracture Mechanics*, 72(4):577–596, 2005.

[13] V. Kumar, B. I. Schumacher, and M. D. German. Development of a procedure for incorporating secondary stresses in the engineering approach. *EPRI Report EPRI NP-3607*, 1985.

[14] R. A. Ainsworth and D. G. Hooton. R6 and R5 procedures: The way forward. *International Journal of Pressure Vessels and Piping*, 85(3):175–182, 2008.

[15] Y.C. Hou and J. Pan. A fracture parameter for welded structures with residual stresses. *Computational Mechanics*, 22(3):281–288, 1998.

[16] Y. J. Chao and Poh-Sang Lam. Constraint effect in fracture-what is it? In *Proceeding of the 12th Intermational Conference of Fracture*, 2009.

[17] X. B. Ren, Z. L. Zhang, and B. Nyhus. Effect of residual stress on crack-tip constraint in a boundary layer model. *International Journal of Solids and Structures*, 46(13):2629–2641, 2009.

[18] Z. L. Zhang, M. Hauge, and C. Thaulow. Two-parameter characterization of the near-tip stress fields for a bi-material elastic-plastic interface crack. *International Journal of Fracture*, 79(1):65–83, 1996.

[19] C. Betegón and I. Peñuelas. A constraint based parameter for quantifying the crack tip stress fields in welded joints. *Engineering Fracture Mechanics*, 73(13):1865–1877, 2006.

[20] M. C. Burstow, I. C. Howard, and R. A. Ainsworth. The influence of constraint on crack tip stress fields in strength mismatched welded joints. *Journal of the Mechanics and Physics of Solids*, 46(5):845–872, 1998.

[21] P. A. Eikrem, Z. L. Zhang, and B. Nyhus. Effect of plastic prestrain on the crack tip constraint of pipeline steels. *International Journal of Pressure Vessels and Piping*, 84(12):708–715, 2007.

[22] S. Cravero and C. Ruggieri. A two-parameter framework to describe effects of constraint loss on cleavage fracture and implications for failure assessments of cracked components. *Journal of the Brazilian Society of Mechanical Sciences and Engineering*, 25:403–412, 2003.

[23] A. Neimitz and J. Galkiewicz. Fracture toughness of structural components: influence of constraint. *International Journal of Pressure Vessels and Piping*, 83(1):42–54, 2006.

[24] M. L. Williams. On the stress distribution at the base of a stationary crack. *Journal of Applied Mechanics*, 24:109–1, 1957.

[25] S. G. Larsson and A. J. Carlsson. Influence of non-singular stress terms and specimen geometry on small-scale yielding at crack tips in elastic-plastic materials. *Journal of the Mechanics and Physics of Solids*, 21:263–277, 1973.

[26] Z. Z. Du and J. W. Hancock. The effect of non-singular stresses on crack-tip constraint. *Journal of the Mechanics and Physics of Solids*, 39:17–26, 1991.

[27] J. W. Hutchinson. Singular behaviour at the end of a tensile crack in a hardening material. *Journal of the Mechanics and Physics of Solids*, 16(1):13–31, 1968.

[28] J. R. Rice and G. F. Rosengren. Plane strain deformation near a crack tip in a power law hardening material. *Journal of the Mechanics and Physics of Solids*, 16(1):1–12, 1968.

[29] C. Betegón and J. W. Hancock. Two-parameter characterized of elastic-plastic crack-tip fields. *Journal of Applied Mechanics*, 58:104–110, 1991.

[30] N. P. O'Dowd and C. F. Shih. Family of crack-tip fields characterized by a trixiality paramater-I: structure of fields. *Journal of the Mechanics and Physics of Solids*, 39(8):989–1015, 1991.

[31] N. P. O'Dowd and C. F. Shih. Family of crack-tip fields characterized by a trixiality paramater-II: application. *Journal of the Mechanics and Physics of Solids*, 40(5):939–963, 1992.

[32] Xian-Kui Zhu and Brian N. Leis. Bending modified J-Q theory and crack-tip constraint quantification. *International Journal of Fracture*, 141:115–134, 2006.

[33] Y. J. Chao, S. Yang, and M. A. Sutton. On the fracture of solids characterized by one or two parameters: theory and practice. *Journal of the Mechanics and Physics of Solids*, 42:629–629, 1994.

[34] Y. J. Chao and X. K. Zhu. J-A2 characterization of crack-tip fields: Extent of J-A2 dominance and size requirements. *International Journal of Fracture*, 89(3):285–307, 1998.

[35] H. J. Schindler. An engineering concept to account for crack-tip constraint. *Facta universitatis-series: Mechanics, Automatic Control and Robotics*, 3(13):613–622, 2003.

[36] W. Guo. Elastoplastic three dimensional crack border field-I: Singular structure of the field. *Engineering Fracture Mechanics*, 46(1):93–104, 1993.

[37] W. Guo. Elastoplastic three dimensional crack border field-II: Asymptotic solution for the field. *Engineering Fracture Mechanics*, 46(1):105–113, 1993.

[38] W. Guo. Elasto-plastic three-dimensional crack border field-III: Fracture parameters. *Engineering Fracture Mechanics*, 51(1):51–71, 1995.

[39] Z. L. Zhang, C. Thaulow, and M. Hauge. Effects of crack size and weld metal mismatch on the HAZ cleavage toughness of wide plates. *Engineering Fracture Mechanics*, 57(6):653–664, 1997.

[40] Z. L. Zhang, M. Hauge, and C. Thaulow. The effect of T-stress on the near tip stress field on an elastic-plastic interface crack. In *Advances in Fracture Research,Proceedings of the 9th International Conference on Fracture*, volume 5, pages 2463–2650, Sydney, Australia, 1997. Pergamon, Oxford.

[41] T. L. Panontin and M. R. Hill. The effect of residual stresses on brittle and ductile fracture initiation predicted by micromechanical models. *International Journal of Fracture*, 82(4):317–333, 1996.

[42] M. R. Hill and T. L. Panontin. Effect of residual stress on brittle fracture testing. *Fatigue and Fracture Mechanics: 29th Volume, ASTM STP*, 1332, 1998.

[43] W. G. Xu and F. M. Burdekin. Effects of residual stresses on constraint and fracture behaviour of wide plates. *The Royal Society*, A(454):2505–2528, 1998.

[44] J. Liu, Z. L. Zhang, and B. Nyhus. Residual stress induced crack tip constraint. *Engineering Fracture Mechanics*, 75(14):4151–4166, 2008.

[45] D. A. Curry. Cleavage micromechanisms of crack extension in steels. *Metal Science*, 14:319–326, 1980.

[46] A. Neimitz, M. Graba, and J. Galkiewicz. An alternative formulation of the Ritchie-Knott-Rice local fracture criterion. *Engineering Fracture Mechanics*, 74(8):1308–1322, 2007.

[47] R. O. Ritchie, J. F. Knott, and J. R. Rice. Relationship between critical tensile stress and fracture toughness in mild steel. *Journal of the Mechanics and Physics of Solids*, 21:395–410, 1973.

[48] A. Mirzaee-Sisan, C. E. Truman, D. J. Smith, and M. C. Smith. Interaction of residual stress with mechanical loading in a ferritic steel. *Engineering Fracture Mechanics*, 74(17):2864–2880, 2007.

[49] Z. L. Zhang. *Nonlinear Fracture and Damage Mechnics*, chapter 8, pages 223–248. WIT Press Southampton, 2001.

[50] S. H. Goods and L. M. Brown. The nucleation of cavities by plastic deformation. *Acta Metall.*, 27(1):1–15, 1979.

[51] A. H. Sherry, M. A. Wilkes, J. K. Sharples, and P. J. Budden. The assessment of residual stress effects on ductile tearing using continuum damage mechanics. *Journal of Pressure Vessel Technology*, 130:041212–1–8, 2008.

[52] J. K. Sharples, C .C. France, and R. A. Ainsworth. Experimental validation of R6 treatment of residual stresses. *ASME PVP*, 392:225–238, 1999.

[53] A. Mirzaee-Sisan, C. E. Truman, D. J. Smith, and M. C. Smith. Interaction of residual stress with mechanical loading in an austenitic stainless steel. *Fatigue & Fracture of Engineering Materials & Structures*, 31(3-4):223–233, 2008.

[54] A. H. Mahmoudi, C. E. Truman, and D. J. Smith. Using local out-of-plane compression (LOPC) to study the effects of residual stress on apparent fracture toughness. *Engineering Fracture Mechanics*, 75(6):1516–1534, 2008.

[55] J. Liu. Literature review on current residual stress treatment in integrity assessment. Technical report, SINTEF Materials Technology, 2005.

[56] BS7910. Guidance on methods for assessing the acceptability of flaws in metallic structures. *British Standards Institution*, 1999.

[57] R6. Assessment of the integrity of structures containing defects, Rev. 4. *British Energy Generation Ltd, UK*, 2004.

[58] R5. Assessment procedure for the high temperature response of structures, Issue 3. *British Energy Generation Ltd, UK*, 2003.

[59] SINTAP. Structural integrity assessment procedures for european industry, final procedure. Technical report, British Steel, Sheffield, 1999.

[60] R. A. Ainsworth, F. Gutierrez-Solana, and J. R. Ocejo. Analysis levels within the SINTAP defect assessment procedures. *Engineering Fracture Mechanics*, 67(6):515–527, 2000.

[61] A. R. Dowling and C. H. A. Townley. The effect of defects on structural failure: a two-criteria approach. *International Journal of Pressure Vessels and Piping*, 3(2):77–107, 1975.

[62] R. P. Harrison, K. Loosemore, and I. Milne. Assessment of Structures Containing Defects. *Central Electricity Generating Board Report R/H/R6*, 1976.

[63] E. Smith. Describing the effect of secondary stresses on crack exten-sion in the Kr-Lr format. *International Journal of Pressure Vessels and Piping*, 72(1):51–55, 1997.

[64] A. Stacey, J. Y. Barthelemy, R. H. Leggatt, and R. A. Ainsworth. In-corporation of residual stresses into the SINTAP defect assessment procedure. *Engineering Fracture Mechanics*, 67(6):573–611, 2000.

[65] R. A. Ainsworth. A constraint-based failure assessment diagram for fracture assessment. *The International Journal of Pressure Vessels and Piping*, 64(3):277–285, 1995.

[66] I. J. MacLennan and J. W Hancock. Constraint-based failure assess-ment diagrams. *The International Journal of Pressure Vessels and Piping*, 64(3):287–298, 1995.

[67] R. A. Ainsworth and N. P. O'Dowd. Constraint in the failure assess-ment diagram approach for fracture assessment. *Journal of Pressure Vessel Technology*, 117:260, 1995.

[68] R. A. Ainsworth, I. Sattari-Far, A. H. Sherry, D. G. Hooton, and I. Hadley. Methods for including constraint effects within the SIN-TAP procedures. *Engineering Fracture Mechanics*, 67(6):563–571, 2000.

[69] H. Y. Lee, F. R. Biglari, R. Wimpory, and K. M. Nikbin. Treatment of residual stress in failure assessment procedure. *Engineering Fracture Mechanics*, 73(13):1755–1771, 2006.

[70] R. E. Dolby, R. Leggatt, I. C. Howard, D. Smith, and A. H. Sherry. Some challenges in the treatment of residual stress in flaw tolerance calculations-A TAGSI view. *International Journal of Pressure Vessels and Piping*, 85(3):166–174, 2008.

[71] P. J. Withers and H. K. D. H. Bhadeshia. Residual stress Part 1-Measurement techniques. *Materials Science and Technology*, 17:355–365, 2001.

[72] H. K. D. H. Bhadeshia. Material factors. *ASM International, Mem-ber/Customer Service Center, Materials Park, OH 44073-0002, USA, 2002.*, pages 3–10, 2002.

[73] M. R. Hill and D. V. Nelson. The inherent strain method for residual stress determination and its application to a long welded joint. *ASME, Pressure Vessels and Piping Division*, 318:343–352, 1995.

[74] T. Mura. *Micromechanics of defects in solids*. Kluwer Academic Pub, 1987.

[75] P. Dong. Length scale of secondary stresses in fracture and fatigue. *International Journal of Pressure Vessels and Piping*, 85(3):128–143, 2008.

[76] F. A. Kandil, J. D. Lord, A. T. Fry, and P. V. Grant. A review of residual stress measurement methods: a guide to technique selection. Technical report, National Physical Laboratory, 2001.

[77] N.J. Rendler and I. Vigness. Hole-drilling strain-gage method of measuring residual stresses. *Experimental Mechanics*, 6(12):577–586, 1966.

[78] M.R. Hill. *Determination of residual stress based on the estimation of eigenstrain*. PhD thesis, Stanford University, 1996.

[79] G. S. Schajer. Measurement of non-uniform residual stresses using the hole-drilling method. *Journal of Engineering Materials and Technology*, 103:338–349, 1988.

[80] M. B. Prime. Cross-sectional mapping of residual stresses by measuring the surface contour after a cut. *Journal of Engineering Materials and Technology*, 123(2):162–168, 2001.

[81] M. B. Prime. Residual stress measurement by successive extension of a slot: the crack compliance method. *Applied Mechanics Reviews*, 52:75, 1999.

[82] H. H. Lester and R. H. Aborn. Behaviour under Stress of the Iron Crystals in Steel. *Army Ordnance*, 6:120–129, 1925.

[83] D. Deng and H. Murakawa. Numerical simulation of temperature field and residual stress in multi-pass welds in stainless steel pipe and comparison with experimental measurements. *Computational Materials Science*, 37(3):269–277, 2006.

[84] X. K. Zhu and Y. J. Chao. Effects of temperature-dependent material properties on welding simulation. *Computers and Structures*, 80(11):967–976, 2002.

[85] L. E. Lindgren. Finite element modeling and simulation of welding. Part 1: Increased complexity. *Journal of thermal stresses*, 24(2):141–192, 2001.

[86] L. E. Lindgren. Finite element modeling and simulation of welding. Part 2: Improved material modeling. *Journal of thermal stresses*, 24(3):195–231, 2001.

[87] L. E. Lindgren. Finite element modeling and simulation of welding. Part 3: efficiency and integration. *Journal of thermal stresses*, 24(4):305–334, 2001.

[88] L. E. Lindgren. Numerical modelling of welding. *Computer Methods in Applied Mechanics and Engineering*, 195(48-49):6710–6736, 2006.

[89] *WeldsimS reference manual, Version 4.0*.

[90] RC McClung. A literature survey on the stability and significance of residual stresses during fatigue. *Fatigue and Fracture of Engineering Materials and Structures*, 30(3):173–205, 2007.

[91] M.F. Ashby and D.R.H. Jones. Engineering Materials: An Introduction to Their Properties and Applications. Pergamon, 1980.

[92] P. J. Bouchard, P. J. Withers, S. A0 McDonald, and R. K. Heenan. Quantification of creep cavitation damage around a crack in a stainless steel pressure vessel. *Acta Materialia*, 52(1):23–34, 2004.

[93] J. Toribio and M. Elices. Influence of residual stresses on hydrogen embrittlement susceptibility of prestressing steels. *International Journal of Solid Structures*, 28(6):791–803, 1991.

[94] J. Toribio and V. Kharin. Effect of residual stress-strain profiles on hydrogen-induced fracture of prestressing steel wires. *Materials Science*, 42(2):263–271, 2006.

[95] L. Xue and T. Wierzbicki. Ductile fracture characterization of aluminum alloy 2024-T351 using damage plasticity theory. *International Journal of Applied Mechanics*, 1(2):267–304, 2009.

[96] A. L. Gurson. Continuum theory of ductile rupture by void growth: Part I–Yield criteria and flow rules for porous ductile media. *Journal of Engineering Materials and Technology*, 99(2):2–15, 1977.

[97] J. R. Rice and D. M. Tracey. On the ductile enlargement of voids in triaxial stress fields. *Journal of Mechanics and Physics of Solids*, 17(3):201–217, 1969.

[98] F. A. McClintock. A criterion for ductile fracture by the growth of holes. *Joural of Applied Mechanics*, 35(6):363–371, 1968.

[99] V. Tvergaard. Influence of voids on shear band instabilities under plane strain conditions. *International Journal of Fracture*, 17(4):389–407, 1981.

[100] V. Tvergaard. On localization in ductile materials containing spherical voids. *International Journal of Fracture*, 18(4):237–252, 1982.

[101] V. Tvergaard and A. Needleman. Analysis of the cup-cone fracture in a round tensile bar. *Acta Metallurgica*, 32(1):157–169, 1984.

[102] L. M. Brown and J. D. Embury. Initiation and Growth of Voids at Second-Phase Particles. In *Proc. Conf. on Microstructure and Design of Alloys, Institute of Metals and Iron and Steel Insitute, London. 1973, 1,(33), 164-169*, 1973.

[103] J. Koplik and A. Needleman. Void growth and coalescence in porous plastic solids. *International Journal of Solids and Structures*, 24(8):835–853, 1988.

[104] Z.L. Zhang. *A micro-mechanical model based local approac methodology for the analysis of ductile fracture of welded T-joints*. PhD thesis, Lappeenranta University of Technilogy, Finland, 1994.

[105] Z. L. Zhang, C. Thaulow, and J. Ødegård. A complete Gurson model approach for ductile fracture. *Engineering Fracture Mechanics*, 67(2):155–168, 2000.

[106] P. F. Thomason. A three-dimensional model for ductile fracture by the growth and coalescence of microvoids. *Acta Metallurgica*, 33(6):1087–1095, 1985.

[107] P. F. Thomason. Three-dimensional models for the plastic limit-loads at incipient failure of the intervoid matrix in ductile porous solids. *Acta Metallurgica*, 33(6):1079–1085, 1985.

[108] P. F. Thomason. *Ductile Fracture of Metals*. Pergamon, 1990.

[109] E. Østby, C. Thaulow, and Z. L. Zhang. Numerical simulations of specimen size and mismatch effectsin ductile crack growth-Part I:Tearing resistance and crack growth paths. *Engineering Fracture Mechanics*, 74:1770–1792, 2007.

[110] T. Pardoen and J. W. Hutchinson. An extended model for void growth and coalescence. *Journal of the Mechanics and Physics of Solids*, 48(12):2467–2512, 2000.

[111] Z. L. Zhang and E. Niemi. A class of generalized mid-point algorithms for the Gurson-Tvergaard material model. *International Journal for Numerical Methods in Engineering*, 38(12):2033–53, 1995.

[112] Z. L. Zhang. On the accuracies of numerical integration algorithms for Gurson-based pressure-dependent elastoplastic constitutive models. *Computer Methods in Applied Mechanics and Engineering*, 121(1-4):15–28, 1995.

[113] Z. L. Zhang. Explicit consistent tangent moduli with a return mapping algorithm for pressure-dependent elastoplasticity models. *Computer methods in applied mechanics and engineering*, 121(1-4):29–44, 1995.

[114] *ABAQUS Version 6.7 User's Manual*. Hibbit, Karlsson and Sorensen, Inc., 2007.

[115] René. de Borst. Numerical aspects of cohesive-zone models. *Engineering Fracture Mechanics*, 70(14):1743–1757, 2003.

[116] M. Elices, G. V. Guinea, J. Gomez, and J. Planas. The cohesive zone model: advantages, limitations and challenges. *Engineering Fracture Mechanics*, 69(2):137–163, 2002.

[117] A. Cornec, I. Scheider, and K. H. Schwalbe. On the practical application of the cohesive model. *Engineering Fracture Mechanics*, 70(14):1963–1987, 2003.

[118] G. I. Barenblatt. The mathematical theory of equilibrium cracks in brittle fracture. *Advances in Applied Mechanics*, 7:55–129, 1962.

[119] D. S. Dugdale. Yielding of steel sheets containing slits. *Journal of the Mechanics and Physics of Solids*, 8(2):100–104, 1960.

[120] A. Hillerborg, M. Modeer, and P. E. Petersson. Analysis of crack formation and crack growth in concrete by means of fracture mechanics and finite elements. *Cement and Concrete Research*, 6(6):773–782, 1976.

[121] V. Olden, C. Thaulow, R. Johnsen, E. Østby, and T. Berstad. Application of hydrogen influenced cohesive laws in the prediction of hydrogen induced stress cracking in 25% Cr duplex stainless steel. *Engineering Fracture Mechanics*, 75(8):2333–2351, 2008.

[122] V. Tvergaard and J. W. Hutchinson. The relation between crack growth resistance and fracture process parameters in elastic–plastic solids. *Journal of the Mechanics and Physics of Solids*, 40(6):1377–1397, 1992.

[123] A. Needleman. A continuum model for void nucleation by inclusion debonding. *Journal of Applied Mechanics*, 54(3):525–531, 1987.

[124] X. P. Xu and A. Needleman. Numerical simulations of fast crack growth in brittle solids. *Journal of the Mechanics and Physics of Solids*, 42(9):1397–1407, 1994.

[125] J. L. Chaboche, F. Feyel, and Y. Monerie. Interface debonding models: a viscous regularization with a limited rate dependency. *International Journal of Solids and Structures*, 38(18):3127–3160, 2001.

[126] M. Pezzotta and Z. L. Zhang. Effect of thermal mismatch induced residual stresses on grain boundary micro-cracking of Titanium Diboride ceramics. *Journal of Material Science, doi:10.1007/s10853-009-3952-3*, 45:382–391, 2010.

[127] Y. Ueda, K. Fukuda, K. Nakacho, and S. Endo. A new measuring method of residual stresses with the aid of finite element method and reliability of estimated values. *Trans. Japan Welding Research Institute*, 4(2):123–131, 1975.

[128] M. Mochizuki, M. Hayashi, and T. Hattori. Residual stress analysis by simplified inherent strain at welded pipe junctures in a pressure vessel. *Journal of Pressure Vessel Technology*, 121(4):353–357, 1999.

[129] Y. Ueda, K. Nakacho, and M. Yuan. Application of FEM to theoretical analysis, measurement and prediction of welding residual stresses. *Transactions of the JWRI(Japan Welding Research Institute)(Japan)*, 20(1):97–107, 1991.

[130] Robert H. Dodds, Jr., C. Fong Shin, and Ted L. Anderson. Continuum and micromechanics treatment of constraint in fracture. *International Journal of Fracture*, 64:101–133, 1993.

[131] B. A. Bilby, G. E. Cardew, M. R. Goldthorpe, and I. C. Howard. A finite element investigation of the effect of specimen geometry on the fields of stress and strain at the tips of stationary cracks. *Size Effects in Fracture. Institution of Mechanical Engineers, London, England*, pages 36–46, 1986.

[132] X. B. Ren, Z .L. Zhang, and B. Nyhus. Residual stress induced crack-tip constraint: a paramteric study. In *Proceedings of 17th European Conference on Fracture, ECF17*, 2008.

[133] X Gao and R. H. Dodds Jr. An engineering approach to assess constraint effects on cleavage fracture toughness. *Engineering Fracture Mechanics*, 68(3):263–283, 2001.

[134] Y. Ueda and K. Fukuda. New measuring method of three-dimensional residual stresses in long welded joints using inherent strains as parameters–L_z method. *Journal of Engineering Materials and Technology*, 111(1):1–8, 1989.

[135] P. J. Bouchard and P. J. Withers. Identification of residual stress length scales in welds for fracture assessment. In *Residual Stress and Its Effects on Fatigue and Fracture: Proceedings of a Special Symposium*

Held Within the 16th European Conference of Fracture-ECF16, Alexandroupolis, Greece, 3-7 July, 2006, page 163, 2006.

[136] X. Gao, C. F. Shih, V. Tvergaard, and A. Needleman. Constraint effects on the ductile-brittle transition in small scale yielding. *J. Mech. Phys. Solids*, 44:1255–1282, 1996.

[137] V. Tvergaard and J. W. Hutchinson. Effect of T-stress on mode I crack growth resistance in a ductile solid. *International Journal of Solids and Structures.*, 31(6):823–833, 1994.

[138] J.C. Sobotka, R.H. Dodds, and P. Sofronis. Effects of hydrogen on steady, ductile crack growth:computational studies. *International Journal of Solids and Structures*, 46:4095–4106, 2009.

[139] L. Xia and C. F. Shih. Ductile crack growth-I. A numerical study using computational cells with microstructurally-based length scales. *Journal of the Mechanics and Physics of Solids*, 43(2):233–259, 1995.

[140] P. A. Eikrem, Z. L. Zhang, E. Østby, and B. Nyhus. Numerical study on the effect of prestrain history on ductile fracture resistance by using the complete gurson model. *Engineering Fracture Mechanics*, 75:4568–4582, 2008.

[141] E. Østby, C. Thaulow, and Z. L. Zhang. Numerical simulations of specimen size and mismatch effects in ductile crack growth Part II: Near-tip stress fields. *Engineering Fracture Mechanics*, 74:1793–1809, 2007.

"Reliability Analysis of Structural Systems using Nonlinear Finite Element Methods",
C. A. Holm, 1990:23, ISBN 82-7119-178-0.

"Uniform Stratified Flow Interaction with a Submerged Horizontal Cylinder",
Ø. Arntsen, 1990:32, ISBN 82-7119-188-8.

"Large Displacement Analysis of Flexible and Rigid Systems Considering Displacement-Dependent Loads and Nonlinear Constraints",
K. M. Mathisen, 1990:33, ISBN 82-7119-189-6.

"Solid Mechanics and Material Models including Large Deformations",
E. Levold, 1990:56, ISBN 82-7119-214-0, ISSN 0802-3271.

"Inelastic Deformation Capacity of Flexurally-Loaded Aluminium Alloy Structures",
T. Welo, 1990:62, ISBN 82-7119-220-5, ISSN 0802-3271.

"Visualization of Results from Mechanical Engineering Analysis",
K. Aamnes, 1990:63, ISBN 82-7119-221-3, ISSN 0802-3271.

"Object-Oriented Product Modeling for Structural Design",
S. I. Dale, 1991:6, ISBN 82-7119-258-2, ISSN 0802-3271.

"Parallel Techniques for Solving Finite Element Problems on Transputer Networks",
T. H. Hansen, 1991:19, ISBN 82-7119-273-6, ISSN 0802-3271.

"Statistical Description and Estimation of Ocean Drift Ice Environments",
R. Korsnes, 1991:24, ISBN 82-7119-278-7, ISSN 0802-3271.

"Properties of concrete related to fatigue damage: with emphasis on high strength concret",
G. Petkovic, 1991:35, ISBN 82-7119-290-6, ISSN 0802-3271.

"Turbidity Current Modelling",
B. Brørs, 1991:38, ISBN 82-7119-293-0, ISSN 0802-3271.

"Zero-Slump Concrete: Rheology, Degree of Compaction and Strength. Effects of Fillers as Part Cement-Replacement",
C. Sørensen, 1992:8, ISBN 82-7119-357-0, ISSN 0802-3271.

"Nonlinear Analysis of Reinforced Concrete Structures Exposed to Transient Loading",
K. V. Høiseth, 1992:15, ISBN 82-7119-364-3, ISSN 0802-3271.

"Finite Element Formulations and Solution Algorithms for Buckling and Collapse Analysis of Thin Shells",
R. O. Bjærum, 1992:30, ISBN 82-7119-380-5, ISSN 0802-3271.

"Response Statistics of Nonlinear Dynamic Systems",
J. M. Johnsen, 1992:42, ISBN 82-7119-393-7, ISSN 0802-3271.

"Digital Models in Engineering. A Study on why and how engineers build and operate digital models for decisison support",
J. Høyte, 1992:75, ISBN 82-7119-429-1, ISSN 0802-3271.

"Sparse Solution of Finite Element Equations",
A. C. Damhaug, 1992:76, ISBN 82-7119-430-5, ISSN 0802-3271.

"Some Aspects of Floating Ice Related to Sea Surface Operations in the Barents Sea",
S. Løset, 1992:95, ISBN 82-7119-452-6, ISSN 0802-3271.

"Modelling of Cyclic Plasticity with Apňplication to Steel and Aluminium Structures",
O. S. Hopperstad, 1993:7, ISBN 82-7119-461-5, ISSN 0802-3271.

"The Free Formulation: Linear Theory and Extensions with Applications to Tetrahedral Elements with Rotational Freedoms",
G. Skeie, 1993:17, ISBN 82-7119-472-0, ISSN 0802-3271.

"Høyfast betongs motstand mot piggdekkslitasje. Analyse av resultater fra prøving i Veisliter'n",
T. Tveter, 1993:62, ISBN 82-7119-522-0, ISSN 0802-3271.

"A Nonlinear Finite Element Based on Free Formulation Theory for Analysis of Sandwich Structures",
O. Aamlid, 1993:72, ISBN 82-7119-534-4, ISSN 0802-3271.

"The Effect of Curing Temperature and Silica Fume on Chloride Migration and Pore Structure of High Strength Concrete",
C. J. Hauck, 1993:90, ISBN 82-7119-553-0, ISSN 0802-3271.

"Failure of Concrete under Compressive Strain Gradients",
G. Markeset, 1993:110, ISBN 82-7119-575-1, ISSN 0802-3271.

"An experimental study of internal tidal amphidromes in Vestfjorden",
J. H. Nilsen, 1994:39, ISBN 82-7119-640-5, ISSN 0802-3271.

"Structural analysis of oil wells with emphasis on conductor design",
H. Larsen, 1994:46, ISBN 82-7119-648-0, ISSN 0802-3271.

"Adaptive methods for non-linear finite element analysis of shell structures",
K. M. Okstad, 1994:66, ISBN 82-7119-670-7, ISSN 0802-3271.

"On constitutive modelling in nonlinear analysis of concrete structures",
O. Fyrileiv, 1994:115, ISBN 82-7119-725-8, ISSN 0802-3271.

"Fluctuating wind load and response of a line-like engineering structure with emphasis on motion-induced wind forces",
J. Bogunovic Jakobsen, 1995:62, ISBN 82-7119-809-2, ISSN 0802-3271.

"An experimental study of beam-columns subjected to combined torsion, bending and axial actions",
A. Aalberg, 1995:66, ISBN 82-7119-813-0, ISSN 0802-3271.

"Scaling and cracking in unsealed freeze/thaw testing of Portland cement and silica fume concretes",
S. Jacobsen, 1995:101, ISBN 82-7119-851-3, ISSN 0802-3271.

"Damping of water waves by submerged vegetation. A case study of laminaria hyperborea",
A. M. Dubi, 1995:108, ISBN 82-7119-859-9, ISSN 0802-3271.

"The dynamics of a slope current in the Barents Sea",
Sheng Li, 1995:109, ISBN 82-7119-860-2, ISSN 0802-3271.

"Modellering av delmaterialenes betydning for betongens konsistens",
Ernst Mørtsell, 1996:12, ISBN 82-7119-894-7, ISSN 0802-3271.

"Bending of thin-walled aluminium extrusions",
Birgit Søvik Opheim, 1996:60, ISBN 82-7119-947-1, ISSN 0802-3271.

"Material modelling of aluminium for crashworthiness analysis",
Torodd Berstad, 1996:89, ISBN 82-7119-980-3, ISSN 0802-3271.

"Estimation of structural parameters from response measurements on sub-merged floating tunnels",
Rolf Magne Larssen, 1996:119, ISBN 82-471-0014-2, ISSN 0802-3271.

"Numerical modelling of plain and reinforced concrete by damage mechanics",
Mario A. Polanco-Loria, 1997:20, ISBN 82-471-0049-5, ISSN 0802-3271.

"Nonlinear random vibrations - numerical analysis by path integration methods",
Vibeke Moe, 1997:26, ISBN 82-471-0056-8, ISSN 0802-3271.

"Numerical prediction of vortex-induced vibration by the finite element method",
Joar Martin Dalheim, 1997:63, ISBN 82-471-0096-7, ISSN 0802-3271.

"Time domain calculations of buffeting response for wind sensitive structures",
Ketil Aas-Jakobsen, 1997:148, ISBN 82-471-0189-0, ISSN 0802-3271.

"A numerical study of flow about fixed and flexibly mounted circular cylinders",
Trond Stokka Meling, 1998:48, ISBN 82-471-0244-7, ISSN 0802-3271.

"Estimation of chloride penetration into concrete bridges in coastal areas",
Per Egil Steen, 1998:89, ISBN 82-471-0290-0, ISSN 0802-3271.

"Stress-resultant material models for reinforced concrete plates and shells",
Jan Arve Øverli, 1998:95, ISBN 82-471-0297-8, ISSN 0802-3271.

"Chloride binding in concrete. Effect of surrounding environment and concrete composition",
Claus Kenneth Larsen, 1998:101, ISBN 82-471-0337-0, ISSN 0802-3271.

"Rotational capacity of aluminium alloy beams",
Lars A. Moen, 1999:1, ISBN 82-471-0365-6, ISSN 0802-3271.

"Stretch Bending of Aluminium Extrusions",
Arild H. Clausen, 1999:29, ISBN 82-471-0396-6, ISSN 0802-3271.

"Aluminium and Steel Beams under Concentrated Loading",
Tore Tryland, 1999:30, ISBN 82-471-0397-4, ISSN 0802-3271.

"Engineering Models of Elastoplasticity and Fracture for Aluminium Alloys",
Odd-Geir Lademo, 1999:39, ISBN 82-471-0406-7, ISSN 0802-3271.

"Kapasitet og duktilitet av dybelforbindelser i trekonstruksjoner",
Jan Siem, 1999:46, ISBN 82-471-0414-8, ISSN 0802-3271.

"Etablering av distribuert ingeniørarbeid; Teknologiske og organisatoriske erfaringer fra en norsk ingeniørbedrift",
Lars Line, 1999:52, ISBN 82-471-0420-2, ISSN 0802-3271.

"Estimation of Earthquake-Induced Response",
Símon Ólafsson, 1999:73, ISBN 82-471-0443-1, ISSN 0802-3271.

"Coastal Concrete Bridges: Moisture State, Chloride Permeability and Aging Effects" Ragnhild Holen Relling, 1999:74, ISBN 82-471-0445-8, ISSN 0802-3271.

"Capacity Assessment of Titanium Pipes Subjected to Bending and External Pressure",
Arve Bjørset, 1999:100, ISBN 82-471-0473-3, ISSN 0802-3271.

"Validation of Numerical Collapse Behaviour of Thin-Walled Corrugated Panels",
Håvar Ilstad, 1999:101, ISBN 82-471-0474-1, ISSN 0802-3271.

"Strength and Ductility of Welded Structures in Aluminium Alloys",
Miroslaw Matusiak, 1999:113, ISBN 82-471-0487-3, ISSN 0802-3271.

"Thermal Dilation and Autogenous Deformation as Driving Forces to Self-Induced Stresses in High Performance Concrete",
Øyvind Bjøntegaard, 1999:121, ISBN 82-7984-002-8, ISSN 0802-3271.

"Some Aspects of Ski Base Sliding Friction and Ski Base Structure",
Dag Anders Moldestad, 1999:137, ISBN 82-7984-019-2, ISSN 0802-3271.

"Electrode reactions and corrosion resistance for steel in mortar and concrete",
Roy Antonsen, 2000:10, ISBN 82-7984-030-3, ISSN 0802-3271.

"Hydro-Physical Conditions in Kelp Forests and the Effect on Wave Damping and Dune Erosion. A case study on Laminaria Hyperborea",
Stig Magnar Løvås, 2000:28, ISBN 82-7984-050-8, ISSN 0802-3271.

"Random Vibration and the Path Integral Method",
Christian Skaug, 2000:39, ISBN 82-7984-061-3, ISSN 0802-3271.

"Buckling and geometrical nonlinear beam-type analyses of timber structures",
Trond Even Eggen, 2000:56, ISBN 82-7984-081-8, ISSN 0802-3271.

"Structural Crashworthiness of Aluminium Foam-Based Components",
Arve Grønsund Hanssen, 2000:76, ISBN 82-7984-102-4, ISSN 0809-103X.

"Measurements and simulations of the consolidation in first-year sea ice ridges, and some aspects of mechanical behaviour",
Knut V. Høyland, 2000:94, ISBN 82-7984-121-0, ISSN 0809-103X.

"Kinematics in Regular and Irregular Waves based on a Lagrangian Formulation",
Svein Helge Gjøsund, 2000-86, ISBN 82-7984-112-1, ISSN 0809-103X.

"Self-Induced Cracking Problems in Hardening Concrete Structures",
Daniela Bosnjak, 2000-121, ISBN 82-7984-151-2, ISSN 0809-103X.

"Ballistic Penetration and Perforation of Steel Plates",
Tore Børvik, 2000:124, ISBN 82-7984-154-7, ISSN 0809-103X.

"Freeze-Thaw resistance of Concrete. Effect of: Curing Conditions, Moisture Exchange and Materials",
Terje Finnerup Rønning, 2001:14, ISBN 82-7984-165-2, ISSN 0809-103X

"Structural behaviour of post tensioned concrete structures. Flat slab. Slabs on ground",
Steinar Trygstad, 2001:52, ISBN 82-471-5314-9, ISSN 0809-103X.

"Slipforming of Vertical Concrete Structures. Friction between concrete and slipform panel",
Kjell Tore Fosså, 2001:61, ISBN 82-471-5325-4, ISSN 0809-103X.

"Some numerical methods for the simulation of laminar and turbulent incompressible flows",
Jens Holmen, 2002:6, ISBN 82-471-5396-3, ISSN 0809-103X.

"Improved Fatigue Performance of Threaded Drillstring Connections by Cold Rolling",
Steinar Kristoffersen, 2002:11, ISBN: 82-421-5402-1, ISSN 0809-103X.

"Deformations in Concrete Cantilever Bridges: Observations and Theoretical Modelling",
Peter F. Takâcs, 2002:23, ISBN 82-471-5415-3, ISSN 0809-103X.

"Stiffened aluminium plates subjected to impact loading",
Hilde Giæver Hildrum, 2002:69, ISBN 82-471-5467-6, ISSN 0809-103X.

"Full- and model scale study of wind effects on a medium-rise building in a built up area",
Jónas Thór Snæbjørnsson, 2002:95, ISBN82-471-5495-1, ISSN 0809-103X.

"Evaluation of Concepts for Loading of Hydrocarbons in Ice-infested water",
Arnor Jensen, 2002:114, ISBN 82-417-5506-0, ISSN 0809-103X.

"Numerical and Physical Modelling of Oil Spreading in Broken Ice",
Janne K. Økland Gjøsteen, 2002:130, ISBN 82-471-5523-0, ISSN 0809-103X.

"Diagnosis and protection of corroding steel in concrete",
Franz Pruckner, 20002:140, ISBN 82-471-5555-4, ISSN 0809-103X.

"Tensile and Compressive Creep of Young Concrete: Testing and Modelling",
Dawood Atrushi, 2003:17, ISBN 82-471-5565-6, ISSN 0809-103X.

"Rheology of Particle Suspensions. Fresh Concrete, Mortar and Cement Paste with Various Types of Lignosulfonates",
Jon Elvar Wallevik, 2003:18, ISBN 82-471-5566-4, ISSN 0809-103X.

"Oblique Loading of Aluminium Crash Components",
Aase Reyes, 2003:15, ISBN 82-471-5562-1, ISSN 0809-103X.

"Utilization of Ethiopian Natural Pozzolans",
Surafel Ketema Desta, 2003:26, ISSN 82-471-5574-5, ISSN:0809-103X.

"Behaviour and strength prediction of reinforced concrete structures with discontinuity regions",

Helge Brå, 2004:11, ISBN 82-471-6222-9, ISSN 1503-8181.

"High-strength steel plates subjected to projectile impact. An experimental and numerical study",
Sumita Dey, 2004:38, ISBN 82-471-6281-4 (electronic version), ISBN 82-471-6282-2 (printed version), ISSN 1503-8181.

"Alkali-reactive and inert fillers in concrete. Rheology of fresh mixtures and expansive reactions",
Bård M. Pedersen, 2004:92, ISBN 82-471-6401-9 (printed version), ISBN 82-471-6400-0 (electronic version), ISSN 1503-8181.

"On the Shear Capacity of Steel Girders with Large Web Openings",
Nils Christian Hagen, 2005:9 ISBN 82-471-6878-2 (printed version), ISBN 82-471-6877-4 (electronic version), ISSN 1503-8181.

"Behaviour of aluminium extrusions subjected to axial loading",
Østen Jensen, 2005:7, ISBN 82-471-6872-3 (electronic version) , ISBN 82-471-6873-1 (printed version), ISSN 1503-8181.

"Thermal Aspects of corrosion of Steel in Concrete",
Jan-Magnus Østvik, 2005:5, ISBN 82-471-6869-3 (printed version) ISBN 82-471-6868 (electronic version), ISSN 1503-8181.

"Mechanical and adaptive behaviour of bone in relation to hip replacement. A study of bone remodelling and bone grafting",
Sébastien Muller, 2005:34, ISBN 82-471-6933-9 (printed version) (ISBN 82-471-6932-0 (electronic version), ISSN 1503-8181.

"Analysis of geometrical nonlinearities with applications to timber structures",
Lars Wollebæk, 2005:74, ISBN 82-471-7050-5 (printed version), ISBN 82-471-7019-1 (electronic version), ISSN 1503-8181.

"Pedestrian induced lateral vibrations of slender footbridges",
Anders Rönnquist, 2005:102, ISBN 82-471-7082-5 (printed version), ISBN 82-471-7081-7 (electronic version), ISSN 1503-8181.

"Initial Strength Development of Fly Ash and Limestone Blended Cements at Various Temperatures Predicted by Ultrasonic Pulse Velocity",
Tom Ivar Fredvik, 2005:112, ISBN 82-471-7105-8 (printed version), ISBN 82-471-7103-1 (electronic version), ISSN 1503-8181.

"Behaviour and modelling of thin-walled cast components",
Cato Dørum, 2005:128, ISBN 82-471-7140-6 (printed version), ISBN 82-471-7139-2 (electronic version), ISSN 1503-8181.

"Behaviour and modelling of selfpiercing riveted connections",
Raffaele Porcaro, 2005:165, ISBN 82-471-7219-4 (printed version), ISBN 82-471-7218-6 (electronic version), ISSN 1503-8181.

"Behaviour and Modelling og Aluminium Plates subjected to Compressive Load",
Lars Rønning, 2005:154, ISBN 82-471-7169-1 (printed version), ISBN 82-471-7195-3 (electronic version), ISSN 1503-8181

"Bumper beam-longitudinal system subjected to offset impact loading",
Satyanarayana Kokkula, 2005:193, ISBN 82-471-7280-1 (printed version), ISBN 82-471-7279-8 (electronic version), ISSN 1503-8181.

"Control of Chloride Penetration into Concrete Structures at Early Age",
Guofei Liu, 2006:46, ISBN 82-471-7838-9 (printed version), ISBN 82-471-7837-0 (electronic version), ISSN 1503-8181.

"Modelling of Welded Thin-Walled Aluminium Structures",
Ting Wang, 2006:78, ISBN 82-471-7907-5 (printed version), ISBN 82-471-7906-7 (electronic version), ISSN 1503-8181.

"Time-variant reliability of dynamic systems by importance sampling and probabilistic analysis of ice loads",
Anna Ivanova Olsen, 2006:139, ISBN 82-471-8041-3 (printed version), ISBN 82-471-8040-5 (electronic version), ISSN 1503-8181.

"Fatigue life prediction of an aluminium alloy automotive component using finite element analysis of surface topography",
Sigmund Kyrre Ås, 2006:25, ISBN 82-471-7791-9 (printed version), ISBN 82-471-7791-9 (electronic version), ISSN 1503-8181.

"Constitutive models of elastoplasticity and fracture for aluminium alloys under strain path change",
Dasharatha Achani, 2006:76, ISBN 82-471-7903-2 (printed version), ISBN 82-471-7902-4 (electronic version), ISSN 1503-8181.

"Simulations of 2D dynamic brittle fracture by the Element-free Galerkin method and linear fracture mechanics",
Tommy Karlsson, 2006:125, ISBN 82-471-8011-1 (printed version), ISBN

144

82-471-8010-3 (electronic version), ISSN 1503-8181.

"Penetration and Perforation of Granite Targets by Hard Projectiles",
Chong Chiang Seah, 2006:188, ISBN 82-471-8150-9 (printed version), ISBN
82-471-8149-5 (electronic version) ISSN 1503-8181.

"Deformations, strain capacity and cracking of concrete in plastic and early
hardening phases",
Tor Arne Hammer, 2007:234, ISBN 978-82-471-5191-4 (printed version),
ISBN 978-82-471-5207-2 (electronic version) ISSN 1503-8181.

"Crashworthiness of dual-phase high-strength steel: Material and Compo-
nent behaviour",
Venkatapathi Tarigopula, 2007:230, ISBN 82-471-5076-4 (printed version)
ISBN 82-471-5093-1 (electronic version) ISSN 1503-8181.

"Fibre reinforcement in load carrying concrete structures",
Åse Lyslo Døssland, 2008:50, ISBN 978-82-471-6910-0 (printed version),
ISBN 978-82-471-6924-7 (electronic version), ISSN 1503-8181.

"Low-velocity penetration of aluminium plates",
Frode Grytten, 2008:46, ISBN 978-82-471-6826-4 (printed version) ISBN
978-82-471-6843-1 (electronic version) ISSN 1503-8181.

"Robustness studies of structures subjected to large deformations",
Ørjan Fylling, 2008:24, ISBN 978-82-471-6339-9 (printed version) ISBN 978-
82-471-6342-9 (electronic version) ISSN 1503-8181.

"Constitutive modelling of morsellised bone",
Knut Birger Lund, 2008:92, ISBN 978-82-471-7829-4 (printed version) ISBN
978-82-471-7832-4 (electronic version) ISSN 1503-8181.

"Experimental Investigations of Wind Loading on a Suspension Bridge
Girder",
Bjørn Isaksen, 2008:131, ISBN 978-82-471-8656-5 (printed version) ISBN
978-82-471-8673-2 (electronic version) ISSN 1503-8181.

"Cracking Risk of Concrete Structures in the Hardening Phase",
Guomin Ji, 2008:198, ISBN 978-82-471-1079-9 (printed version), ISBN 978-
82-471-1080-5 (electronic version) ISSN 1503-8181.

"Modelling and numerical analysis of the porcine and human mitral ap-
paratus",
Victorien Emile Prot, 2008:249, ISBN 978-82-471-1192-5 (printed version),

ISBN 978-82-471-1193-2 (electronic version) ISSN 1503-8181.

"Strength analysis of net structures",
Heidi Moe, 2009:48, ISBN 978-82-471-1468-1 (printed version), ISBN 978-82-471-1469-8 (electronic version) ISSN1503-8181.

"Numerical analysis of ductile fracture in surface cracked shells",
Espen Berg, 2009:80, ISBN 978-82-471-1537-4 (printed version), ISBN 978-82-471-1538-1 (electronic version) ISSN 1503-8181.

"Subject specific finite element analysis of bone-for evaluation of the healing of a leg lengthening and evaluation of femoral stem design",
Sune Hansborg Pettersen, 2009:99, ISBN 978-82-471-1579-4 (printed version), ISBN 978-82-471-1580-0 (electronic version) ISSN 1503-8181.

"Evaluation of fracture parameters for notched multi-layered structures",
Lingyun Shang, 2009:137, ISBN 978-82-471-1662-3 (printed version), ISBN 978-82-471-1663-0 (electronic version) ISSN 1503-8181.

"Modelling of Dynamic Material Behaviour and Fracture of Aluminium Alloys for Structural Applications",
Yan Chen, 2009:69, ISBN 978-82-471-1515-2 (printed version), ISBN 978-82 471-1516-9 (electronic version) ISSN 1503-8181.

"Nanomechanics of polymer and composite particles",
Jianying He, 2009:213, ISBN 978-82-471-1828-3 (printed version), ISBN 978-82-471-1829-0 (electronic version) ISSN 1503-8181.

"Mechanical properties of clear wood from Norway spruce",
Kristian Berbom Dahl, 2009:250, ISBN 978-82-471-1911-2 (printed version), ISBN 978-82-471-1912-9 (electronic version) ISSN 1503-8181.

"Modeling of the degradation of TiB_2 mechanical properties by residual stresses and liquid Al penetration along grain boundaries",
Micol Pezzotta, 2009:254, ISBN 978-82-471-1923-5 (printed version), ISBN 978-82-471-1924-2 (electronic version) ISSN 1503-8181